Anticorrosion studies of benzaldehyde derivatives on iron in HCl using experimental and theoretical analysis

TH Baloyi

orcid.org **0000-0003-4304-1761**

Dissertation accepted in fulfilment of the requirements for the degree Master of Science in Chemistry at the North-West University

Supervisor: Dr ME Mashuga

Graduation: October 2024

DECLARATION

I declare that this study, submitted in fulfilment of the requirements of the Master of Science in Chemistry (MSc) degree, has not been previously submitted to this university or any other institution. I conducted and wrote the following research. The quotations are marked by proper punctuation. There is a reference list to acknowledge all the sources used in this research.

TH BALOYI

DEDICATION

This work is lovingly dedicated to the memory of my dear brother, Omphemetse Baloyi. May his bright spirit and promising future, though unfulfilled, continue to inspire me and may this achievement be a testament to the potential and dreams that will forever be cherished in my heart.

ACKNOWLEDGMENT

I am deeply grateful to God for His guidance and presence throughout my academic journey. I would like to express my heartfelt appreciation to my supervisor, Dr. M.E. Mashuga, for his unwavering support, patience, motivation, and expertise throughout my MSc studies and research. His exceptional guidance and mentorship have been invaluable, and I feel fortunate to have had the pleasure of working under his supervision.

I would also like to extend my sincere gratitude to Sasol-NRF and NWU bursary for their financial support, without which I would not have been able to pursue my studies. Additionally, I appreciate the assistance provided by the technicians from the chemistry department at North-west University, who helped me with my experiments.

Lastly, I would like to thank my family, particularly my parents, Julia Baloyi and Albert Tladinyane, for their unwavering support and love throughout my life. I am also proud of myself for persevering and staying committed to my goals.

Thank you all for your contributions to my success…

ABSTRACT

A recent investigation explored the corrosion-fighting potential of five benzaldehyde derivatives: 4-Formylbenzonitrile (BA 1), 4-Nitrobenzaldehyde (BA 2), 2-Hydroxy-5-methoxy-3-nitrobenzaldehyde (BA 3), 3,5-Bis(trifluoromethyl)benzaldehyde (BA 4), and 4-Fluorobenzaldehyde (BA 5). These compounds were tested for their ability to protect mild steel from corrosion in 1 M hydrochloric acid solution using a range of techniques, including potentiodynamic polarization (PDP), electrochemical impedance spectroscopy (EIS), adsorption isotherms, and computational methods. Supporting techniques like Fourier transform infrared spectroscopy (FTIR), and ultraviolet-visible (UV-Vis) spectroscopy, were also employed to validate the results. Despite sharing a common benzaldehyde ring, the molecules differ in their substituents, allowing for a comprehensive examination of the substituents' impact on corrosion inhibition. After a thorough analysis of the PDP and EIS data, the inhibitors demonstrated outstanding inhibitory efficiency, with the following ranking: BA 2 > BA 1 > BA 3 > BA 4 > BA 5. The Tafel analysis revealed that the inhibitors exhibited mixed-type inhibition behaviour, meaning they interacted with both the anodic and cathodic reactions, influencing the corrosion process. EIS analysis revealed that benzaldehyde derivatives formed a protective passive film on mild steel, exhibiting high corrosion resistance by shielding the alloy from corrosive attacks. The benzaldehyde inhibitors conformed to the Langmuir adsorption isotherm, with high R^2 values approaching unity, indicating a monolayer adsorption mechanism. Furthermore, the negative values of ΔG^o_{Ads} (less than -20 kJ mol^{-1}) for five inhibitors suggested a physisorption interaction between the inhibitors and the mild steel surface.

The computational study produced promising results, with the highest occupied molecular orbital (HOMO) and lowest unoccupied molecular orbital (LUMO) figures indicating that the benzaldehyde ring and substituents are capable of donating and accepting electrons. The calculated parameters indicate that all molecules possess a high affinity for adsorption on the metal surface, confirming their potential as effective corrosion inhibitors. The E_{HOMO} values reveal that these inhibitors possess high electron-donating ability, with BA 3 exhibiting the highest E_{HOMO} value among them. This is likely attributed to the presence of electron-donating methoxy and hydroxy groups. Furthermore, these inhibitors showed lower E_{LUMO} values, indicating their ability to accept electrons, with BA 2 having the lowest value, signifying a high electron-accepting ability. The presence of the nitro group ($-NO_2$) in BA 2 likely enhances its electron-accepting capability, facilitating the acceptance of electrons from the metal surface. FTIR and UV-Vis spectroscopy revealed the molecular interactions between mild steel and the inhibitor molecules, providing insight into the binding mechanism.

Keywords: Benzaldehyde derivatives; corrosion inhibitor; mild steel; electrochemical techniques; density functional theory.

LIST OF ABBREVIATIONS

Ag/AgCl	Silver/Silver Chloride
B3LYP	Becke, 3-parameter, Lee-Yang-Parr
CE	Counter Electrode
CPE	Constant Phase Element
DFT	Density Functional Theory
EIS	Electrochemical Impedance Spectroscopy
FMO	Frontier molecular orbital
FeO	Iron II oxide
Fe_2O_3	Iron III oxide
Fe_3O_4	Iron (II, III) oxide
$Fe(OH)_2$	Ferrous hydroxide
FTIR	Fourier Transform Infrared Spectroscopy
GDP	Gross Domestic Product
HCl	Hydrochloric Acid
HOMO	Highest Occupied Molecular Orbital

I.E	Inhibition Efficiency
LSV	Linear Sweep Voltammetry
LUMO	Lowest Unoccupied Molecular Orbital
MO	Molecular Orbital
MS	Mild Steel
OCP	Open Circuit Potential
Ppm	Parts per million
PDP	Potentiodynamic Polarization
RE	Reference Electrode
WE	Working Electrode

LIST OF SYMBOLS

ac	Alternating current
b_a	Anodic Tafel slope
b_c	Cathodic Tafel slope
C_{dI}	Double layer capacitance
ε	Dielectric constant
eV	Electron volt
E^o	Standard electrochemical potential
E	Electrochemical potential
E_a	Activation energy
π	Pi
h	Hour
Hz	Hertz
K	Kelvin
$kJmol^{-1}$	Kilo Joule per mole
M	Molar

mM	Millimolar
min	Minute
mL	Millilitre
mV	Millivolt
nm	Nanometre
R	Universal gas constant
R_{ct}	Charger transfer resistance
R_p	Polarization resistance
R_s	Solution resistance
s	second
% wt	Percentage weight
ω	Angular frequency
W	Warburg impedance

LIST OF FIGURES

LIST OF TABLES

TABLE OF CONTENTS

CHAPTER 1 - INTRODUCTION

1.1 Background and motivation for the study

The concept of corrosion, commonly referred to as rust, has been a natural occurrence since the dawn of time. It's a detrimental process that dulls the appearance and shortens the lifespan of materials, particularly metals. The ancient Roman philosopher Pliny (23-79 AD) discussed this phenomenon in his essay titled 'Ferrum Corrumpitar', and highlighted in detail the effects of corrosion on metal, particularly iron [1]. Corrosion negatively impacts industrial, national, and, by extension, global economies [2, 3]. Compared to other metals and alloys, mild steel is preferred for many metalworks due to its inexpensive cost and outstanding mechanical qualities. Many industrial gadgets are made of mild steel, which is prone to corrosion when exposed to industrial environments. Hydrochloric acid is a commonly used aqueous acid solution in various industrial processes. However, the use of such acidic solutions can significantly reduce the lifespan of metal equipment by accelerating corrosion, leading to premature deterioration [4].

1.2 Problem statement

It has been established that corrosion has a direct or indirect significant impact on humans, directly influencing the valuable lives of our belongings and the possibility of product contamination or efficiency loss (indirect cost) [5]. Furthermore, manufacturers and providers of goods and services suffer corrosion costs which they then pass on to customers. The worldwide financial impact of corrosion is staggering, exceeding $1.8 trillion annually. In South Africa, the direct economic cost of corrosion is estimated to be approximately R130 billion, underscoring the substantial economic burden of corrosion on the country's economy [6]. Several studies have assessed financial losses and concluded that early material degradation costs industrialized countries about 3% of their gross domestic product (GDP). Corrosion has a daily impact on the national economy, causing the failure

of bridges, destruction and damage to buildings, automobiles, water and waste systems, and many more [7].

1.3 Justification of the study

The world's technological advancements have significantly decreased the time it takes to complete tasks, both in the present and the future. Metals have always been the common materials for industrialization and urbanization. Metals are the basis of contemporary structures, transportation, electricity, and civilization. The significant advancements in technology and industry have led to tremendous rise in the use of metals and alloys. Eventually corrosion resistance is significant, it has not received enough attention. Understanding corrosion, its nature and mechanisms will significantly help the global economy. Affordable and environmentally friendly methods of corrosion mitigation are crucial. Fortunately, researchers have been actively exploring organic corrosion inhibitors as a safer and more effective alternative. This study reveals that benzaldehyde-based inhibitors possess exceptional potential as effective and eco-friendly corrosion protectants, offering a promising solution for mitigating corrosion-related issues.

1.4 Research questions

The natural tendency of metals and alloys to transform into their relatively more stable constituents, known as ores, causes corrosion [8]. Iron has a natural tendency to revert to its most stable form, which is iron(III) oxide. Even when alloyed with small amounts of carbon to form mild steel, iron readily reacts with atmospheric oxygen to revert to its ore form, a process that occurs spontaneously and effortlessly, as shown in equation (1.1). This reaction is a natural consequence of iron's inherent tendency to combine with oxygen and form an ore. The current

study aims to determine whether it is possible to control a natural occurrence like rusting and, if so, how best to do so by using benzaldehyde molecules as inhibitors.

$$4Fe + 3O_2 \rightarrow 2Fe_2O_3 \quad (1.1)$$

1.5 Aim and Objective

This research aims to employ a multi-faceted approach, combining spectroscopy, quantum chemistry, and electrochemistry techniques to assess the effectiveness of benzaldehyde and its derivatives as corrosion inhibitors for mild steel in a highly corrosive 1 M hydrochloric acid solution.

The objectives are to:

- examine the impact of varying concentrations of benzaldehyde inhibitors on their effectiveness in mitigating mild steel corrosion in 1 M HCl solution, employing electrochemical methods to assess corrosion inhibition performance,
- use a combination of electrochemical and spectroscopic techniques to study the adsorption behaviour and surface interactions of benzaldehyde derivatives on mild steel in an acidic environment, aiming to understand how these inhibitors bind to and protect the metal surface,
- ascertain the impact of molecular structure on the effectiveness of benzaldehyde derivatives' corrosion inhibition and evaluate the structure-activity relationship,
- Perform quantum chemical calculations on the benzaldehyde compounds to determine their molecular properties and correlate the calculated quantum chemical parameters with the experimentally measured inhibition efficiencies, seeking to establish a theoretical-experimental relationship that explains their corrosion inhibition behaviour.

1.6 Research hypothesis

Organic corrosion inhibitors work by adsorbing onto the metal surface, creating a protective layer that acts as a barrier, preventing corrosion from occurring and shielding the metal from damage. Compounds containing phosphorus, sulphur, nitrogen, oxygen, or multiple bonds are particularly effective at preventing corrosion. These elements and bonds act as focal points for adsorption, allowing the inhibitor molecule to attach to the metal and shield it from corrosion. Benzaldehyde molecules used in this study possess oxygen, nitrogen, and various heteroatoms in their structural ring. In addition to having adjacent heteroatoms, benzaldehydes possess an aromatic ring, which is renowned for its ability to donate electrons from its π (pi) bond, a characteristic typical of aromatic rings. Therefore, since benzaldehyde and its relative derivatives fit the criteria as mentioned above, they promise to exhibit good results as corrosion inhibitors.

1.7 Scope of the study

This research examines the corrosion-inhibiting properties of five benzaldehyde derivatives in a 1 M hydrochloric acid solution. These derivatives were chosen based on their structural characteristics and potential to prevent corrosion. This research employs a multidisciplinary approach, integrating electrochemical, quantum chemical, and spectroscopic methods, to thoroughly evaluate the corrosion-inhibiting properties of these benzaldehyde derivatives.

CHAPTER 2 – LITERATURE REVIEW

2.1 Historical background

Industries have intensively used metallic materials for structural and functional application due to their excellent mechanical strength. However, due to their high level of reactivity, these materials also experience corrosion, which reduces their performance and durability [9]. These materials are chosen based on their accessibility, affordability, and mechanical durability. Corrosion is a pervasive issue that affects both developed and developing nations worldwide, impacting various physical and chemical properties of metallic materials, such as hardness, flexibility, density, elasticity, tensile strength, and electrical conductivity, which are compromised by corrosion, thereby restricting the usefulness of metals in various applications. Rust, a persistent and familiar example of metal corrosion, has been a longstanding problem that has afflicted humanity since ancient times, posing significant challenges and limitations [10]. Our understanding of corrosion has its roots in the 17th century when Robert Boyle discovered the mechanical basis of corrosiveness and corrodibility in 1675. This foundational knowledge was later expanded upon by Austin in 1788, who discovered that the corrosion of iron causes water to become alkaline, a crucial insight into the chemical mechanisms driving corrosion [11]. The understanding of corrosion has undergone significant advancements throughout history, notably including the ground-breaking work by Epelboiu in 1970, who pioneered the use of EIS to investigate the corrosion process [12]. Corrosion-induced degradation of iron and steel structures results in significant loss of strength, potentially leading to catastrophic failure or collapse of these metals. Their degradation and damage cause this weakening due to corrosion [13]. Corrosion can impact metals in diverse ways, depending on the metal's properties, environmental factors, and the specific type of corrosion. While corrosion can be mitigated, it often comes at a significant cost, highlighting the need for effective and efficient corrosion prevention and control strategies [14].

2.2 Forms of corrosion

Eight distinguishable visual forms of corrosion represent the fundamental types of corrosion and are distinct from one another. This distinction makes it possible to study a sample and reasonably assume the general cause of corrosion and potential remedial actions[15].

Different types of corrosion

Uniform corrosion: is a corrosion type that affects the entire exposed surface of a material equally, leading to a comprehensive and uniform degradation. This phenomenon can swiftly render substantial amounts of material unusable, as the corrosion progresses evenly across the entire surface area, leaving no area unaffected [16].

Galvanic corrosion: occurs when two dissimilar metals come into contact, creating an electrochemical reaction that accelerates the corrosion process. This phenomenon happens when two metals with different electrical potentials are connected, causing the more noble metal to catalyse the corrosion of the less noble metal, leading to accelerated degradation. [17].

Pitting corrosion: A form of localized corrosion characterized by the formation of holes or pits on the metal surface, ranging from small, microscopic depressions to larger, more visible cavities, which can occur randomly and unpredictably [18].

Crevice corrosion: occurs in small, confined spaces where liquid can seep in but not flow freely, creating a stagnant environment. This type of corrosion often affects areas like gaskets, paint edges, screw heads, heat exchanger tubes, and overlapping joints. Many materials, including stainless steels, aluminium, and low-alloy steels, are susceptible to crevice corrosion, especially when exposed to chloride-containing corrosive media or other salt solutions. In these cases, the

material may initially undergo passivation, a process that can actually precede crevice corrosion [19].

Corrosion fatigue: is a category of damage that appears when metals are exposed to both cyclic stresses and a corrosive environment, leading to reduction in their ability to withstand repeated loading and unloading. This combination of stress and corrosion weakens the metal's fatigue resistance, making it more susceptible to cracking and failure, particularly in dynamically loaded components operating in corrosive environments [20].

Stress Corrosion Cracking (SCC): A type of degradation that occurs when a metal is subjected to a combination of tensile stress, corrosive environment, and susceptible material conditions, leading to the formation and propagation of cracks, often resulting in sudden and catastrophic failure [21].

Intergranular corrosion: occurs at the boundaries between grains, weakening the bonds that hold them together. This type of corrosion is particularly damaging because it reduces the material's ability to withstand tension, leading to a decrease in toughness and potentially sudden failure. As a result, the material may crack or break apart without warning, and the grains may even detach, forming pits or grooves on the surface [22].

Filiform corrosion: is a type of corrosion that specifically affects painted surfaces. It typically occurs when water or moisture seeps through the coating, coming into contact with the underlying metal and causing corrosion to spread in a thread-like pattern [23].

Microbial Induced Corrosion: also known as Bio corrosion, is a type of corrosion that occurs when microorganisms such as bacteria, archaea, or fungi interact with metals and cause corrosion [24].

Fretting corrosion occurs when two surfaces in contact experience slight, repeated movements, causing wear and corrosion at the interface, especially in environments prone to corrosion. This

type of corrosion is often seen in joints, bearings, and other areas where mechanical stress and environmental factors combine, leading to material degradation and potential failure [25].

2.3 Classification of corrosion

Corrosion can be classified into three primary categories based on its underlying mechanisms and influencing factors: chemical corrosion, electrochemical corrosion, and physical corrosion, each with distinct characteristics [26].

2.3.1 Chemical corrosion

Chemical corrosion occurs in the absence of a liquid phase, typically when the temperature exceeds the dew point or in dry environments. In such cases, vapours and gases act as corrodents, leading to material degradation. This type of corrosion is often seen at high temperatures, where dry rust forms, and is commonly associated with oxidation of metals in air at elevated temperatures (e.g., scaling of steel)

Examples of chemical corrosion include:

- Carburization: corrosion of metals in carbon-rich environments

- Nitridation: corrosion of metals in nitrogen-rich environments

- Sulfidation: corrosion of metals in sulphur-rich environments

2.3.2 Electrochemical corrosion

Electrochemical corrosion occurs when an electric potential difference exists between two dissimilar metals or between a metal and its environment, leading to the flow of electrons and corrosion. This type of corrosion is characterized by the presence of an electrolyte (e.g., moisture, saltwater).

Examples of electrochemical corrosion include:

- Galvanic corrosion: corrosion between two dissimilar metals in contact

- Pitting corrosion: localized corrosion due to electrochemical reactions

- Crevice corrosion: corrosion in shielded areas, such as under deposits or gaskets

2.3.3 Physical corrosion

This kind of corrosion process results from the physical breakdown of the material rather than any chemical reactions. Chemical reactions should not be confused with these dissolutions. A good illustration of this phenomenon is dissolving a substance in liquid metals such as mercury.

Examples of physical corrosion include:

-Abrasion: wear due to friction or rubbing against another surface

-Erosion: wear due to the impact of particles or fluids

-Cavitation: damage due to the formation and collapse of bubbles in fluids

-Fretting: wear due to small oscillatory movements between surfaces

-Impact: damage due to sudden collisions or impacts

2.4 Mechanism of corrosion

An electrochemical process results in the corrosion phenomena. When metal atoms come into contact with water molecules, they lose electrons and turn into positively charged ions (assuming the electrical current is complete[27]. This process can lead to the deterioration of metals and other materials, causing them to degrade and weaken due to chemical reactions with their environment.

The electrochemical corrosion process that results in the rusting of a metal goes through the following stages:

Anodic reaction: The metal dissolution process at the anode can be described by the following electrochemical reaction as shown in Equation 2.1:

$$M \rightarrow M^{2+}ne^{-} \qquad (2.1)$$

This is the process of oxidation, where the metal atoms surrender their electrons, leading to a loss of electrons.

Cathodic reaction: The reduction reaction that takes place at the cathode, where electrons from the anodic dissolution are used up, varies depending on the environment. The most common reactions that take place at the cathode in corrosion processes are as follows:

(A) Oxygen reduction (Acid solution)

$$O_2 + 4H^+ + 4e^- \rightarrow 2H_2O \qquad (2.2)$$

(B) Oxygen reduction (Neutral or basic solution)

$$O_2 + H_2O + 4e^- \rightarrow 2(OH)^- \qquad (2.3)$$

(C) Hydrogen evolution

$$2H^+ + 2e^- \rightarrow H_2 \uparrow \qquad (2.4$$

(D) Metal ion reduction: Metal ions present in solution may be reduced:

$$M + e^- \rightarrow M^{(n-1)+} \quad (2.5)$$

This reaction can only occur when there is a high concentration of M^{n+} ions present. In this process, the metal ion reduces its valence state by gaining an electron, resulting in a decrease in its oxidation number.

(E) Metal deposition: Metal may be reduced from an ionic to a neutral metallic state:

$$M^{n+} + e^- \rightarrow M \quad (2.6)$$

Understanding the corrosion mechanism opens options for tackling this critical issue as shown in Schematic diagram 2.1:

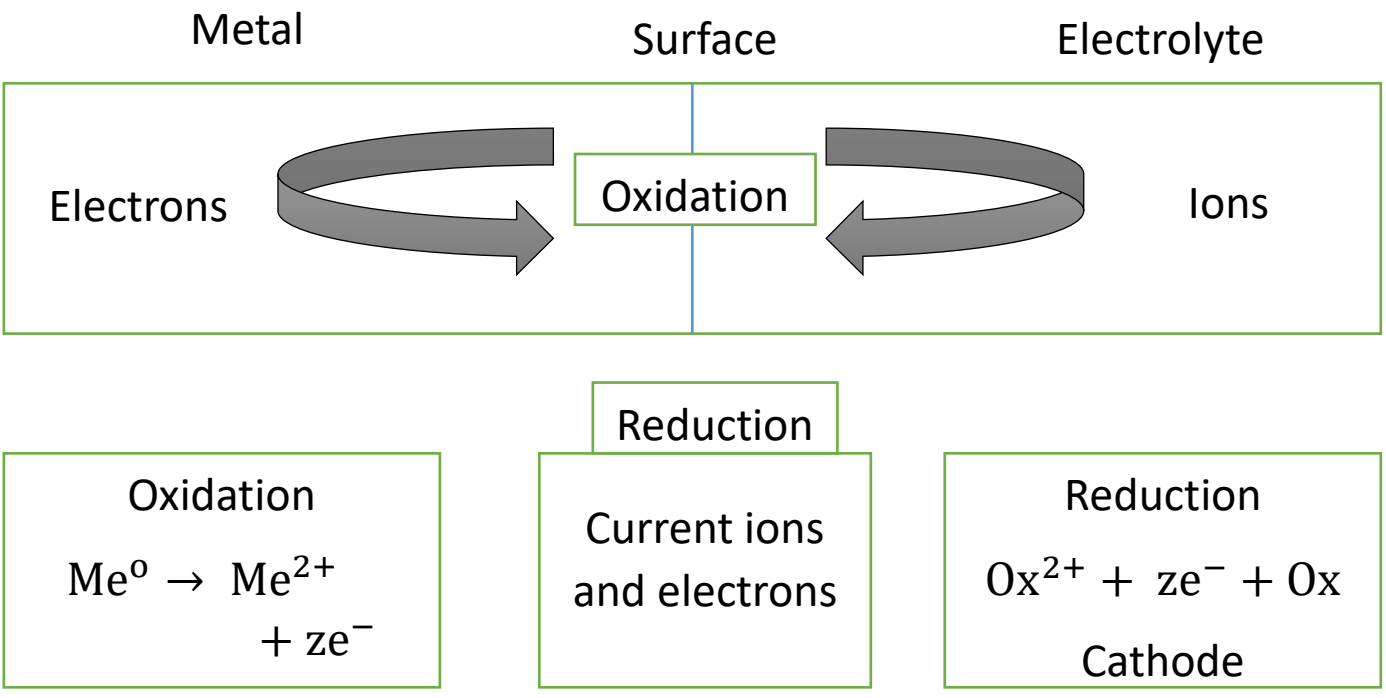

Figure 2.1 Schematic diagram of a corroding metal electrode

2.5 Corrosion of mild steel

Mild steel is a multi-component alloy, with iron (Fe) being the predominant element, making up approximately 99.321% of its composition. The remaining components include trace amounts of various elements, specifically: 0.02% phosphorus (P), 0.37% manganese (Mn), 0.03% sulphur (S), 0.01% molybdenum (Mo), 0.039% nickel (Ni), and 0.21% carbon (C) [28]. Iron is primarily involved in mild steel corrosion in the following steps under listed equations 2.7 – 2.10, schematically represented in figure 2.2 [29]:

$$Fe_{(s)} \rightarrow Fe^{2+}{}_{(aq)} + 2e^{-} \quad (2.7)$$

Then, ferrous (Fe^{2+}) ions are oxidized to ferric ions (Fe^{3+})

$$Fe^{2+}{}_{(aq)} \rightarrow Fe^{3+}{}_{(aq)} + e^{-} \quad (2.8)$$

Then the next step involves the reduction of oxygen electrons from the above equations (2.7 and 2.8)

$$O_{2(g)} + 2H_2O_{(l)} + 4e^{-} \rightarrow 4OH^{-}{}_{(aq)} \quad (2.9)$$

The final step involves the reaction between ferrous ions Fe^{2+} and oxygen O_2, resulting in the formation of ferric oxide, also known as iron(III) oxide or rust.

$$4Fe^{2+}{}_{(aq)} + O_{2(g)} + XH_2O_{(l)} \rightarrow 2Fe_2O_3.XH_2O_{(s)} + 8H^{+}{}_{(aq)} \quad (2.10)$$

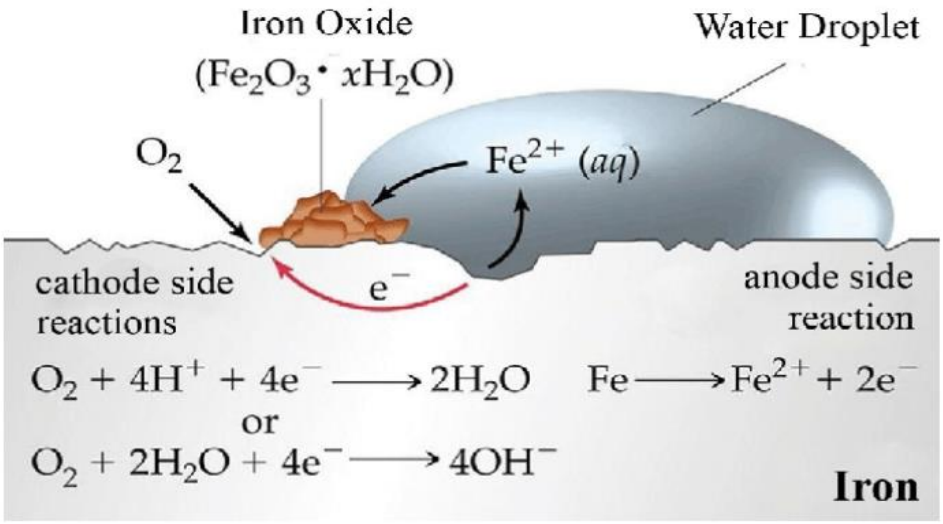

Figure 2.2 Schematic representation of corrosion of iron in the presence of water droplet and associated anode and cathode side reactions [29].

2.6 Electrochemical characterisation methods

It is necessary to set up an electrochemical cell to characterise electrochemical reactions. The electrochemical cell may contain two, three, or four electrons in an electrochemical experiment. The cell's most basic design for corrosion investigations has three electrodes. In a typical electrochemical setup, the reference electrode tracks the electrode potential of the working electrode, while the counter electrode completes the electrical circuit. The working electrode monitors the oxidation or reduction of species at its surface. The electrodes are typically submerged in a 1 M hydrochloric acid (HCl) solution, with and without the test inhibitor, as depicted in Figure 2.3, which shows a three-electrode cell setup [30].

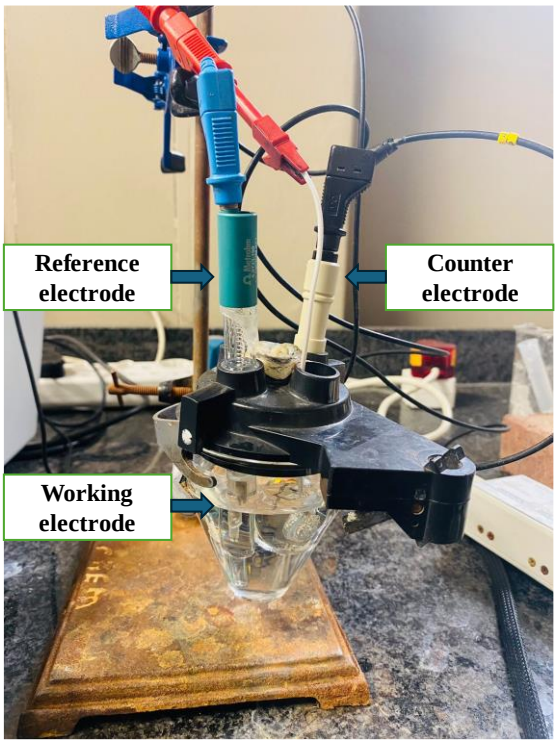

Figure 2.3 Three-electrode electrochemical cell.

2.6.1 Linear sweep voltammetry (LSV)

Linear sweep voltammetry is an electrochemical technique that records the current changes at the working electrode while the voltage between the working and reference electrodes is gradually and linearly varied, enabling the study of electrochemical reactions as a function of voltage [31]. This technique is frequently used to detect rusting. It is part of sweeping the working electrode's voltage and measuring the current response. With the help of linear sweep voltammetry, significant information on the mechanism, rate, and susceptibility of materials to corrosion in various environments may be obtained. Electrochemical technologies offer an alternative to traditional approaches to determining the corrosion rate. Simple electrochemical experiments, such as linear sweep voltammetry, can be used to directly and quantitatively evaluate corrosion rates [32].

$$R_M = \frac{M}{nF\rho} i_{corr} \qquad (2.11)$$

where M represents the metal's atomic weight, for its density, n for the number of electrons that were transferred during the reaction, and F, the Faraday constant, is identified as having a value of 96.485 C/mol. The determination of corrosion rates depends on the understanding of corrosion currents, which can be calculated using Tafel slope analysis when the corrosion reaction mechanism is known. Current theories of aqueous corrosion are based on electrode kinetics. The corrosion current can be quantitatively represented by using the Butler-Volmer equation and mixed potential theory, which takes into account both the anodic and cathodic reactions that take place in the corrosion system [33].

$$i = i_{corr}(e^{2.303\frac{n}{b_a}} - e^{2.203\frac{n}{b_c}}) \quad (2.12)$$

$$\eta = E - E_{corr} \quad (2.13)$$

E in the above equation stands for the measured current density and the applied potential. The overpotential (η) is known as the voltage difference between the applied potential and the corrosion potential (E_{corr}). The open circuit potential of a metal undergoing corrosion is known as the corrosion potential (E_{corr}). The data can be used to calculate the Tafel constants b_a and b_c as well as the corrosion current (i_{corr}).

For η/b_a greater than 1 (large anodic overpotentials), the Butler-Volmer equation provides a simplified version of the Tafel equation, specifically for the anodic reaction as follows:

$$\eta = \log(i_{corr}) + b_a.\log(i) \quad (2.14$$

On the other hand, for η/b_c less than -1 (large cathodic overpotentials), The Tafel equation for the cathodic reaction is expressed as:

$$\eta = \log(i_{corr}) + b_a . \log|i| \quad (2.15)$$

According to the Tafel equation, the difference between the potential and current density logarithms should be a straight line. Tafel plots, which are semilogarithmic, are therefore widely employed to show currents. The open circuit potential, also known as the corrosion potential E_{corr}, can be found using the Tafel curve. One can ascertain the coefficient of charge transfer by calculating the Tafel curve's slope as shown in figure 2.4.

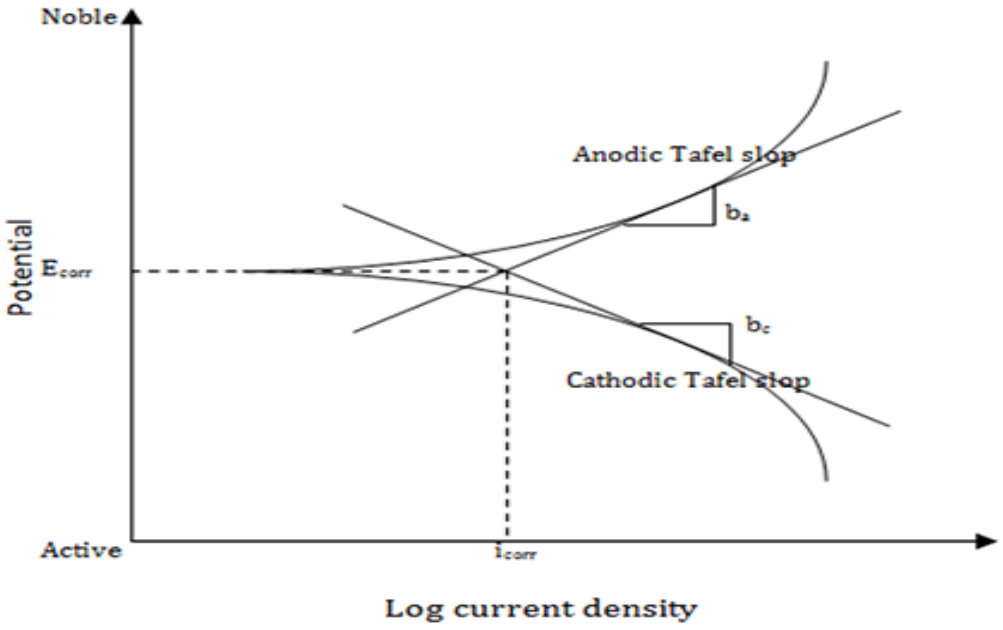

Figure 2.4 Tafel slope diagram [34].

Using equation 2.16 below, the inhibition efficiency can be determined using the corrosion current (i_{corr}) values derived from the Tafel slope:

$$\%IE_{PDP}\% = \frac{i^{o}corr - i^{i}corr}{i^{o}corr} \quad (2.16)$$

The corrosion inhibition efficiency can be calculated by comparing the current density with and without the inhibitor. The current density in the presence of the inhibitor is represented by i_{corr}, while the current density in the absence of the inhibitor by i^{o}_{corr}.

2.6.2. Electrochemical Impedance Spectroscopy (EIS)

Electrochemical Impedance Spectroscopy (EIS) is a crucial analytical technique that provides real-time insights into the electrochemical behaviour of a system, enabling the elucidation of corrosion mechanisms and kinetics. This is especially important when studying passive, active, or combined protection forms, as EIS helps track changes in the system over time, offering a deeper understanding of the corrosion dynamics [35, 36]. Most importantly, it offers quantitative data regarding the processes within the system [37].

Electrochemical Impedance Spectroscopy (EIS) involves applying a small, sinusoidal potential perturbation (typically 5-10 mV) to the working electrode in a conventional three-electrode electrochemical cell, scanning a wide range of frequencies (typically 100 kHz to 10 MHz), to measure the resulting current response and analyse the impedance spectra [38]. Concerning the perturbation, the current response is a sinusoidal signal with the same frequency but a different phase and amplitude Figure 2.5. [36]. The impedance (Z) is calculated as the complex ratio of the applied potential sine wave (V) to the response current (I), yielding both the real (Zre) and imaginary (Zim) components, also represented as the magnitude (|Z|) and phase angle (θ) of the impedance as shown in equation 2.17 and figure 2.5 [39].

$$Z(j\omega)=V(j\omega)/I(j\omega) \quad (2.17)$$

where j is the imaginary unit that equals $(-1)^{1/2}$ and ω is the angular frequency.

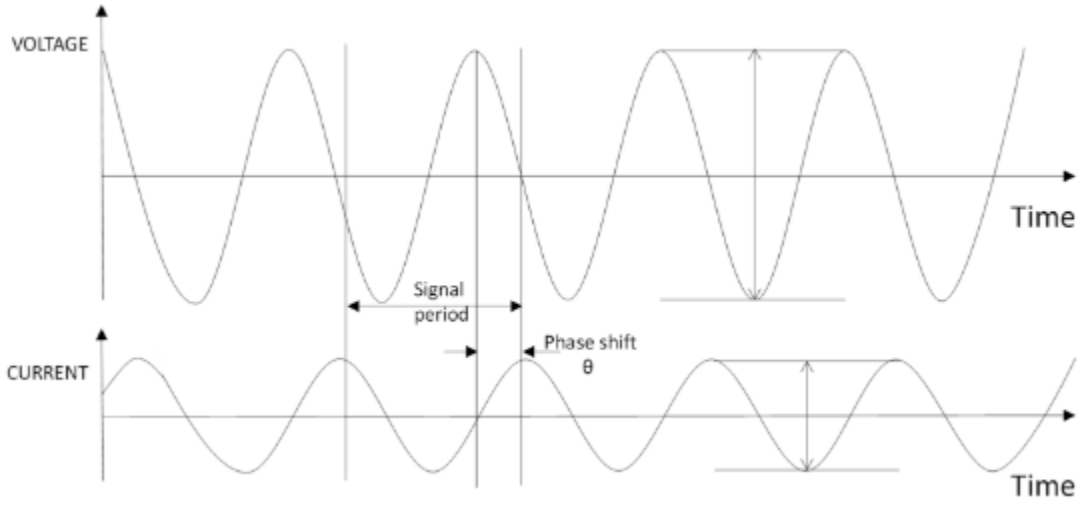

Figure 2.5 Graphic representation of the current and voltage as a function of time [40].

Electrochemical Impedance Spectroscopy (EIS) data is typically visualized in two types of plots: Nyquist plots and Bode plots. Nyquist plots illustrate the relationship between the imaginary (Z″) and real (Z′) components of impedance at different frequencies, whereas Bode plots display the impedance magnitude (|Z|) and phase angle (θ) as a function of frequency, with both axes scaled logarithmically. While both plots provide valuable insights into the electrochemical system's behaviour, Nyquist plots are often preferred for analysing complex impedance data due to their ability to clearly display relaxation processes, time constants, and electrode kinetics[38, 41]. In contrast, bode plots are more useful for identifying frequency-dependent phenomena and characterizing the system's response over a wide frequency range. As a result, this analysis may draw more heavily from Nyquist plots to elucidate specific aspects of the electrochemical system's behaviour.

To extract meaningful corrosion properties like resistance and impedance from the EIS data, researchers use a modelling approach. They fit the frequency response data to an equivalent

electrical circuit, which combines various components like resistors, capacitors, constant phase elements, inductors, and Warburg impedance in series or parallel configurations. This circuit modelling enables the conversion of EIS data into valuable insights on corrosion behaviour [42, 43]. Specialised software, such as ZView (version 3.0a, Scribner Associates, Inc., Southern Pines, NC, USA), can be employed to analyse the impedance data by fitting it to an equivalent circuit model, facilitating the interpretation of the electrochemical properties [44]. The accuracy of the fit is commonly evaluated using the chi-squared ($\chi 2$) value, which quantifies the discrepancy between the measured data and the predicted model, allowing for an assessment of the fitting quality [45]. For the equivalent circuit to accurately represent the system, its components must be directly related to the specific electrochemical reactions and corrosion mechanisms occurring in the system being studied.

EIS data must be validated as a prerequisite for impedance analysis, confirming that the data is accurate, reliable, and free from errors or artifacts that could compromise the integrity of the analysis [46]. The Kramer-Kronig (K-K) transformation can be applied to validate electrochemical impedance data by checking if it meets certain fundamental conditions: causality, linearity, stability, and finite value. By comparing the original experimental data with the transformed data, we can confirm that the system satisfies these conditions, ensuring the reliability and accuracy of the impedance measurements.

Principle of EIS

EIS analysis is a technique that assesses the electrical properties of an electrochemical cell by applying an alternating current (AC) voltage and measuring the resulting current response.

Ohm's law governs the relationship between voltage, current, and resistance in a DC circuit, as shown in Figure 2.5(a). Similarly, in an AC circuit, the impedance (Z) is defined as the ratio of voltage to current, $\frac{V_{(\omega)}}{I_{(\omega)}}$, which is an extension of Ohm's law to AC circuits. In essence, impedance represents the opposition to current flow when an AC voltage is applied, analogous to resistance in DC circuits. The opposition to current flow in an electrochemical cell is represented by a combination of circuit elements, including resistors, inductors, and conductors, which collectively make up the total impedance. Unlike a simple resistor-based model, an actual electrochemical system contains a variety of these elements in complex configurations, making impedance a more comprehensive and accurate concept for understanding and representing the system's behaviour.

Additionally, when an alternating voltage (V) is applied with an angular frequency (ω), a phase shift (Ø) occurs between the voltage and current (I). As shown in Figure 2.6, the voltage and current in the AC circuit can be represented by equations that include the maximum values of voltage (Vm) and current (Im) [47].

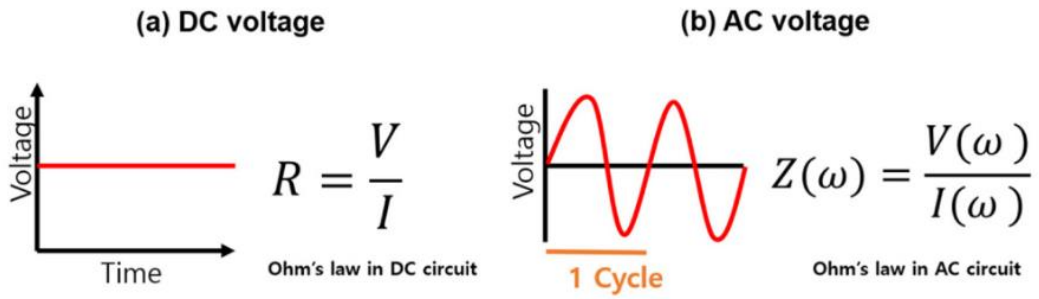

Figure 2.6 Schematic diagram and equation showing Ohm's law for D.C. circuits where D.C. voltages are formed by direct current and (b) A.C. circuits from which A.C [47].

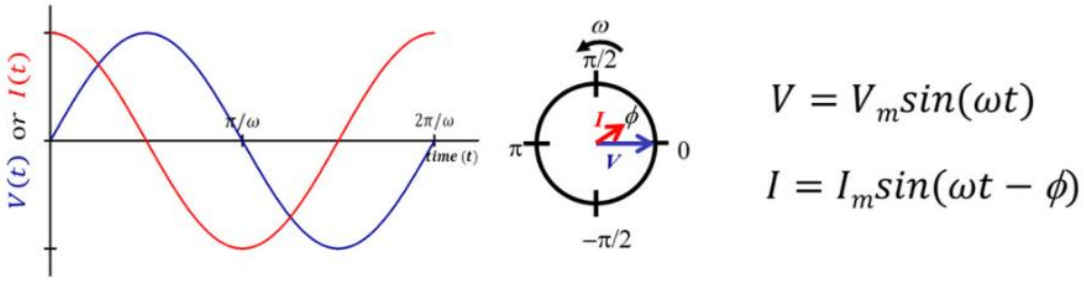

Figure 2.7 Diagram and formula showing how voltage and current are related when an A.C. voltage with an angular frequency of ω is applied [47].

Advantages of EIS

The advantages of Electrochemical Impedance Spectroscopy (EIS) over other methods like DC include [48]:

- Fast and efficient results, thanks to its linear technique, which aligns with linear systems theory.
- Comprehensive data extraction, as impedance encompasses all information obtainable from the system through linear electrical perturbation and response techniques, provided it is measured over an infinite frequency range.
- High data transfer efficiency, with a high ratio of acquired data to experimental output.
- Enhanced sensitivity, enabling the detection of much lower corrosion rates than non-electrochemical methods like weight loss or hydrogen evolution measurements.

Limitations of EIS

The limitations of Electrochemical Impedance Spectroscopy (EIS) over other methods like DC include [49, 50]

-Complexity: EIS requires sophisticated instrumentation and expertise to interpret data.

-Time-consuming: Measurements can be slow, especially at low frequencies.

-Limited frequency range: EIS typically explores a limited frequency range (mHz to MHz).

-Assumptions: EIS assumes linearity, causality, and stability of the system.

-Data analysis: Requires complex data analysis and modelling

-Limited spatial resolution: EIS provides averaged information over the electrode surface.

-Difficulties in interpreting: Data can be challenging to interpret, especially in complex systems.

-Limited applicability: EIS may not be suitable for all electrochemical systems or conditions.

-Requires calibration: EIS instruments require calibration and maintenance.

-Cost: EIS instrumentation can be expensive compared to DC methods

2.7 Quantum chemical methods

Quantum chemical methods have proven to be very useful in determining the molecular structure and elucidating the electronic structure and reactivity [51]. Thus, it has become a common practice to conduct quantum chemical calculations in corrosion inhibition studies. The predicted properties of reasonable accuracy can be obtained from density functional theory (DFT) calculations [52], [53]. Some quantum chemical parameters that influence the electronic interaction between surface atoms and inhibitors are the energy of the highest occupied molecular

orbital (E_{HOMO}), the energy of the lowest unoccupied molecular orbital (E_{LUMO}), the energy gap $E_{HOMO} - E_{LUMO}$ (ΔE) and dipole moment (μ).

DFT is one of the most essential theoretical methods for explaining the science of solids. Several chemical concepts have been correlated within the framework of DFT [54]. The most fundamental parameter in DFT is the electron density $\rho(r)$, in which all the chemical quantities are expressed [55]. The structural parameters calculated through the electronic density $\rho(r)$ concept compare well with the parameters calculated by the Schrodinger's equation in terms of the single-electron wave function (Ψ), where the latter can be applied [56]. Since the theory is more straightforward than classical quantum mechanics, which relies upon solving the many-bodied Schrodinger's equation with poorly known electron correlation factors, interest has grown in understanding the structure, properties, reactivity, and dynamics of atoms, molecules, and clusters using DFT, and large systems involving many atoms or molecules are now simulated regularly. DFT overcomes the limitations of wave mechanics [57] by reducing the problem's complexity (number of degrees of freedom) by dealing with electron density functional, each comprising the wave functions for many electrons. It is emerging as a unique approach for studying reaction mechanisms [58], including defining the configurations and energetics of transition states. Recently, as noted above, DFT has been used to analyse the characteristics of inhibitor/surface interaction and hence inhibitor mechanisms and to describe the effect of the structural nature of an inhibitor on the corrosion process [59].

Thanks to numerous studies [60, 61], DFT has become a more accessible and user-friendly tool for corrosion research. This method has provide valuable insights into the adsorption properties of corrosion inhibitors by generating various quantum chemical parameters, such as molecular orbitals, charge density, and binding energies, which help researchers understand the mechanisms

of corrosion inhibition at the molecular level [62, 63]. Below are examples of how chemical methods were used in corrosion inhibition.

The study of the mild steel corrosion inhibition properties of 4-[(E)-[(2E)-3-(4-nitrophenyl) prop-2-en-1-ylidene]amino]benzenethiol (4-NPPABT) and 4-[(E)-[(2E)-3-(4-nitrophenyl)prop-2-en-1-ylidene]amino]cyclohexan-1-ol (4-NPPACH) on mild steel in 0.1 M HCl medium was done. The compounds were optimised using density functional theory (DFT) with Becke three Lee Yang Parr (B3LYP) and 6–31G(d) basis set. The results showed that 4-NPPABT and 4-NPPACH possess high E_{HOMO} values and low-lying LUMO orbitals; hence, they could receive electrons from the metal's d orbitals. The good dipole moment values of 4-NPPABT and 4-NPPACH from the data obtained also suggest good inhibitory efficiency [64].

Corrosion inhibition performance of 2-(2-hydroxybenzylideneamino) phenol (L^1), 2-(5-chloro-2-hydroxybenzylideneamino) phenol (L^2) and 2-(2-hydroxy-5-nitrobenzylideneamino) phenol (L^3) on the corrosion behaviour of mild steel surface in a 1 M hydrochloric acid (HCl) solution was done using DFT. The data obtained showed that these inhibitor molecules with higher electronegativity would strongly interact with the metal surface, and higher inhibition efficiency was observed [65].

A computational study was conducted to investigate the corrosion inhibition properties of three amine derivatives - diethylenetriamine (I), triethylenetetramine (II), and pentaethylene hexamine (III) - on carbon steel. Using Density Functional Theory (DFT), quantum chemical parameters such as HOMO and LUMO energies, hardness (η), and dipole moment (μ) were calculated and analyzed. The results revealed that pentaethylene hexamine (III) exhibited the most promising corrosion inhibition potential, characterized by the highest HOMO energy value and lowest LUMO energy value, indicating its exceptional ability to protect carbon steel from corrosion [66].

These studies demonstrate the power of DFT in understanding corrosion mechanisms and designing corrosion-resistant materials. However, further research is needed to address limitations, such as scalability and accuracy, and to explore new applications in corrosion research.

2.8 Corrosion control

Various methods used to control corrosion include cathodic protection, linings and coatings, and corrosion inhibitors [66].

- Cathodic protection (CP) is a technology that utilizes direct current to protect structures like gas pipelines and storage tanks from corrosion. By applying an electric current, CP prevents corrosion from occurring in the first place and halts its progression, thereby preserving the integrity and extending the lifespan of these structures.
- Corrosion inhibitors are substances that slow down the corrosion rate of metals in specific environments, thereby prolonging the lifespan of equipment and preventing failures, shutdowns, and costly repairs. Additionally, these inhibitors can maintain heat transfer efficiency, prevent contamination, and preserve the appearance of structures, making them a valuable solution for various industries.
- Linings and coatings are the frontline defence against corrosion, and when combined with cathodic protection (CP), they offer the most comprehensive and cost-effective corrosion protection. Additionally, coating repairs and additional coatings can be applied as part of a corrosion control strategy to maintain optimal protection and extend the lifespan of equipment and structures.

2.9 Corrosion inhibitors

Corrosion inhibitors are cost-effective and inexpensive techniques that prevent corrosion [67]. Literature survey also reveals that the most popular inhibitors are those molecular structures containing N, O, P, S, and heterocyclic rings or polar functional groups [68] because these compounds have active adsorption centres that can strongly adsorb onto the mild steel surface by charge sharing or transferring to form a stable bond [69]. Corrosion inhibitors may be classified as cathodic, anodic, or mixed, depending on whether their influence is mainly on retarding the cathodic or anodic reaction of the corrosion process or both. In this study, the anti-corrosion and adsorption potential ability of benzaldehyde and its derivatives is observed. In this regard, benzaldehyde derivatives are promising corrosion inhibitors as they are organic compounds that are eco-friendly and contain heteroatoms such as nitrogen, oxygen, pi-electrons systems, and other electronegative atoms from various substituent groups; therefore, they may exhibit excellent properties as corrosion inhibitors.

2.10 Preliminary literature review

2.10.1. Benzaldehydes and their derivatives

Benzaldehydes and their relative derivatives are promising corrosion inhibitors. They are eco-friendly organic compounds and contain heteroatoms such as nitrogen, oxygen, π-electron systems, and other electronegative atoms from various substituent groups. Benzaldehydes such as benzaldehyde (C_6H_5CHO) are aromatic aldehydes formed from benzene rings bearing formyl (-CHO) substituents, as shown in Figure 2.8.

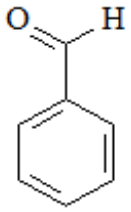

Figure 2.8: Structure of benzaldehyde.

2.10.2. Synthesis of benzaldehyde and its derivatives

Benzaldehyde can be made in a variety of ways, one of which is the hydrolysis of cinnamaldehyde to benzaldehyde under mild reaction conditions efficiently, where 2-hydroxypropyl-β-cyclodextrin (2-HPβ-CD) is used to catalyse the hydrolysis of cinnamaldehyde. Figure 2.9 shows the synthetic pathway to benzaldehyde [70].

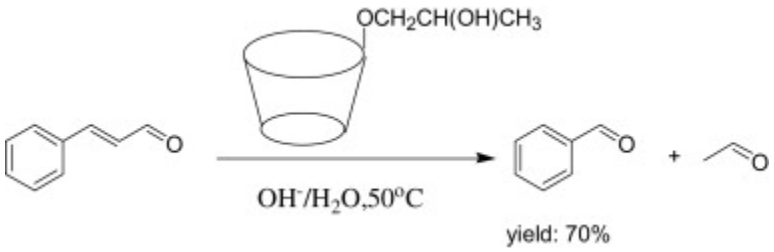

Figure 2.9 Alkaline hydrolysis of cinnamaldehyde to benzaldehyde promoted by the 2-HPβ-CD [70].

One of the other ways of preparing benzaldehyde derivatives is the synthesis of benzaldehyde derivatives by oxygenation of methylenes. First, ArCHO is formed in an E.T.–O.T. oxygenation reaction, and then H_2 as the additional product is released by electrolysis [71].

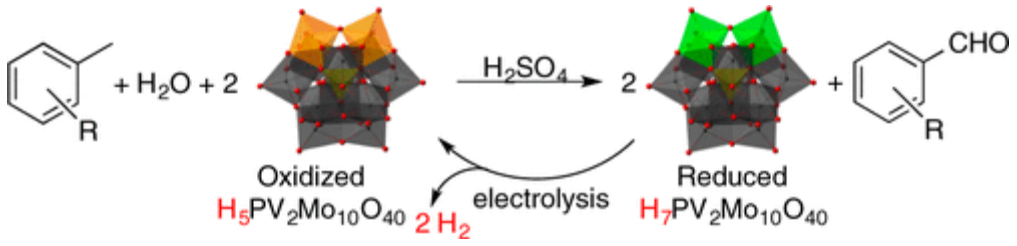

Figure 2.10 Scheme for the ET-OT oxygenation of ArCHO followed by electrolytic release of H_2 [71].

2.10.3. Application of benzaldehydes

Benzaldehydes have a wide range of applications across various industries, including [72]:

- Food flavouring: used to give almond flavour to foods.
- Cosmetics and personal care: used in certain products.
- Dye manufacturing: used in the production of dyes like acridine and aniline.
- Soap manufacturing: used in the production of soap.
- Odour control: used to control and eliminate unpleasant Odours.
- Baking: used in almond extract for cakes and baked goods, and serves as a preservative with antibacterial and antifungal properties
- Chemical synthesis: used as an intermediate product in the synthesis of compounds like cinnamic acid and benzoic acid.
- Solvents: used to dissolve solvents, resins, ethers, and oils in water.

In summary, benzaldehydes are versatile compounds with various applications across food, cosmetics, manufacturing, and chemical synthesis industries.

2.10.4 Benzaldehyde as a corrosion inhibitor

Benzaldehydes and their related derivatives fit the criteria of being corrosion inhibitors as they are heterocyclic organic compounds composed of heteroatoms, namely oxygen and some other heteroatoms found in the benzaldehyde derivatives. Though there has not been much research on the usage of benzaldehydes and their derivatives as corrosion inhibitors, some researchers have ventured to experiment with benzaldehydes as corrosion inhibitors, as shown below.

Singh et al. [73] investigated the corrosion inhibition of 4(N,N-dimethylamino) benzaldehyde nicotinic hydrazone on mild steel in 1 M HCl, using electrochemical analysis, scanning electron microscopy, and quantum studies; the results obtained showed that the inhibition efficiency increases with increasing inhibitor concentration. The surface morphology of mild steel, as revealed by FE-SEM and AFM images, provided visual evidence of the inhibitor's strong adsorption onto the metal surface. This adsorption was correlated with a high inhibition efficiency of 80.5%, demonstrating the inhibitor's effectiveness in mitigating corrosion. Furthermore, quantum chemical parameters calculated from theoretical models were in good agreement with the experimentally determined inhibition efficiency, providing a comprehensive understanding of the inhibitor's performance.

Zhang and Chen [74] investigated the inhibition behaviour of three benzaldehyde thiosemicarbazone derivatives, namely p-methoxybenzaldehyde thiosemicarbazone (MOBT), p-carboxybenzaldehyde thiosemicarbazone (COBT), and p-ethylbenzaldehyde thiosemicarbazone (EBT), for mild steel in 1 M HCl solution. Their research used analysis techniques such as gravimetric spectroscopy, electrochemical, scanning electron microscopy and energy dispersive spectrum. Gravimetric measurements showed that the corrosion rate reduced when inhibitor concentration was increased, and that the COBT inhibitor had the best inhibition efficiency at 300

M, at 96.4%. Potentiodynamic polarization results indicated that these three substances functioned as mixed-type inhibitors. These three inhibitors adhere to the Langmuir adsorption isotherm when adsorbing on mild steel surfaces in 1.0 M HCl solutions. Moreover, theoretical calculations were made, and the outcomes matched the experimental findings well.

Arrousse et al. [75] investigated the influence of (2E)-2-(acetylamino)-3-(4-nitrophenyl) prop-2-enoic acid (NPP) which was synthesized following a facile chemical method from 4-nitrobenzaldehyde (NB) and thoroughly characterized using spectroscopic techniques. These compounds were applied as novel inhibitors for corrosion of mild steel in 1M HCl using various methods such as absorbance difference, potentiodynamic polarization, and electrochemical impedance spectroscopy (EIS). According to the results, these inhibitors exhibit corrosion inhibition effectiveness values of 84% for NB and 94% for NPP, respectively, demonstrating good protective performance. The scanning electron microscopy (SEM) technique was used to examine the surface analysis of mild steel. Additionally, the DFT approach at B3LYP/6-31G (+d,p) was computed using Gaussian 09, and quantum chemical simulations were examined and showed a strong connection with the experimental data.

As was already mentioned, there hasn't been much research done on benzaldehyde and its derivatives, which has essentially led us to look more closely at how these compounds inhibit mild steel corrosion in acidic media.

CHAPTER 3 - MATERIALS AND METHODS

3.1 Experimental

This chapter describe the experimental techniques used to investigate the corrosion behaviour of Benzaldehyde derivatives in 1 M HCl. The experiments were designed to simulate real-world exposure conditions and assess the material's resistance to corrosion. The experimented procedure includes:

3.1.1 Materials and preparations

The benzaldehyde derivatives were purchased from a commercial source and used as received, without any additional processing or purification. Meanwhile, a 1 M hydrochloric acid (HCl) solution was prepared in the laboratory by diluting a 37% concentrated HCl bench reagent with distilled water, using the appropriate formula to achieve the desired concentration as shown in equation 3.1 and 3.2.

$$C_{(m)} = \left(\frac{\%\times d}{M_r} \times 100\right) \quad (3.2)$$

$$V_1 = \frac{C_2 \times V_2}{C_1} \quad (3.2)$$

where $C_{(m)}$ represents the concentration in moles per liter (molar), calculated using the density (d), molar mass (M_r), and volume (V) as shown in Equation 3.1, which enables the determination of the stock reagent's concentration, while Equation 3.2 facilitates the calculation of the volume required to prepare a 1 M solution. Specifically, in this experiment, various concentrations of benzaldehyde compounds, ranging from 100 ppm to 500 ppm, were prepared in an acidic medium, and the corrosion behaviour of mild steel, composed of 0.46% manganese, 0.26% silicon, 0.17%

carbon, 0.019% phosphorus, 0.017% sulphur, and the remaining balance of iron (Fe), was investigated using the mild steel working electrode.

3.1.2 Mild steel coupon (working electrode)

A mild steel specimen, measuring 1 cm x 1 cm, was mounted in a Teflon holder using epoxy resin, exposing a single surface area of 1 cm^2. To ensure reliable results, the mild steel surface was prepared before each test by polishing with a 220-grit diamond wheel (Struers MD Piano^{TM}) on a Struers LaboPol-1 machine to remove any residual epoxy resin. The surface was then progressively polished with silicon carbide (SiC) paper of increasing grit sizes (600-1200) to achieve a high shine, followed by washing with distilled water, acetone rinsing, and air drying. The freshly prepared mild steel surface was immediately used for Tafel polarization (PDP) and electrochemical impedance spectroscopy (EIS) measurements.

3.1.3 Corrosion inhibitors

Benzaldehyde derivatives, obtained from Sigma Aldrich, were prepared in various concentrations (100 ppm to 500 ppm) by serial dilution with distilled water. Initially, 1 g of each derivative was dissolved in a 100 ml volumetric flask to create a 1000 ppm stock solution. Then, 50 ml volumetric flasks were used to prepare five different concentrations through serial dilution, with 10 ml of each solution used as the test solution. This study employed a multi-faceted approach, combining electrochemical, computational, spectroscopic, and Langmuir methods to investigate the efficacy of benzaldehyde derivatives as corrosion inhibitors for mild steel in a 1 M HCl solution. Based on various substituents in their ring structures, the inhibitors were contrasted. Table 3.1 contains a list of the IUPAC names and chemical structures. By evaluating the different concentrations of the

inhibitors (100 ppm- 500 ppm) in the acidic medium, the effect of the inhibitor concentration was investigated.

Table 3.1 Benzaldehyde derivatives chosen for investigation in this study.

Name of inhibitors	Molecular structure	Chemical formula	Molecular weight
4-Formylbenzonitrile **(BA 1)**	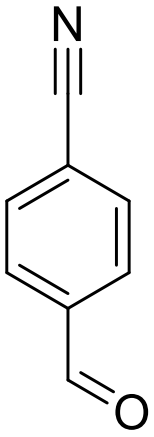	C_8H_5NO	131.13g/mol
4-Nitrobenzaldehyde **(BA 2)**	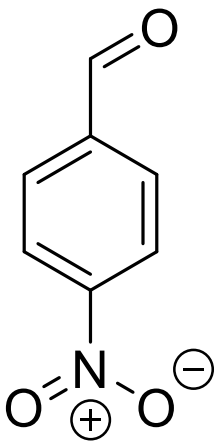	$C_7H_5NO_3$	151.12 g/mol

2-Hydroxy-5-methoxy-3-nitrobenzaldehyde **(BA 3)**	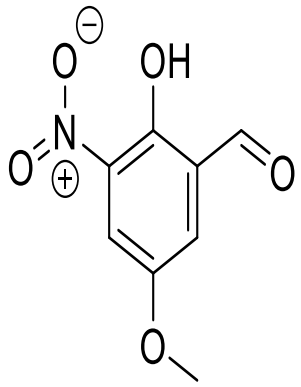	$C_8H_7NO_5$	197.14g/mol
3,5-Bis(trifluoromethyl)benzaldehyde **(BA 4)**	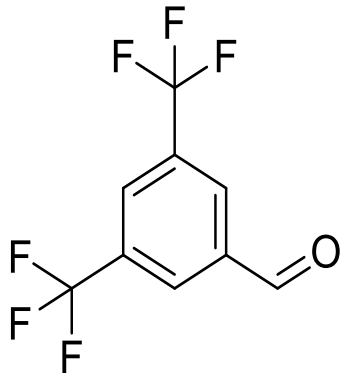	$C_9H_4F_6O$	242.12g/mol
4-Fluorobenzaldehyde **(BA 5)**	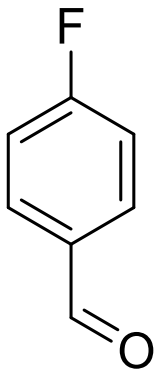	C_7H_5FO	124.11g/mol

3.2 Corrosion testing

3.2.1 Electrochemical measurement

The Auto lab electrochemical workstation from Metrohm was used to conduct the electrochemical measurements at room temperature. Before the measurements were taken, a steady period of 30 minutes was given. This period was regarded as adequate for obtaining a consistent open circuit potential value.

The electrochemical experiments utilised a three-electrode configuration, comprising a platinum counter electrode, a silver-silver chloride reference electrode in a saturated potassium chloride solution, and a carbon steel working electrode. PDP investigations were run by polarizing the working electrode potential between -250 and + 250Mv relative to OCP at the scan rate of 0.001V/s, with all potentials referenced to the Ag/AgCl electrode in saturated 3M KCl electrolyte. Additionally, The behaviour of mild steel/electrolyte system was further investigated by using the AC frequency modulation measurements at the corrosion potential (E_{corr}) by analysing the response of the system between 100 kHz and 0.1 Hz at 0.01 V amplitude and an AC signal at the corrosion potential (E_{corr}), under potentiodynamic conditions.

3.2.2 Potentiodynamic Polarization (PDP)

The potentiodynamic polarization technique was used to determine several corrosion parameters, including corrosion potential (E_{corr}), corrosion current density (i_{corr}), anodic and cathodic Tafel slopes (b_a and b_c), Polar Resistance (R_p), and Corrosion Rate. The corrosion current density (i_{corr}) was determined by extrapolating the linear Tafel segments of the anodic and cathodic curves to the corrosion potential, and then used to calculate the inhibition efficiency using the formula 3.3 below:

$$E_{PDP}\% = \frac{i^{o}corr - i^{i}corr}{i^{o}corr} \qquad (3.3)$$

where i^{o}_{corr} and i^{i}_{corr} represent the corrosion current densities measured in the absence and presence of an inhibitor, respectively.

3.2.3 Electrochemical Impedance Spectroscopy (EIS)

Electrochemical impedance spectroscopy (EIS) was used to determine critical parameters, including charge transfer resistance (R_{ct}) and double layer capacitance (Cdt), which were then used to calculate the inhibition efficiency using the equation 3.4:

$$E_{EIS}\% = \left(1 - \frac{R^{o}_{ct}}{R_{ct}}\right) x\ 100 \qquad (3.4)$$

where R^{o}_{ct} represents the charge transfer resistance without the inhibitor, and R_{ct} represents the charge transfer resistance with the inhibitor present.

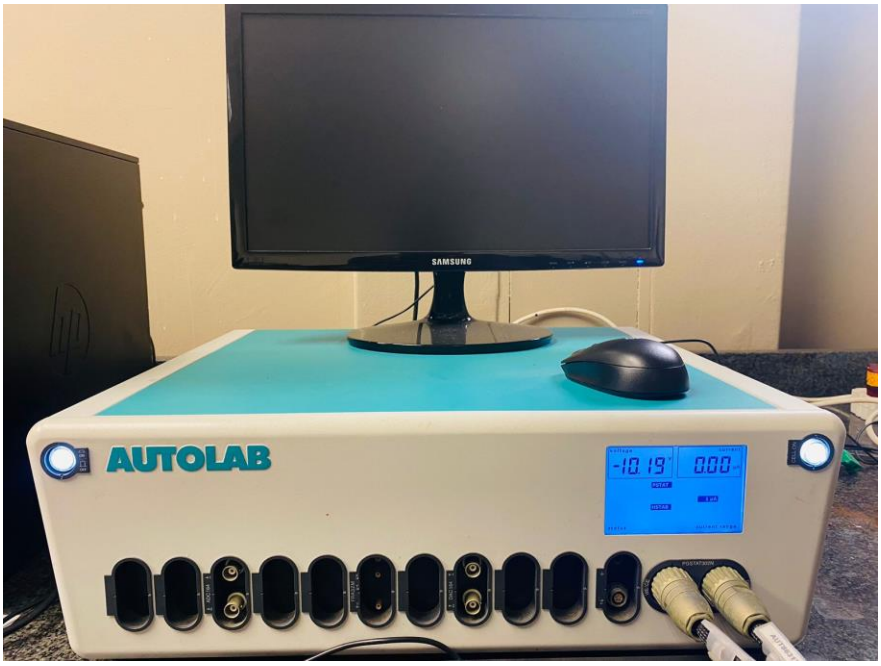

Figure 3.1 Auto lab setup for electrochemical measurement.

3.3 Spectroscopic studies

3.3.1 Fourier Transform Infrared (FTIR) spectroscopy.

The initial FTIR (Fourier Transform Infrared) spectra of pure benzaldehyde derivatives, used as corrosion inhibitors, were collected. Additionally, FTIR of benzaldehyde molecules adsorbed on the steel surface were recorded. To prepare the samples, mild steel sheets were polished and then immersed in a 500 ppm solution of the inhibitors for seven days, allowing the molecules to adsorb onto the surface. The solution was then evaporated, leaving a thin film of the inhibitor molecules adsorbed on the steel surface, which was subsequently analysed using FTIR spectroscopy.

3.3.2 Ultraviolet-visible (UV-Vis) spectroscopy

Freshly pre-treated metals were dipped in a 500 ppm solution of the studied benzaldehyde compounds for seven days. The adsorbed film of the benzaldehyde molecules on the steel surface was analysed using the Agilent Technology, Cary series UV-vis spectrometer [75]. UV–vis spectra of the benzaldehyde molecule (500 ppm) and the left-over solution after mild steel had been dipped for seven days were recorded using the Carry 50 Ultraviolet Spectrophotometer.

3.4 Quantum chemical study

B3LYP/6-31G+(d, p) model, comprehensive geometry optimisation of benzaldehyde molecules was performed using density functional theory (DFT) [9]. The calculations for the optimized molecular force constants and frequencies were performed at the same theoretical level. The optimised shapes are the molecule's ground state geometries since there is no negative frequency. All the calculations in the gas phase were carried out using the Gaussian 09W D.01 program [10]. The energy gap (ΔE) was computed as the difference of the benzaldehydes frontier molecular orbitals (FMO) energies. Using equation (3.5) below.

$$\Delta E = E_{LUMO} - E_{HOMO} \quad (3.5)$$

where E_{LUMO} is the energy of the lowest unoccupied molecular orbital and E_{HOMO} is the energy of the highest occupied molecular orbital.

The dipole moment (μ), calculated using equation (3.6), represents the overall molecular polarity, equivalent to the product of the charge magnitude (Q) at each end of the molecular dipole and the distance (r) between the charges, reflecting the molecule's net polar properties.

$$\mu = Q \times r \quad (3.6)$$

Using equation (3.7) below, the global chemical hardness (η), a frequently used reactivity parameter [11], was determined.

$$\sigma = \frac{1}{\eta} \cong -2/(E_{HOMO} - E_{LUMO}) \quad (3.7)$$

The electronegativity (χ) of a molecule, calculated using equation (3.8), represents its ability to attract and draw electrons towards itself, reflecting its electron-withdrawing power [76].

$$X \cong -(\frac{1}{2})(E_{HOMO} + E_{LUMO}) \quad (3.8)$$

CHAPTER 4 - RESULTS AND DISCUSSION

Chapter 4 presents the findings and interpretations of the research, which combines electrochemical, quantum chemical, and spectroscopic approaches. Each method is supported by relevant data, which is thoroughly discussed and analysed. The chapter is organized in the following sequence: electrochemical methods, quantum chemical methods, spectroscopic methods, and Langmuir isotherms. This structure allows for a comprehensive examination of the results, facilitating a deeper understanding of the corrosion inhibition mechanisms and the effectiveness of the benzaldehyde derivatives as corrosion inhibitors.

4.1 Electrochemical studies

4.1.1 Potentiodynamic polarization

Figure 4.1 displays the potentiodynamic polarization curves for mild steel in 1 M HCl, both without and with various concentrations (100 - 500 ppm) of the benzaldehyde inhibitors. The corresponding values for corrosion potential (E_{corr}), corrosion current density (i_{corr}), anodic and cathodic Tafel slopes (b_a and b_c), polarization resistance (R_p), and corrosion rate were extracted from the polarization curves and presented in Table 4.1. The corrosion current densities (i_{corr}) were obtained by extrapolating the linear Tafel segments of the anodic and cathodic curves to the corrosion potential. The inhibition efficiency was then calculated using equation 3.3 (Chapter 3) based on the measured i_{corr} values, providing insights into the effectiveness of the inhibitors.

Potentiodynamic polarization curves inform us about the kinetics of the anodic and cathodic reactions [77]. By closely examining the Tafel curves, it is observed that the anodic and cathodic curves current density decreased compared to the blank when the inhibitors are added to the hydrochloric acid. This observation indicates the inhibitors can prevent hydrogen evolution and mild steel dissolution [78]. For most of the inhibitors in the study, the 500 ppm systems showed

the lowest anodic currents. Significant inhibition was seen in the anodic curves, particularly at high concentrations, indicating that the inhibitors could adsorb on the metal surface and create a passive protective film [79]. The addition of inhibitors did not alter the shape of the anodic Tafel curves, suggesting that they did not influence the corrosion reaction mechanism. However, the cathodic curves remained unchanged in shape, except for the BA 2 inhibitor, which showed exhibited a slight modification at higher concentrations, this suggests that BA 2 influences the cathodic reaction mechanism, with this effect becoming more pronounced at higher concentrations [80]. The introduction of inhibitors led to a substantial decrease in the corrosion potential across all concentrations, signifying a shift towards a more noble direction. This reduction indicates that the inhibitors successfully suppressed the anodic dissolution of mild steel, thereby effectively mitigating corrosion and demonstrating their protective effect.

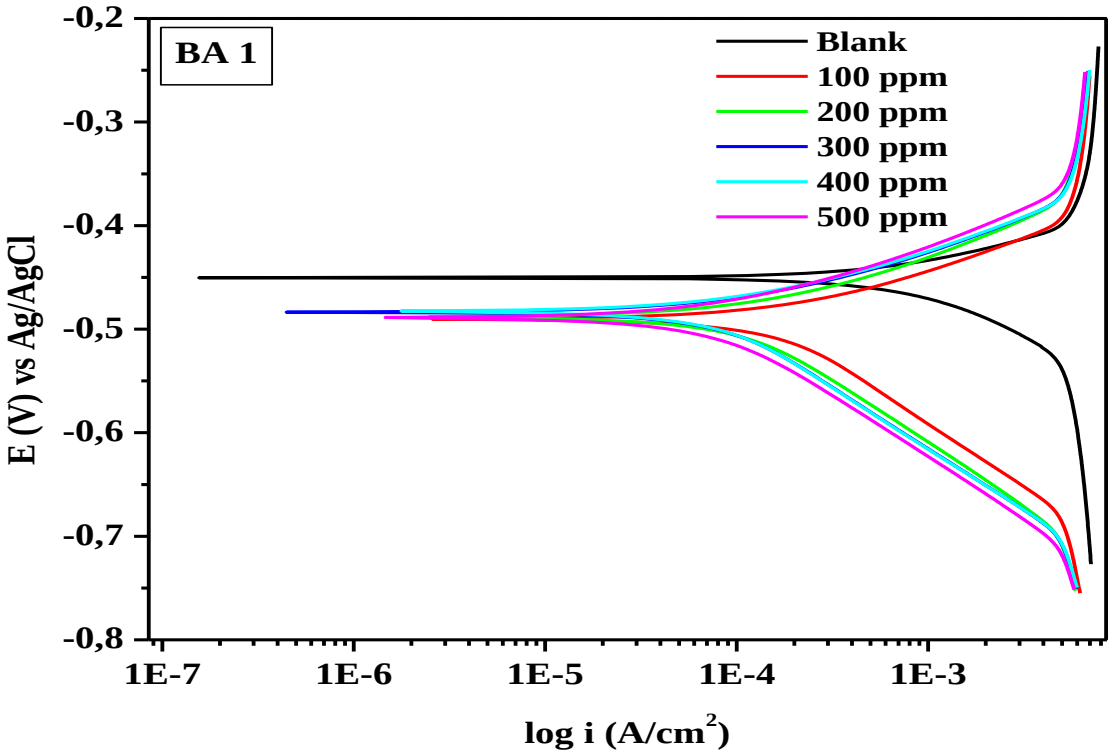

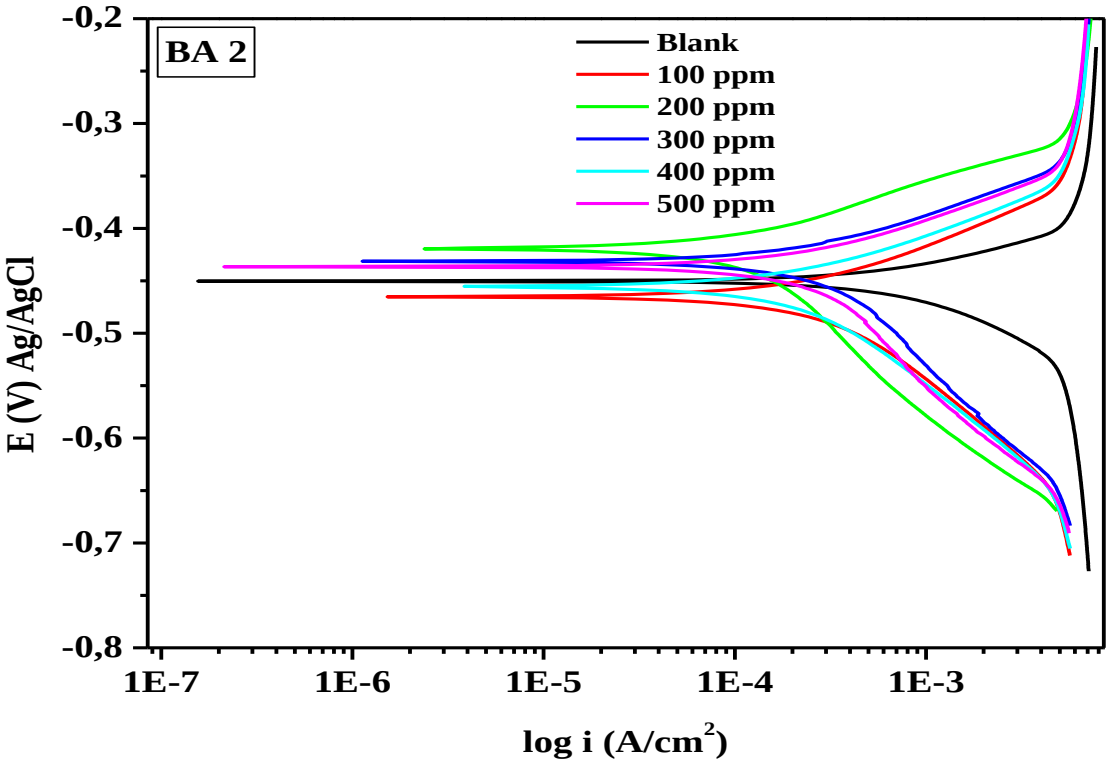
BA 2
Blank
100 ppm
200 ppm
300 ppm
400 ppm
500 ppm
E (V) Ag/AgCl
-0,2
-0,3
-0,4
-0,5
-0,6
-0,7
-0,8
1E-7
1E-6
1E-5
1E-4
1E-3
log i (A/cm2)

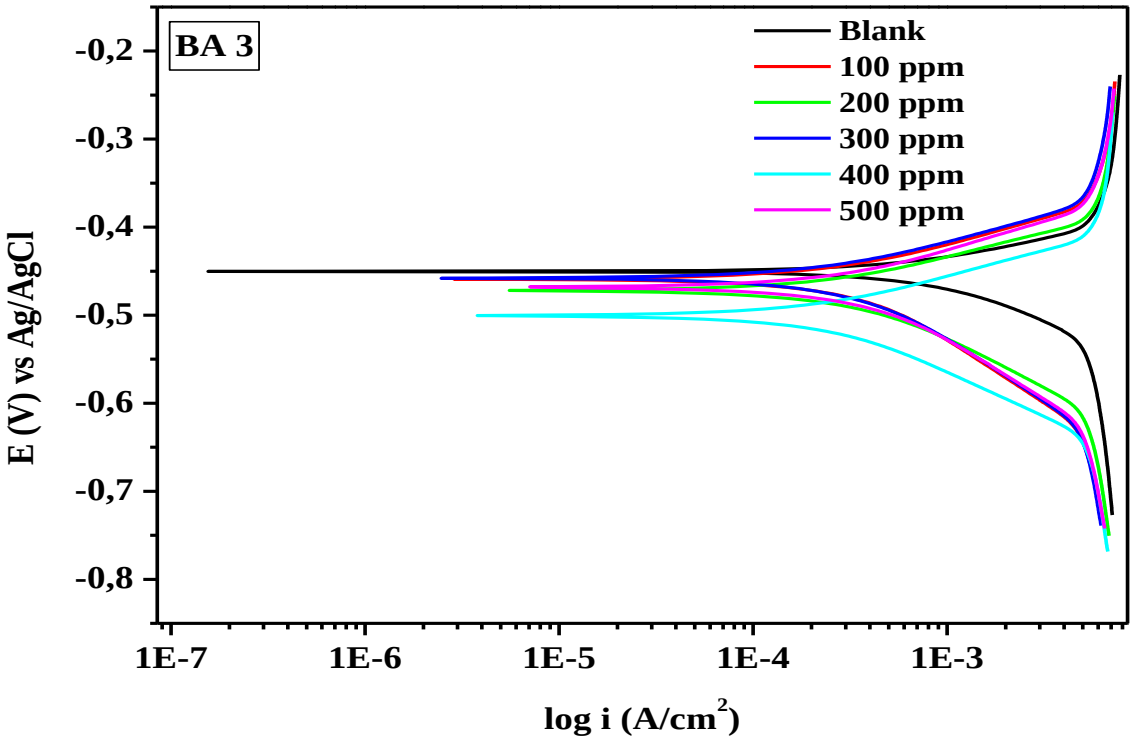
BA 3
Blank
100 ppm
200 ppm
300 ppm
400 ppm
500 ppm
E (V) vs Ag/AgCl
-0,2
-0,3
-0,4
-0,5
-0,6
-0,7
-0,8
1E-7
1E-6
1E-5
1E-4
1E-3
log i (A/cm2)

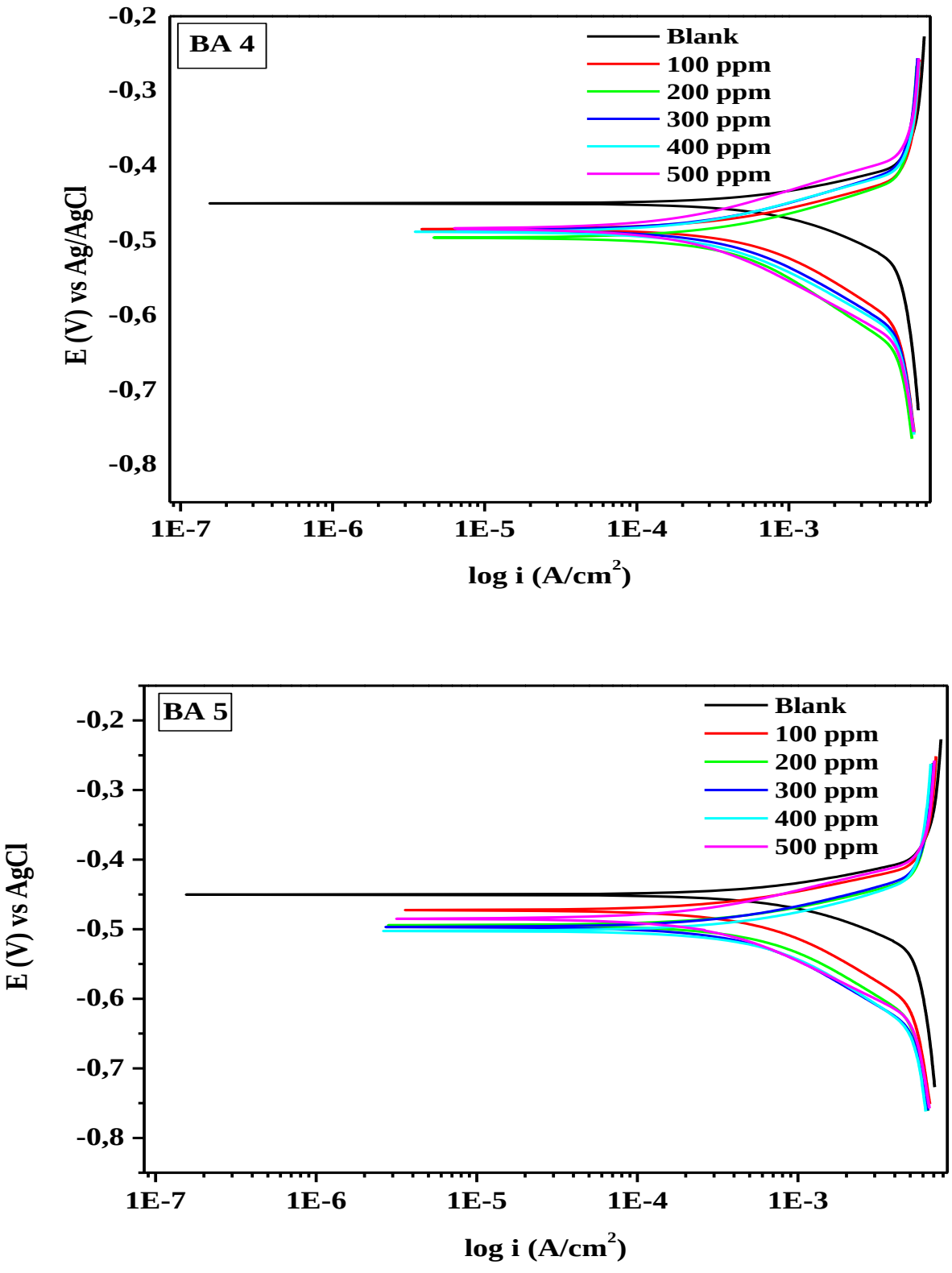

Figure 4.1 Tafel polarization curves for benzaldehydes BA 1 to BA 5 compounds for mild steel corrosion in 1 M HCl solution.

The data in Table 4.1 reveals a significant decrease in corrosion current density (i_{corr}) values when the inhibitor is added to the acid solution, with a consistent decrease in i_{corr} as the inhibitor concentration increases. Meanwhile, the corrosion potential (E_{corr}) values exhibit only a slight shift, indicating a mixed-type inhibition behaviour. According to the classification criteria, an inhibitor is considered anodic if the E_{corr} shift is more than 85 mV in the anodic direction, cathodic if the shift is more than 85 mV in the cathodic direction, and mixed-type if the shift is less than 85 mV [81, 82]. In this case, the small difference in E_{corr} values between the blank and inhibitor-containing systems (as shown in Table 4.1) suggests a mixed-type inhibition mechanism. This implies that the benzaldehyde compounds under investigation are corrosion inhibitors of the mixed type, as they prevent mild steel from dissolving anodically and hydrogen gas from evolving cathodically. The current density (i_{corr}) of the reaction is seen to decrease with the addition of the benzaldehyde inhibitors, which is a definite indicator of the inhibitor's role in lowering the active sites on the metal surface. The slight alteration in βa and βc readings following the inhibitors' addition in comparison to the blank indicates that the inhibitors are adsorbed into the metal surface without impacting the mild steel corrosion mechanism in the acid. Since cathodic reactions are more likely to be prevalent when βc values are higher than βa values, inhibitors will have a greater impact on cathodic reaction sites. As inhibitor concentrations rise, it is evident that the current density (i_{corr}) falls, indicating that the inhibitors under study are effective at inhibiting corrosion. All the inhibitors examined in this study exhibited notable protection efficiencies, calculated using equation 3.3, with some demonstrating superior performance compared to others. The inhibition efficiency of the compounds displayed a positive correlation with the concentration of the inhibitors, with the highest efficiency achieved at a concentration of 500 ppm for all respective inhibitors. This suggests that increasing the inhibitor concentration enhances the protective effect,

with the optimal efficiency attained at the highest concentration tested. BA 2 at 500 ppm yields the highest result, 94.25%, as Table 4.1 illustrates. At 500 ppm, the order of protection efficiency of the compounds is BA 2 > BA 1 > BA 3 > BA 4 > BA 5. The inhibitors BA 1 and BA 2 have comparable levels of inhibition efficiency over the investigated concentration interval. BA 2 inhibitor demonstrated the highest inhibition efficiency among all the inhibitors in the study. The exceptional protection efficiency of BA 2 can be attributed to the presence of the nitro group in its ring, which provides additional pi-electrons, supplementing the pi-electrons already present in the benzaldehyde ring. This enhances the inhibitor's ability to interact with the metal surface, leading to improved corrosion inhibition. The synergistic effect of nitro group and the benzaldehyde ring in BA 2 results in a more effective inhibitor-metal interaction, making it the most efficient inhibitor in the study. BA 3 compound has additional functional groups hydroxyl (OH) at position 2 and methoxy at position 5, these groups can introduce a bit of steric hindrance, which might slightly reduce the molecule's ability to interact with the metal surface [83]. In the instance of BA 4, the molecule's enormous size (242.12 g/mol) may be the cause of a very slight reduction in the molecule's ability to interact with the metal surface. This is because steric barrier between the incoming and already adsorbed molecules may make it difficult for a particularly large molecule to fit into a partially occupied space on a metallic substrate [84]. The BA 5 inhibitor, like the other inhibitors investigated, exhibited enhanced activity at higher concentrations, indicating that its efficacy is concentration dependent.

Table 4.1 Results of the parameters obtained from the extrapolation of the Tafel polarization curve.

Inhibitor concentration (ppm)	$-E_{corr}$ (mV)	β_a ($mVdec^{-1}$)	β_c ($mVdec^{-1}$)	i_{corr} (μAcm^{-2})	IP_{PDP} (%)
Blank					
0	445±1.00	77.52±0.21	38.24±0.12	485.14±1.00	-
BA 1					
100	488±0.50	112.62±0.58	49.27±0.02	127.1±0.20	73.8±0.10
200	488±0.98	112.85±0.65	61.40±0.20	87.66±0.70	81.9±0.65
300	483±0.55	106.19±1.01	84.03±0.31	63.02±0.49	87.0±0.55
400	478±1.48	104.98±0.59	37.27±0.47	54.69±0.18	88.7±0.70
500	489±0.95	86.41±0.58	41.78±0.07	42.38±2.89	91.3±1.30
BA 2					
100	465±1.00	73.41±0.15	38.23±0.45	114.84±0.62	76.3±1.40
200	415±0.58	84.85±0.10	36.40±0.50	55.17±2.42	88.5±1.26
300	432±0.95	22.31±0.58	23.26±1.00	50.06±1.50	89.7±2.66
400	453±0.55	27.70±0.16	14.22±0.20	37.42±0.5	92.3±0.31
500	436±1.48	14.76±0.05	12.60±0.65	27.91±0.48	94.25±1.00
BA 3					
100	452±0.91	155.04±0.74	63.55±0.47	307.81±0.56	36.6±0.67
200	464±1.00	92.822±1.00	49.98±0.58	278.37±1.00	42.6±0.74

300	457±0.21	129.45±1.34	60.99±0.29	250.02±2.66	48.5±0.50
400	497±0.25	89.96±0.30	55.04±1.00	176.61±0.95	63.6±1.06
500	466±0.56	63.548±0.34	46.90±1.13	154.93±0.17	68.1±0.95
BA 4					
100	477±0.52	107.60±0.10	47.69±0.43	351.07±2.01	27.6±0.72
200	491±076	117.11±0.47	53.70±0.10	301.42±0.87	37.9±0.60
300	478±1.00	101.99±0.29	51.66±0.32	269.43±0.20	44.5±0.10
400	485±0.25	79.46±0.30	50.53±0.27	194.68±1.00	60.0±0.25
500	478±0.03	99.32±0.75	59.76±0.98	169.85±0.61	65.0±1.00
BA 5					
100	467±1.08	77.74±0.17	45.12±0.30	319.61±1.28	34.1±0.49
200	476±0.53	83.98±0.61	44.16±1.00	312.82±0.64	35.5±0.76
300	473±0.53	104.50±0.90	36.83±0.43	301.85±1.46	37.8±1.10
400	474±2.10	115.30±0.26	49.68±2.00	223.83±0.63	53.9±1.57
500	480±2.64	94.01±0.48	52.10±0.76	198.45±2.00	59.1±2.00

4.1.2 Electrochemical impedance spectroscopy (EIS)

The impedance approach yields data on the surface characteristics of the systems under investigation as well as the kinetics of the electrode processes. The impedance's shape provides mechanistic details. The approach is frequently utilized to look at procedures for inhibiting corrosion [85]. EIS was employed to study the corrosion behaviour of mild steel in 1 M HCl solution at open circuit potential (OCP) with and without at various concentrations (100-500 ppm) of BA 1, BA 2, BA 3, BA 4, and BA 5 inhibitors after 30 minutes of immersion at 30°C. The

resulting Nyquist and Bode plots (-Phase angle vs log f and log Z vs log f) for mild steel in both uninhibited and inhibited acid solutions containing different concentrations of the benzaldehyde inhibitors are presented in Figures 4.2 and 4.3, respectively. The inhibitors' Nyquist plot shows a sequence of lowered semicircles with each one's centre below the x-axis. The Nyquist semicircles' diameters increase as the concentration of the inhibitor increases. The Nyquist plots show depressed semicircles attributes, this is in relation to a single time constant in the Bode plot (Fig 4.3). These attributes of the Nyquist curves imply that the corrosion of mild steel in the benzaldehyde inhibitors are controlled by single charge transfer process [86]. The depressed Nyquist semicircle is a characteristic feature of solid electrodes, attributed to the frequency dispersion caused by the roughness of the mild steel electrode surface. From the phase angle curves of the Bode plots, it can be observed that the curves of the inhibited system have an increased area under the curves and an increased magnitude of the phase angle compared to the blank system. A high area under the curve for the inhibitors compared to the blank suggests that most of the inhibitors were able to adsorb on the mild steel surface and create a passive coating that protects the mild steel from acid exposure [87, 88]. All inhibitors except BA 4 and BA 5 demonstrated a consistent behaviour. Notably, BA 5 stood out with significantly lower inhibition efficiency values in both PDP and EIS tests, deviating from the expected trend.

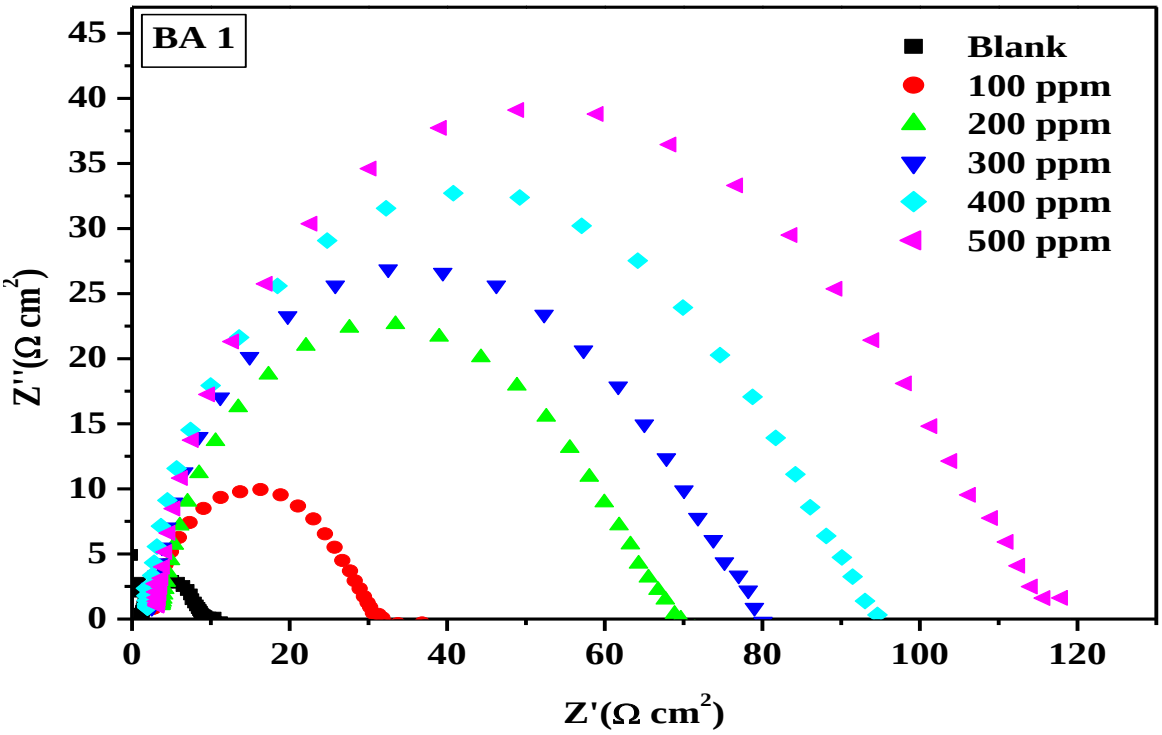
BA 1
Blank
100 ppm
200 ppm
300 ppm
400 ppm
500 ppm
Z''(Ω cm²)
Z'(Ω cm²)
0
5
10
15
20
25
30
35
40
45
0
20
40
60
80
100
120

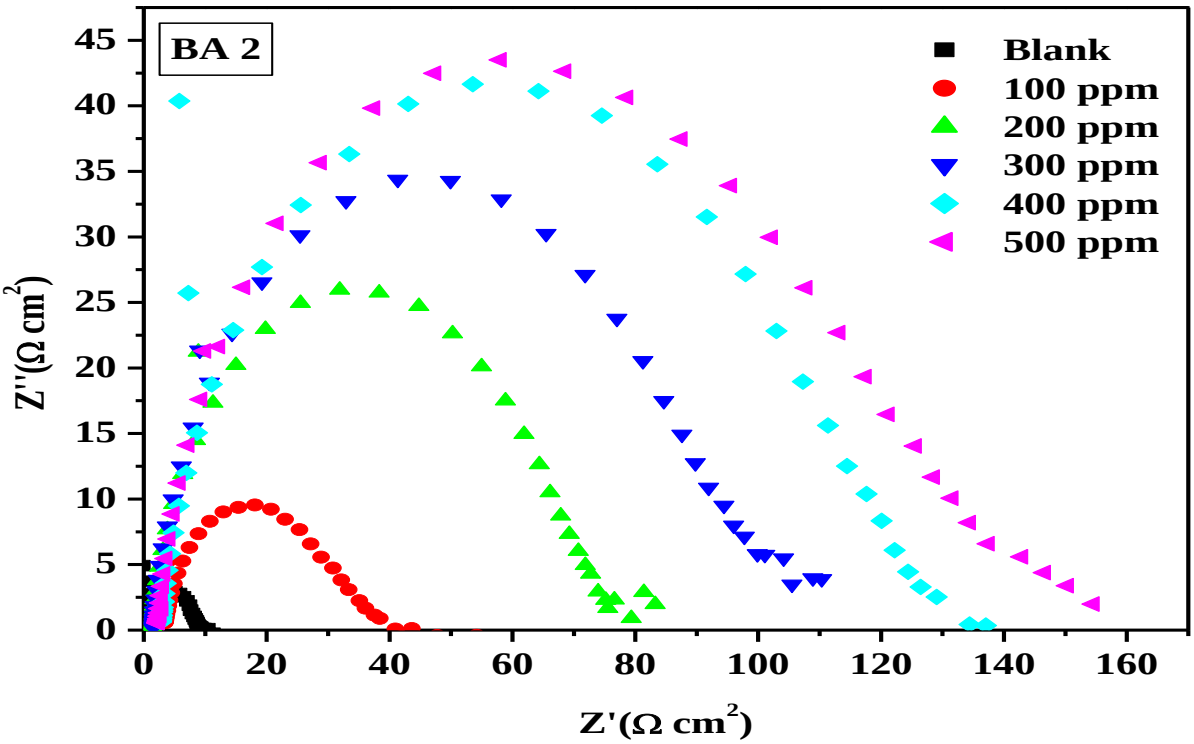
BA 2
Blank
100 ppm
200 ppm
300 ppm
400 ppm
500 ppm
Z''(Ω cm²)
Z'(Ω cm²)
0
5
10
15
20
25
30
35
40
45
0
20
40
60
80
100
120
140
160

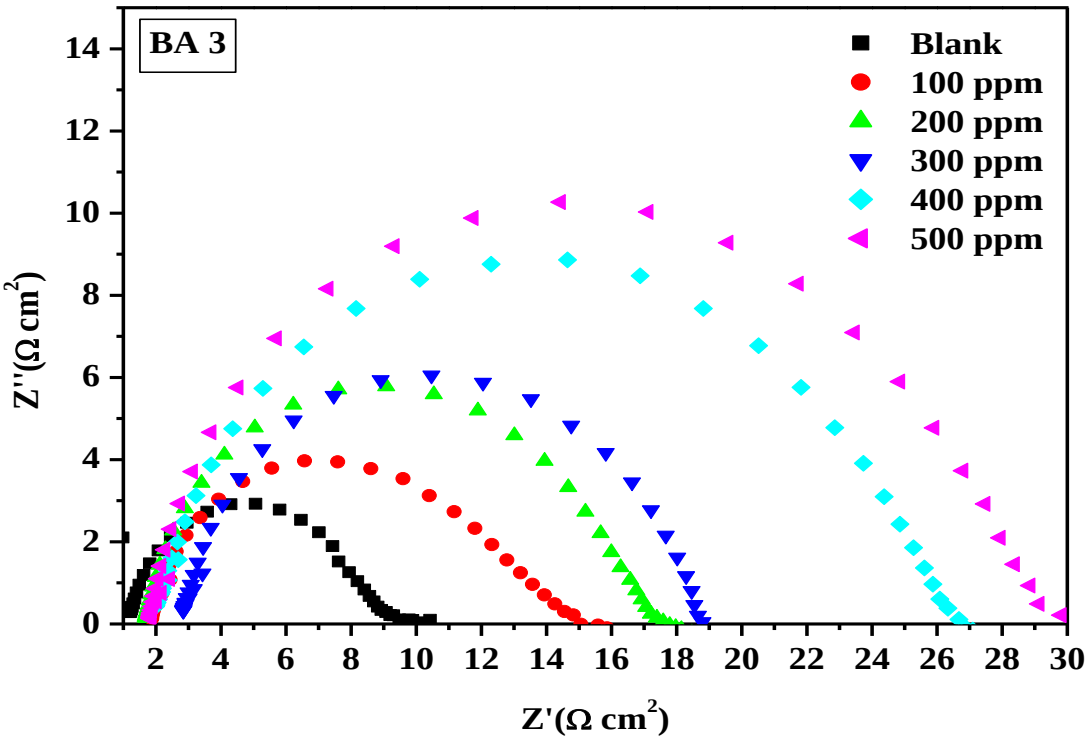
BA 3
Blank
100 ppm
200 ppm
300 ppm
400 ppm
500 ppm
Z''(Ω cm²)
Z'(Ω cm²)

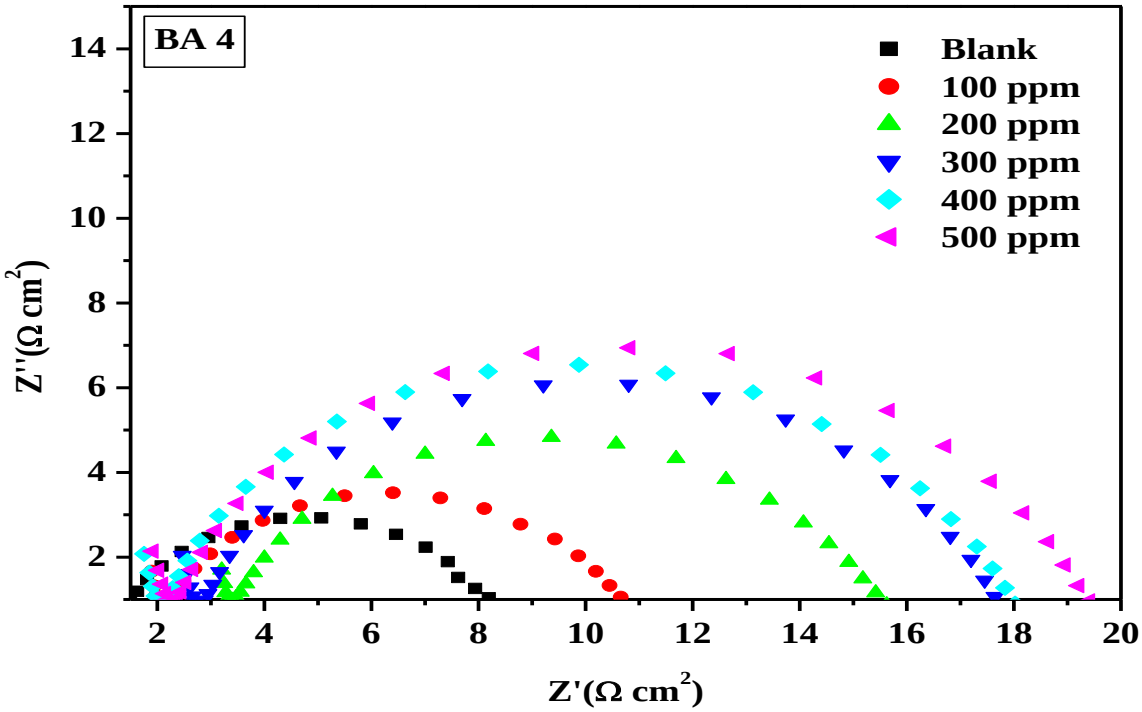
BA 4
Blank
100 ppm
200 ppm
300 ppm
400 ppm
500 ppm
Z''(Ω cm²)
Z'(Ω cm²)

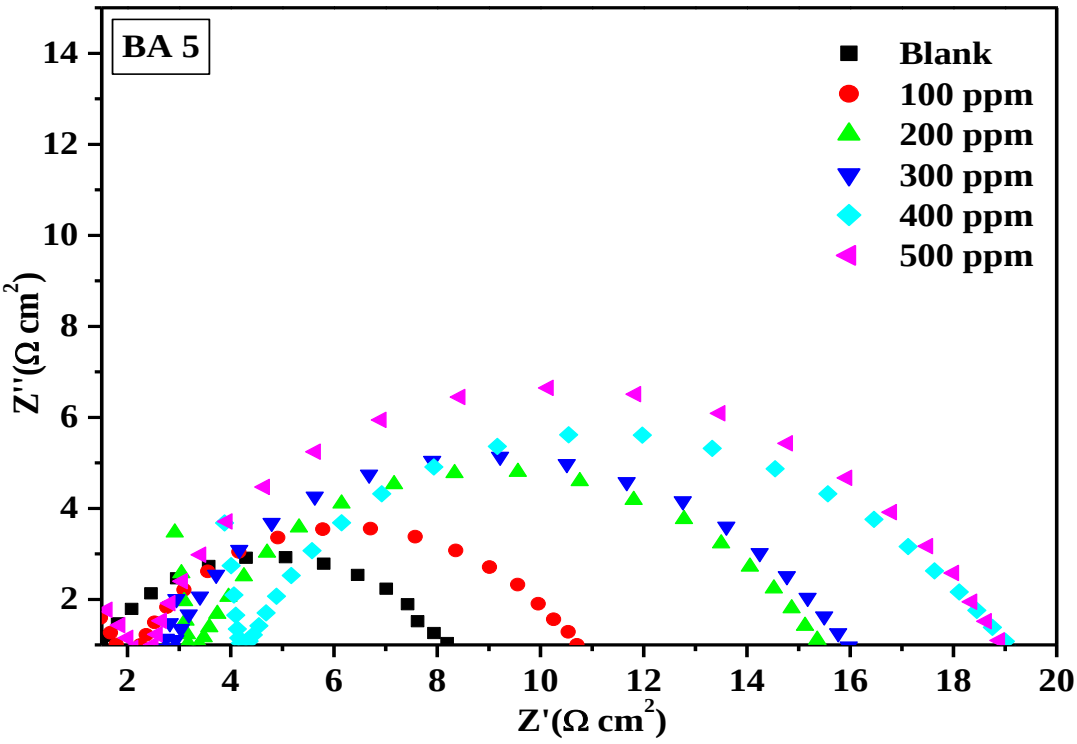

Figure 4.2 Nyquist plot of mild steel in 1 M HCl solution, comparing the corrosion behaviour with and without various concentrations of benzaldehyde inhibitors [90].

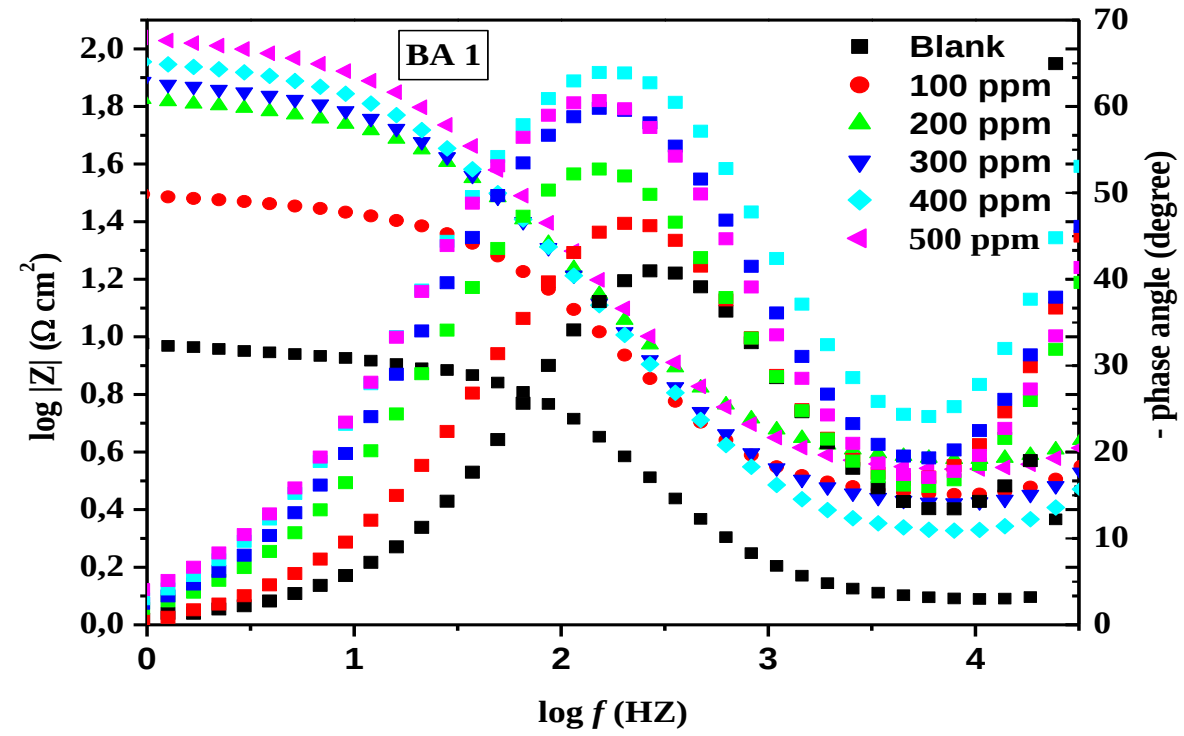
BA 1
Blank
100 ppm
200 ppm
300 ppm
400 ppm
500 ppm
log |Z| (Ω cm²)
- phase angle (degree)
log f (HZ)

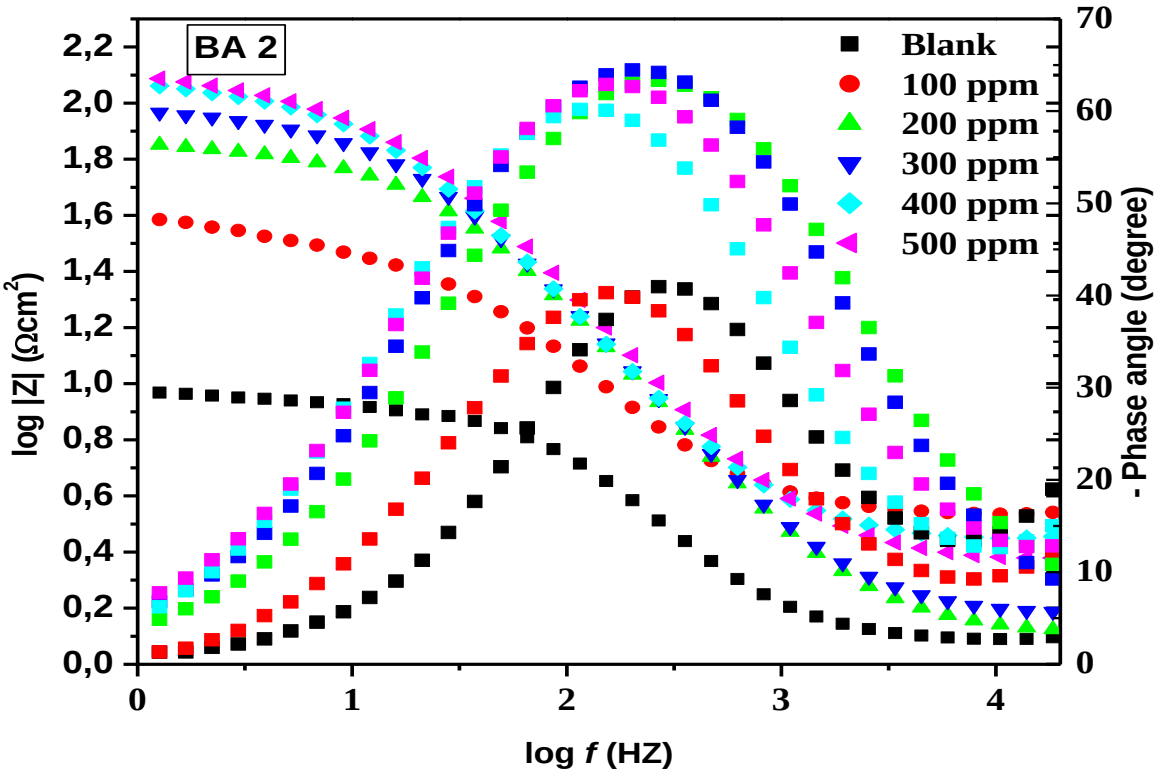
BA 2
Blank
100 ppm
200 ppm
300 ppm
400 ppm
500 ppm
log |Z| (Ωcm²)
- Phase angle (degree)
log f (HZ)

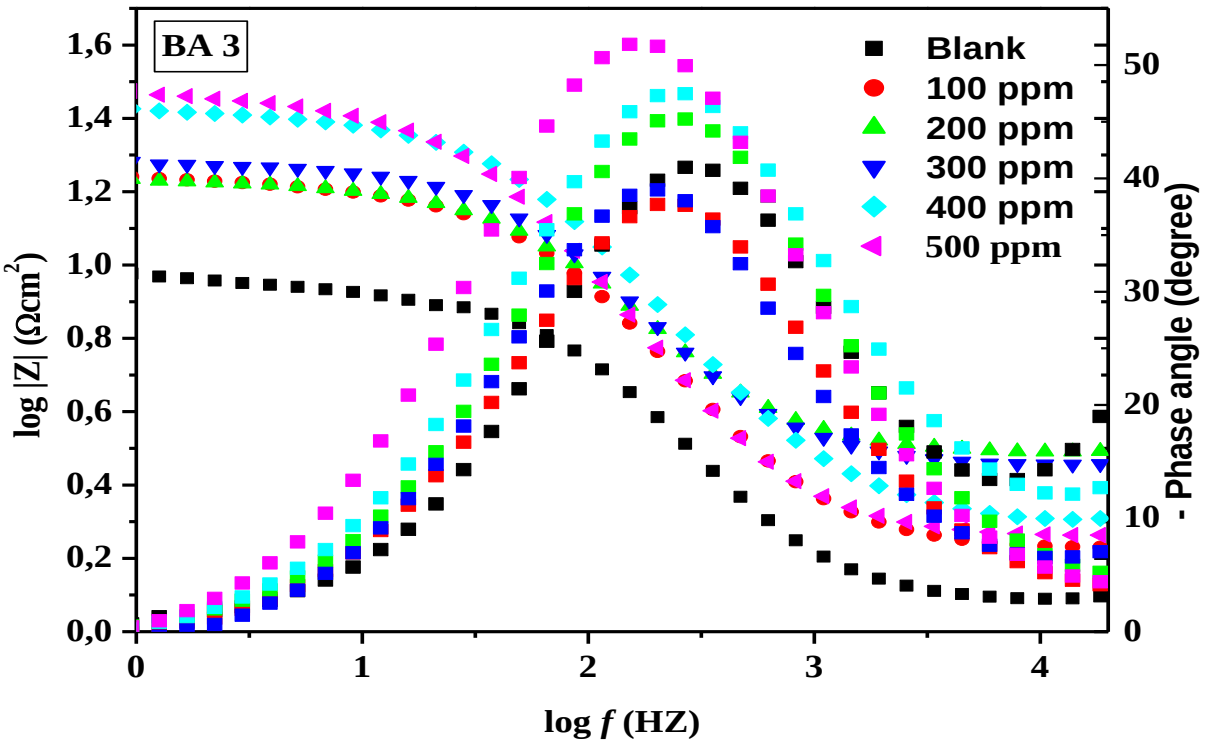
BA 3
Blank
100 ppm
200 ppm
300 ppm
400 ppm
500 ppm
log |Z| (Ωcm²)
- Phase angle (degree)
log f (HZ)

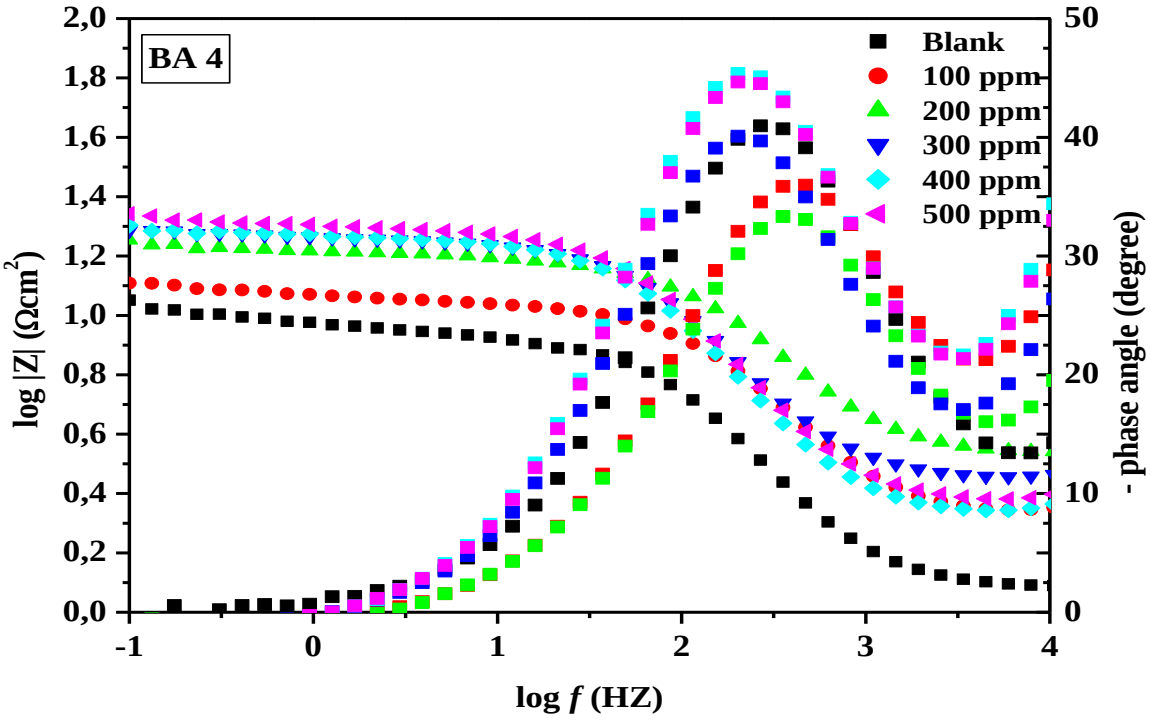
BA 4
Blank
100 ppm
200 ppm
300 ppm
400 ppm
500 ppm
log |Z| (Ωcm²)
- phase angle (degree)
log f (HZ)

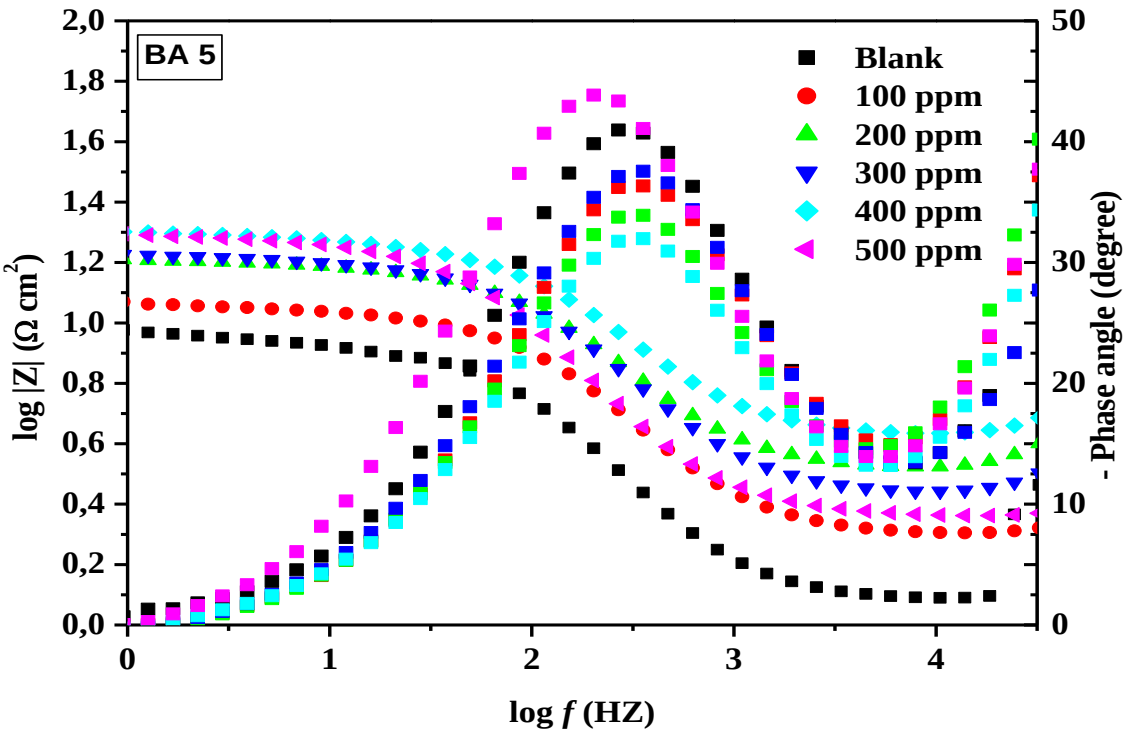

Figure 4.3 Bode plots of mild steel in 1 M HCl solution, comparing the impedance and phase angle responses with and without different concentrations of benzaldehyde inhibitors (BA 1, BA2, BA 3, BA 4, and BA 5).

Figure 4.4 displays the Nyquist plots of the impedance spectra, which were analysed using equivalent circuits. The impedance behaviour of all inhibitors was modelled using Randle's equivalent circuit, consisting of solution resistance (Rs) and charge transfer resistance (Rct) in parallel with a constant phase element (CPE). The CPE accounts for the frequency-independent phase shift between the applied AC potential and its current response, and its behaviour is mathematically described by equation 4.1, which characterizes the CPE's impedance behaviour.

$$Z_{CPE} = Y_0^{-1}(i\omega)^{-n} \qquad (4.1)$$

where; Y_0 is the CPE constant, ω is the angular frequency (in $rads^{-1}$), i^2= -1 is the imaginary number, and n is a CPE exponent that can gauge the surface's heterogeneity or roughness. Depending on the value of n, CPE can represent resistance (n= 0, Y_0 = R), capacitance (n= 1, Y_0 = C), inductance (n = -1, Y_0 = l) or Warburg impedance (n = 0.5, Y_0 = W) [12].

Equation 4.2 below was used to calculate the values of double-layer capacitance, C_d

$$C_{dI} = (Y_0 R_{ct}^{1-n})^{1/n} \quad (4.2)$$

where, Y_0 is the CPE (constant phase element), R_{ct} the charger-transfer resistance and n are CPE exponents that can be used to gauge the surface's heterogeneity or roughness [89].

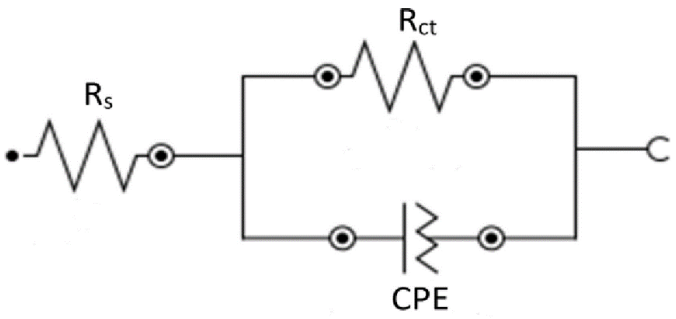

Figure 4.4 The equivalent circuit used for the fitting and simulation of impedance spectra [90].

The impedance data in Table 4.2, obtained by fitting the Nyquist plots in Fig. 4.4, reveals that as the inhibitor concentration increases, the charge transfer resistance (R_{ct}) of the inhibited system also increases. This suggests that the inhibitors bind to the mild steel surface, preventing direct contact with the corrosive acid medium and thereby hindering the oxidation process. The double-layer capacitance and corrosion inhibition efficiency were calculated using equations 4.2 and 3.4, respectively. The trend of all the inhibitor's maximum concentration (500 ppm) protection efficiencies ($\%IE_{EIS}$) agrees with the order determined for polarization studies, their inhibition

efficiency ranking, from the highest to lowest, is as follows: BA 2 > BA 1 > BA 3 > BA 4 >BA 5. From the order we discern that the inhibitors bearing nitrogen atoms tend to be effective for corrosion inhibition. The reduced inhibition efficiency of BA 4 and BA 5 can be attributed to the presence of fluorine, which alters the molecule's electronic properties [91]. Fluorine's electron-withdrawing nature hinders the molecule's ability to form a protective layer on metal surfaces, leading to decreased corrosion protection. The protection efficiencies for EIS were calculated using equation 3.4. These results agreed favourably with other studies reported on mild steel corrosion inhibition in 1 M HCl [92]. Additionally, the data demonstrate that benzaldehyde inhibitors have higher solution resistance (Rs) values than the blank. This correlates with the expected lower conductivity of the solution in the presence of organic compounds [93]. The CPE was the next notable trend, The CPE constant (Q) values of the uninhibited system were substantially higher than those of the inhibited systems, indicating that there might be a formation of a protective film or cover on the mild steel surface by the benzaldehyde inhibitors. The film protected the surface area of the mild steel from ions that could lead to its eventual corrosion. In contrast, the inhibited systems except for BA 5 exhibited n = 1 CPE value indicating that the CPE becomes equivalent to an ideal capacitor [94]. BA 5 inhibitor has a lower CPE value as compared to the blank. The decreased CPE exponent (n) on BA 5 inhibitor suggests adsorption on the mild steel surface, resulting from the increased inhomogeneity of the mild steel electrode surface in the inhibited systems [95]. The double-layer capacitance values for the metal/solution interfaces were lower in the inhibited electrolyte compared to the blank. However, there were exceptions for BA 4 at 500 ppm and BA 5 at 100, 200, 400, and 500 ppm, this might be due to an increase in the dielectric constant, which suggests that the passive film may have absorbed additional water molecules during the corrosion reactions, leading to an increase in the dielectric constant and a

higher C_{dl} value [96]. The decrease in C_{dl} values in the inhibited system can be explained by either a reduction in the dielectric constant of the medium or a decrease in the available surface area of the electrode exposed to corrosive ions, combined with an increase in the thickness of the protective film formed by the inhibitor [97].

Table 4.2 EIS parameters and percentage inhibition efficiency for mild steel corrosion in 1 M HCl solution with different concentrations of BA 1, BA 2, BA 3, BA 4, and BA 5 inhibitors.

Inhibitor Concentration (ppm)	**Rs (Ωcm^{-2})**	**Q,Yo ($\Omega^{-1}S^{n}cm^{-1}\mu$)**	**N**	**R_{ct} (Ωcm^{-2})**	**C_{dl} $\mu F \cdot cm^{-1}$**	**$\%IE_{EIS}$ (%)**
Blank						-
0	1.01±0.05	844±3.19	0.76±0.12	8.59±0.06	13976.41±23.25	-
BA 1						
100	2.40±0.49	449±3.01	0.78±0.05	29.4±1.01	6523.27±2.01	70.8±1.10
200	3.33±0.26	272±2.04	0.82±0.03	65.0±0.05	2327.79±1.11	86.8±1.80
300	2.29±1.18	233±2.80	0.85±0.07	75.9±0.08	1308.98±0.89	88.7±2.00
400	1.74±0.09	224±1.00	0.85±0.12	90.7±0.06	1289.61±0.78	90.5±0.25
500	3.07±0.55	188±3.18	0.85±0.05	109±0.10	1083.99±0.65	92.1±1.00
BA 2						
100	3.26±0.13	320±0.05	0.85±0.02	38.3±2.21	1685.09±1.05	77.6±0.45
200	1.29±0.30	205±0.90	0.86±0.04	71.6±3.15	977.35±0.02	88.0±0.50
300	1.50±0.08	199±2.01	0.86±0.09	95.4±0.79	989.32±1.04	90.1±1.00
400	2.72±0.33	212±0.73	0.85±0.07	119±0.87	1268.06±0,89	92.8±2.00
500	2.30±0.17	199±0.55	0.84±0.04	128±0.39	1374.37±0.65	93.3±0.87

BA 3						
100	1.88±0.69	817±3.01	0.79±0.02	13.3±0.93	9662.79±2.14	35.4±0.82
200	1.72±1.12	395±2.44	0.86±0.04	15.6±0.07	1635.04±2.18	45.0±1.01
300	2.88±0.58	376±3.11	0.86±0.06	16.2±1.72	1553.47±3.07	47.0±0.65
400	1.99±1.05	350±0.97	0.83±0.09	24.7±1.01	2240.75±0.69	65.2±0.43
500	1.88±0.65	341±1.09	0.88±0.05	27.5±0.89	1186.87±1.07	68.8±2.48
BA 4						
100	1.12±2.01	606±0.43	0.85±0.10	12.4±1.08	2927.21±0.25	30.7±0.70
200	2.61±0.75	787±0.65	0.84±0.03	14.5±2.01	4664.47±3.11	40.8±1.63
300	1.90±0.08	558±0.77	0.79±0.07	17.6±0.97	6424.48±0.78	51.2±1.42
400	1.38±0.85	993±1.00	0.85±0.03	18.3±1.55	5605.42±1.04	53.1±0.03
500	1.46±2.09	443±0.55	0.68±0.01	20.0±0.99	31916.81±0.63	57.1±0.25
BA 5						
100	1.37±0.48	432±3.58	0.57±0.02	11.4±1.08	4056.53±0.82	24.6±0.72
200	2.74±0.57	678±3.05	0.72±0.07	13.9±2.18	23810.54±2.58	38.2±1.90
300	2.54±0.35	408±2.17	0.80±0.02	14.4±2.78	3572.04±3.01	40.3±2.01
400	3.65±0.15	558±0.87	0.72±0.08	16.8±3.47	19555.95±0.47	48.9±1.05
500	3.65±0.50	558±1.04	0.70±0.05	19.2±3.98	29767.98±0.36	55,3±0.28

4.2 Langmuir adsorption isotherm and thermodynamic parameters

Adsorption isotherms offer valuable insights into the mechanism of metal surface protection by inhibitor molecules [98]. Analysis of the experimental data revealed that the Langmuir adsorption isotherm best described the adsorption behaviour of benzaldehydes on mild steel in 1 M HCl,

indicating that the Langmuir model accurately captures the underlying adsorption processes. This finding provides a deeper understanding of how benzaldehydes interact with the metal surface, shedding light on the fundamental mechanisms of corrosion inhibition and highlighting the importance of the Langmuir model in elucidating these processes.

Equation 4.3 provides the Langmuir adsorption isotherm.

$$\theta = \frac{K_{ads} C_{inh}}{1+K_{ads} C_{inh}} \quad (4.3)$$

where θ is the surface coverage, C_{inh} is the inhibitory concentration, a is the molecular interaction parameter, and K_{ads} is the equilibrium constant.

The equation can be rewritten as equation 4.4.

$$\frac{C}{\theta} = C + \frac{1}{K_{ads}} \quad (4.4)$$

The near-unity values of (R^2) for the Langmuir adsorption isotherm indicate an excellent fit of the experimental data, thereby validating the use of this model to describe the adsorption behaviour of the investigated inhibitors.

We can determine whether the metal-inhibitor interaction is physical or chemical by looking at the Gibbs free energy (ΔG^{O}_{ads}). A physical adsorption process is suggested by values of -20 kJ mol^{-1} or less negative, and a chemical adsorption process is suggested by values of -40 kJ mol^{-1} or larger [99]. The following formula was used to get the Gibbs free energy of each benzaldehyde corrosion inhibitor, as shown in equation 4.5.

$$\Delta G^{O}_{ads} = - RT \ In \ (55.5 K_{ads}) \quad (4.5)$$

where T is the absolute temperature, R is the universal gas constant, and 55.5 is the water concentration (mol/dm^3) in the bulk solution. The electrochemical impedance spectroscopy plots of Langmuir isotherms for mild steel at 1 M in the presence of benzaldehyde inhibitors are displayed in Figure 4.5.

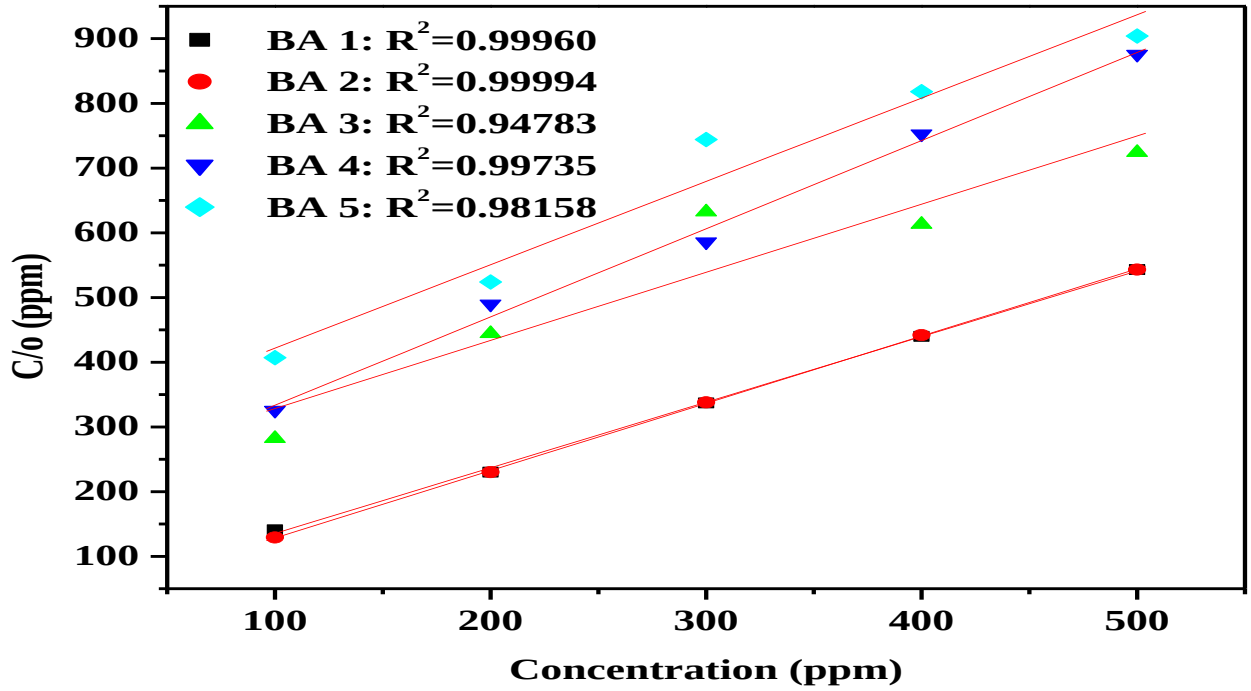

Figure 4.5 Langmuir adsorption isotherm plots for BA 1, BA 2, BA 3, BA 4, and BA 5, constructed using EIS experimental data.

According to Table 4.3, the ΔG_{ads} values fall within the range of -22.56 to -28.98 KJ mol^{-1}, indicating that the adsorption of the benzaldehyde inhibitors onto the mild steel surface is classified as physisorption [100]. This suggests that the film has an electrostatic character, meaning that the inhibitors are attracted to the metal surface through weak electrostatic forces, rather than forming strong chemical bonds [101].

Table 4.3 Adsorption and interaction for the adsorption molecules on the mild steel surface in 1 M HCl medium.

Inhibitor Molecule	$\mathbf{K_{ads}}$ ($\mathbf{dm^3 mol^{-1}}$)	$\mathbf{\Delta G^{\circ}_{ads}}$ (KJ $\mathbf{mol^{-1}}$)
BA 1	3856.76	-27.87
BA 2	6296.67	-28.98
BA 3	884.04	-24.53
BA 4	1227.17	-25.27
BA 5	423.58	-22.56

4.3 Quantum chemical studies

Density Functional Theory (DFT) calculations have corroborated the experimental findings, confirming the efficacy of the inhibitors across various experimental methods. A range of DFT-based parameters were calculated to elucidate the adsorption behaviour of these compounds on the metal surface, including frontier molecular orbital energies (E_{HOMO}, E_{LUMO}), energy band gap (ΔE), electronegativity (χ), hardness, softness (n), dipole moment (μ), and others. A strong correlation was established between the experimental results and DFT study, providing a comprehensive understanding of the adsorption mechanisms and validating the experimental observations. Figure 4.6 displays the optimised molecular structures and the spatial distributions of the highest occupied molecular orbital (HOMO) and lowest unoccupied molecular orbital (LUMO) densities. The optimised geometric structures of the compounds played a crucial role in their corrosion inhibition properties. Planar geometry was found to be a key factor in effective corrosion inhibition, as it

enables inhibitor molecules to cover a larger surface area of the mild steel surface. This is because planar molecules can present most of their atoms to interact with the metal surface, enhancing their corrosion inhibition performance. Benzaldehyde inhibitors under investigation possess a planar shape, which makes them well-suited for corrosion inhibition. A detailed examination of their quantum chemical parameters further revealed their corrosion inhibition capabilities, highlighting the importance of geometric structure in determining their effectiveness.

BA 1

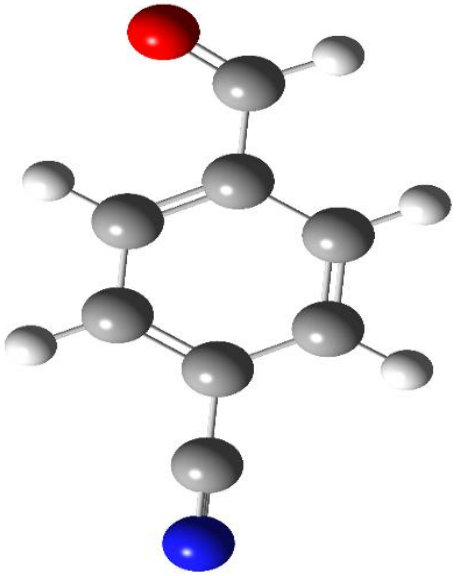

BA 2

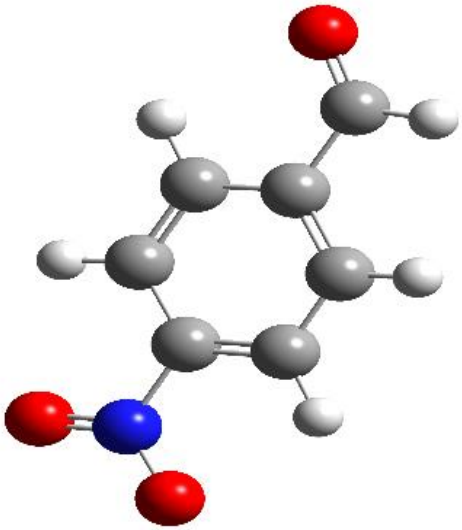

BA 3

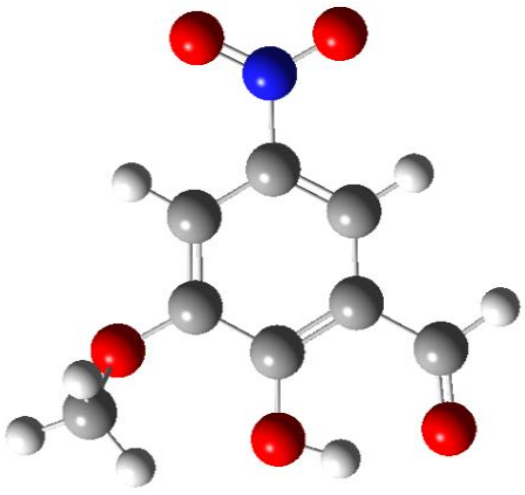

BA 4

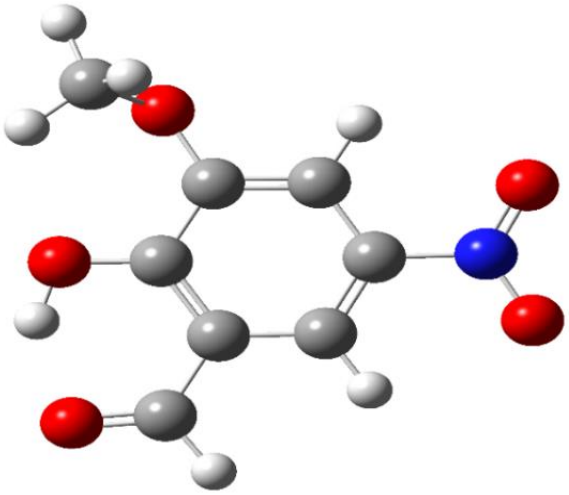

BA 5

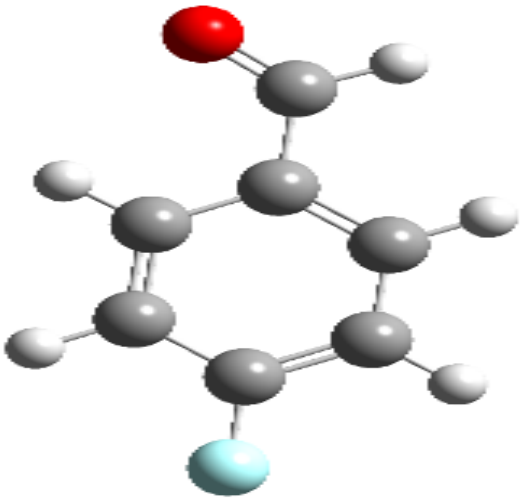

Figure 4.6 Optimised structures of studied molecules: Carbon (grey); Hydrogen (white); Nitrogen (blue); Chlorine (green); Oxygen (Red).

Figure 4.7 displays the electron density distributions of the highest occupied molecular orbital (HOMO) and the lowest unoccupied molecular orbital (LUMO) for the optimised structures of the benzaldehyde inhibitors. The HOMO orbitals of these compounds exhibit widespread electron density delocalization across their molecular frameworks, indicating their susceptibility to electrophilic attack by metal cations. This delocalisation enables the inhibitors' aromatic structures to engage in donor-acceptor interactions with the vacant d-orbitals of Fe (mild steel), facilitating electron donation and promoting strong interactions between the inhibitors and the metal surface. The LUMO diagrams of the inhibitors as shown in figure 4.,7 show a high capacity for accepting electrons from the metal in back-donation interactions, contributing to their effective inhibition efficiency.

HOMO

BA 1

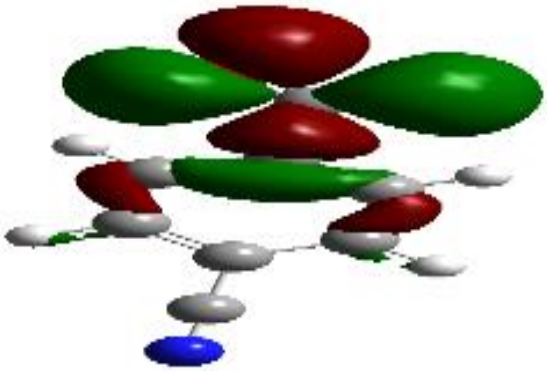

BA 2

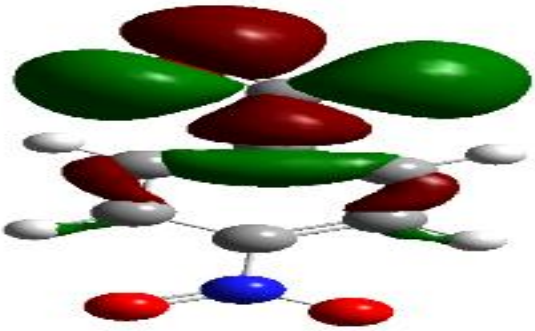

BA 3

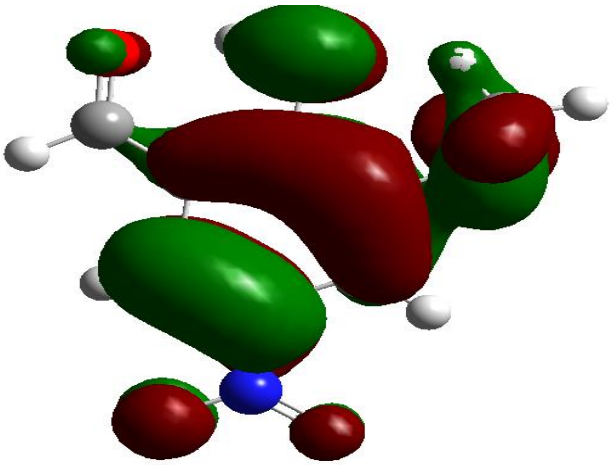

BA 4

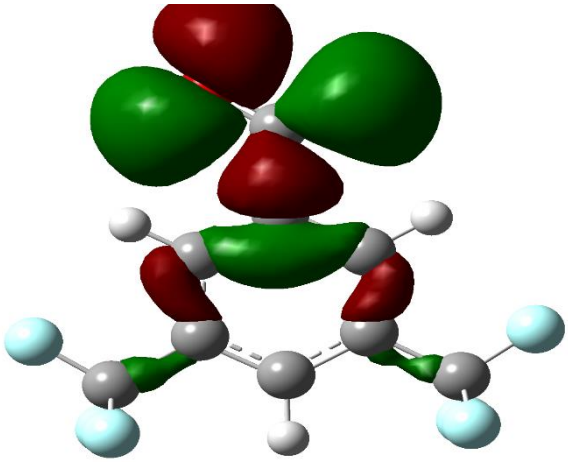

BA 5

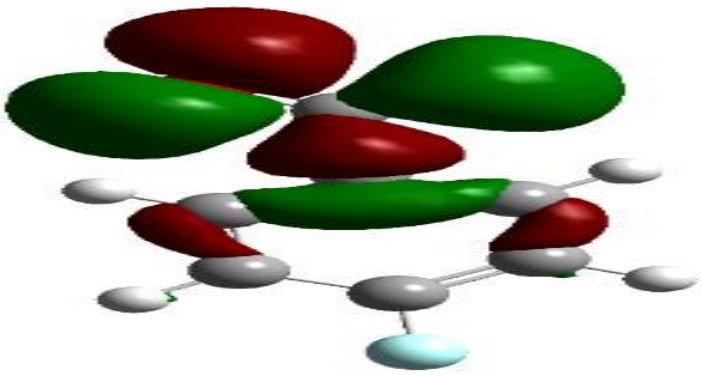

LUMO

BA 1

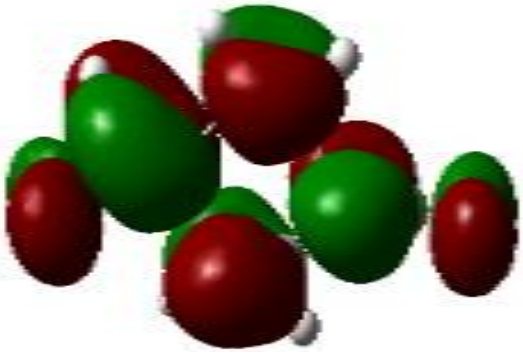

BA 2

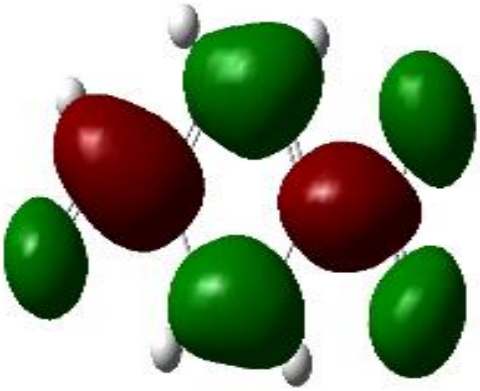

BA 3

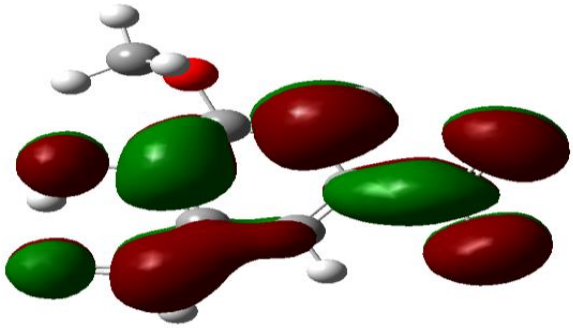

BA 4

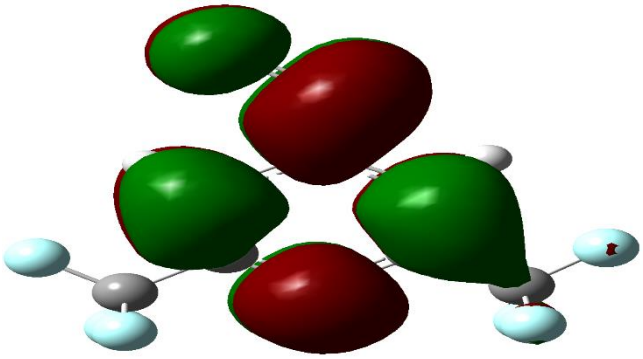

BA 5

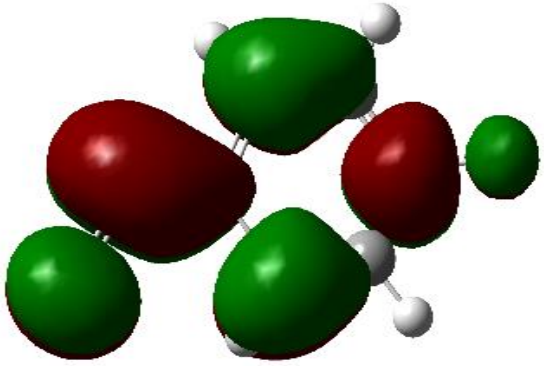

Figure 4.7 Electron density isosurfaces of the (HOMO) and (LUMO) orbitals for the studied benzaldehyde inhibitors.

Table 4.4 shows quantum chemical parameters of benzaldehyde inhibitors. The frontier molecular orbital energies are associated with a molecule's donor/acceptor ability. The ability of a molecule to absorb electrons is known as the LUMO energy (E_{LUMO}), whereas the ability to give electrons is known as the HOMO energy (E_{HOMO}), thus a molecule with high HOMO energy is mostly predicted to have better ability to donate electrons, whereas a molecule with low LUMO energy (E_{LUMO}) is predicted to have better ability to receive charges [102]. The decreasing E_{HOMO} order is BA 3 > BA 5 > BA 1 > BA 2 > BA 4. This trend does not correlate with the electrochemical studies. The presence of the electron-donating methoxy ($-OCH_3$) and hydroxy (O-H) groups in BA 3 may be the reason for its highest electron-donating ability. Through resonance effects, these groups can stabilise the benzene ring by donating. In doing so, these electrons can easily interact with the metal surface, forming a protective layer that prevents corrosion [103]. The increasing order of E_{LUMO} is BA 5 > BA 4 > BA 1 BA 3 > BA 2. From this trend it can be observed that BA 2 has a low E_{LUMO}. The ability of BA 2 to accept electrons from the metal could be due to nitro group ($-NO_2$) present in a molecule. The nitro group is a strong electron-withdrawing group which makes the benzene ring and aldehyde group more polar and electron-deficient [104]. The trend also shows that BA 5 is less prone to accepting electrons from the metal during back donation compared to the rest of the studied inhibitors, this could be the result of a molecule having a fluorine which is a high electronegativity atom. The E_{LUMO} trend is supported by both the Tafel polarization and electrochemical impedance spectroscopy. The energy gap (ΔE) was computed using equation 3.5, according to the frontier orbital theory the inhibitor's adsorption to metal is governed by the energy difference between the HOMO and LUMO. The molecules with small

values of the energy gap are expected to be more reactive than the ones with larger energy gap values. The decreasing trend of energy gap is BA 4 > BA 5 > BA 1 > BA 2 > BA 3. This trend shows that BA 3, BA 2, and BA 1 inhibitors have high reactivity and inhibition ability compared to BA 4 and BA 5 inhibitors, this order confirms that the molecules bearing nitrogen groups tend to be effective as corrosion inhibitors. In addition to the HOMO, LUMO and their energies, a useful parameter for examining corrosion performance is the dipole moment (μ), where a larger positive value is considered for good corrosion performance [105]. The values of μ in the table correspond to the trend of BA 3 > BA 2 > BA 1 > BA 5 > BA 4. This order tallies well with experimental inhibition efficiencies. BA 3 and BA 2 have the highest dipole moment suggesting that these inhibitors might have dipole-dipole interactions with the metal by being more effectively adsorbed on the surface of the metal than the other inhibitors [106]. Additional quantum chemical characteristics used to investigate an inhibitor's corrosion performance include global hardness (n) and electronegativity (χ). Equations 3.6 and 3.8 are utilized to ascertain these parameters, respectively. Molecules that are softer (lower n) are thought to be significantly more reactive than those that are harder [107]. It was established that the decreasing order of global hardness is BA 4 > BA 5 > BA 1 > BA 2 > BA 3, which demonstrated that BA 4 was the hardest compound. The highest value of global hardness on BA 4 could be due to the weight of the molecule (242.12g/mol). Given the high value of electronegativity, it is possible that the molecule may not quickly release its electrons to a species that will receive them. The decreasing order of electronegativity was determined to be BA 2 > BA 1 > BA 4 > BA 3 > BA 5. From the trend BA 2 showed the highest electronegativity, as expected due to the presence of the nitro group ($-NO_2$).

Table 4.4 Quantum chemical parameters for the studied benzaldehyde inhibitors.

Inhibitors molecules	E_{HOMO} (eV)	E_{LUMO} (eV)	ΔE (eV)	μ	η (eV)	χ (eV)
BA 1	-7.83	-3.02	4.81	2.48	2.41	5.43
BA 2	-7.94	-3.57	4.37	2.71	2.19	5.76
BA 3	-7.28	-3.07	4.21	3.29	2.11	5.16
BA 4	-8.06	-2.36	5.71	2.26	2.85	5.21
BA 5	-7.46	-2.23	5.23	2.35	2.62	4.85

4.4 Spectroscopic studies

4.4.1 Fourier transform infrared (FTIR)

Figure 4.7 displays the FTIR spectra of the pure benzaldehyde inhibitors and the adsorbed film of the inhibitors on the mild steel surface after 7 days of exposure to 500 ppm benzaldehyde in 1 M HCl, providing insight into the interaction between the inhibitors and the steel surface through the analysis of the functional groups and adsorption mechanisms. The FTIR spectra of the pure inhibitors exhibit distinctive aromatic C-C stretching vibrations around 1500 cm^{-1}, and a prominent absorption band between 1730 and 1680 cm^{-1}, which is attributed to the stretching vibrations of the carbonyl C=O bond [108]. The C-H vibration bands are observed at 3000 cm^{-1} [109]. In the pure spectra of BA 1 the absorption band around 2200 and 2250 cm^{-1} could be attributed to the (-C≡ N) nitrile group [110], while for BA 2 and BA 3 the strong peak observed at about 1350 and 1550 cm^{-1} is believed to be the (C=N) nitro group [111]. For BA 3, the stretching frequency of (O-H) group which is around 3300 cm^{-1} can be observed [112]. From BA 4 and BA 5 the (C-F) stretching vibration can be observed around 1000 and 1200 cm^{-1}. Through careful observation of all the compounds, it can be noted that in the spectra of the adsorbed film, bands from 500 to about

1500 cm^{-1} disappear as compared with the spectra of pure compounds. Since the C-C, C≡ N, and C=N visible vibration bands are around the region of 500 to 1600 cm^{-1}, it can be assumed that the metal interacted with the benzaldehyde inhibitors through the three functional groups. The hydroxyl group was identified as the broad and large peak seen in the adsorbed film spectra between 3500 and 3100 cm^{-1}, which is recorded for all inhibitors in the investigation. The absence of this peak in the pure spectra of the inhibitors indicates that the inhibitor mild steel complex underwent the formation of new bonds [113].

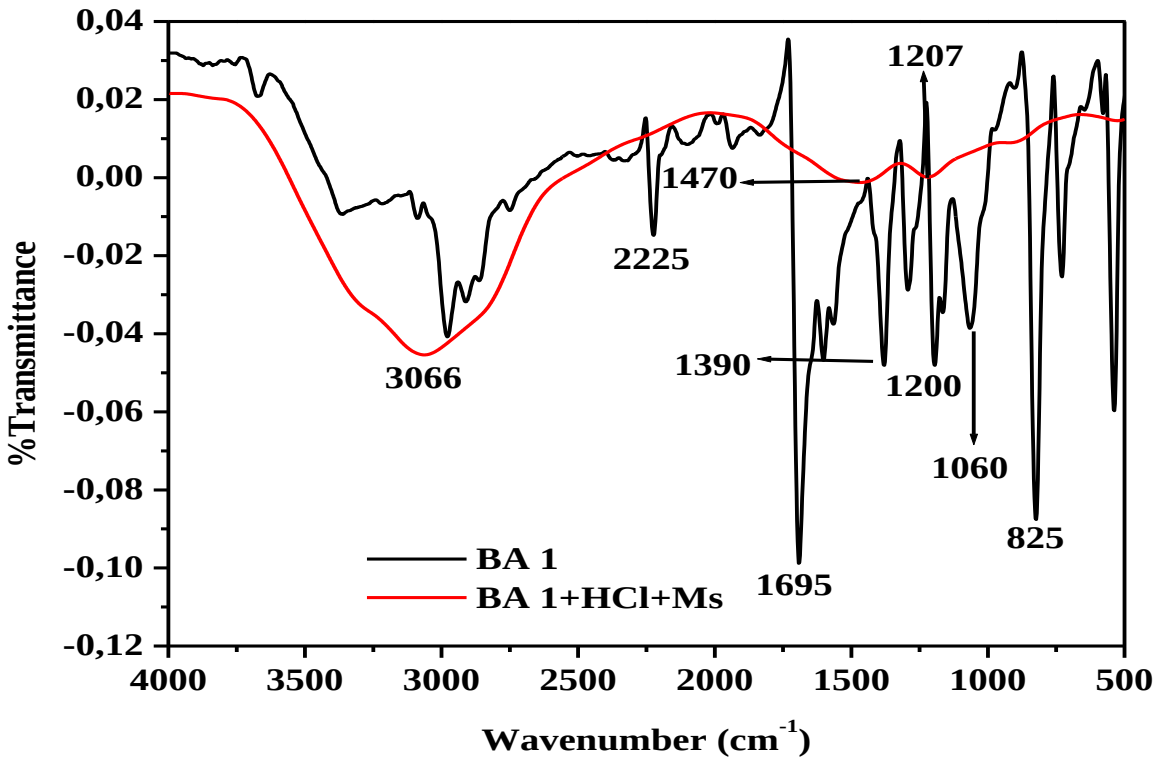

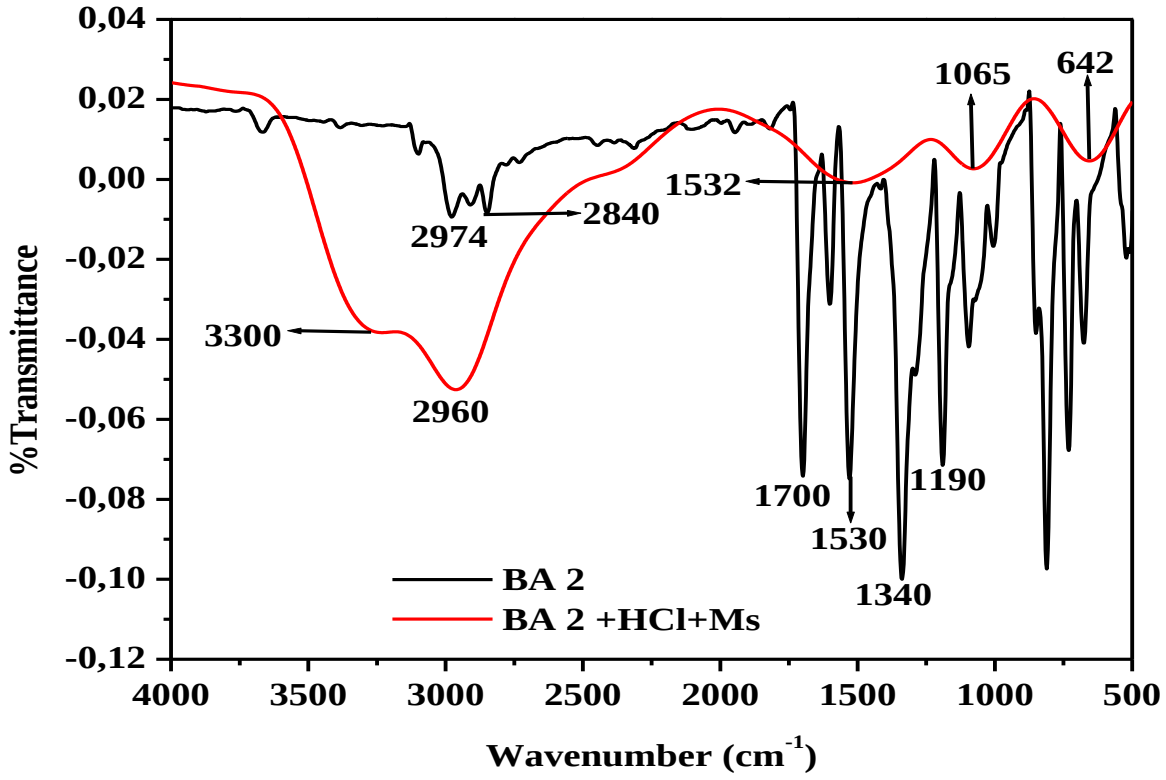
0,04
0,02
0,00
-0,02
-0,04
-0,06
-0,08
-0,10
-0,12
%Transmittance
4000
3500
3000
2500
2000
1500
1000
500
Wavenumber (cm-1)
3300
2960
2974
2840
1532
1065
642
1700
1530
1340
1190
BA 2
BA 2 +HCl+Ms

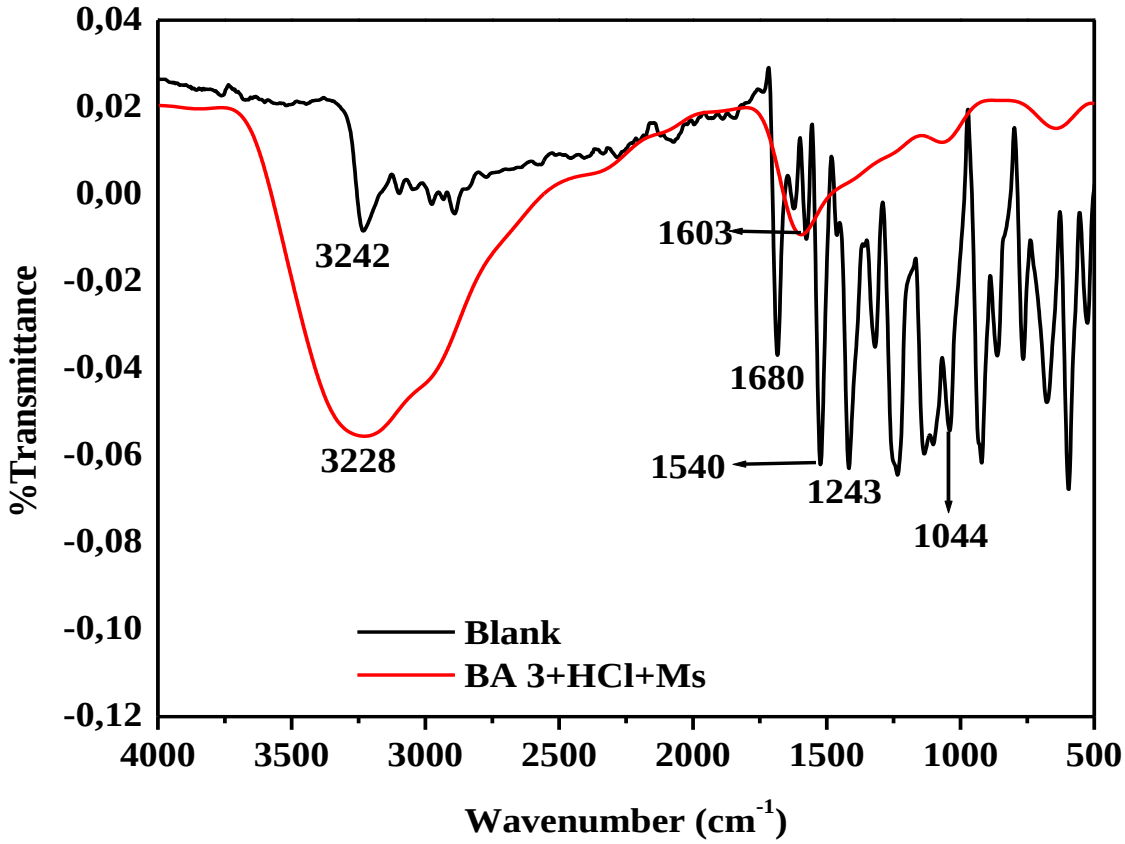
0,04
0,02
0,00
-0,02
-0,04
-0,06
-0,08
-0,10
-0,12
%Transmittance
4000
3500
3000
2500
2000
1500
1000
500
Wavenumber (cm-1)
3242
3228
1603
1680
1540
1243
1044
Blank
BA 3+HCl+Ms

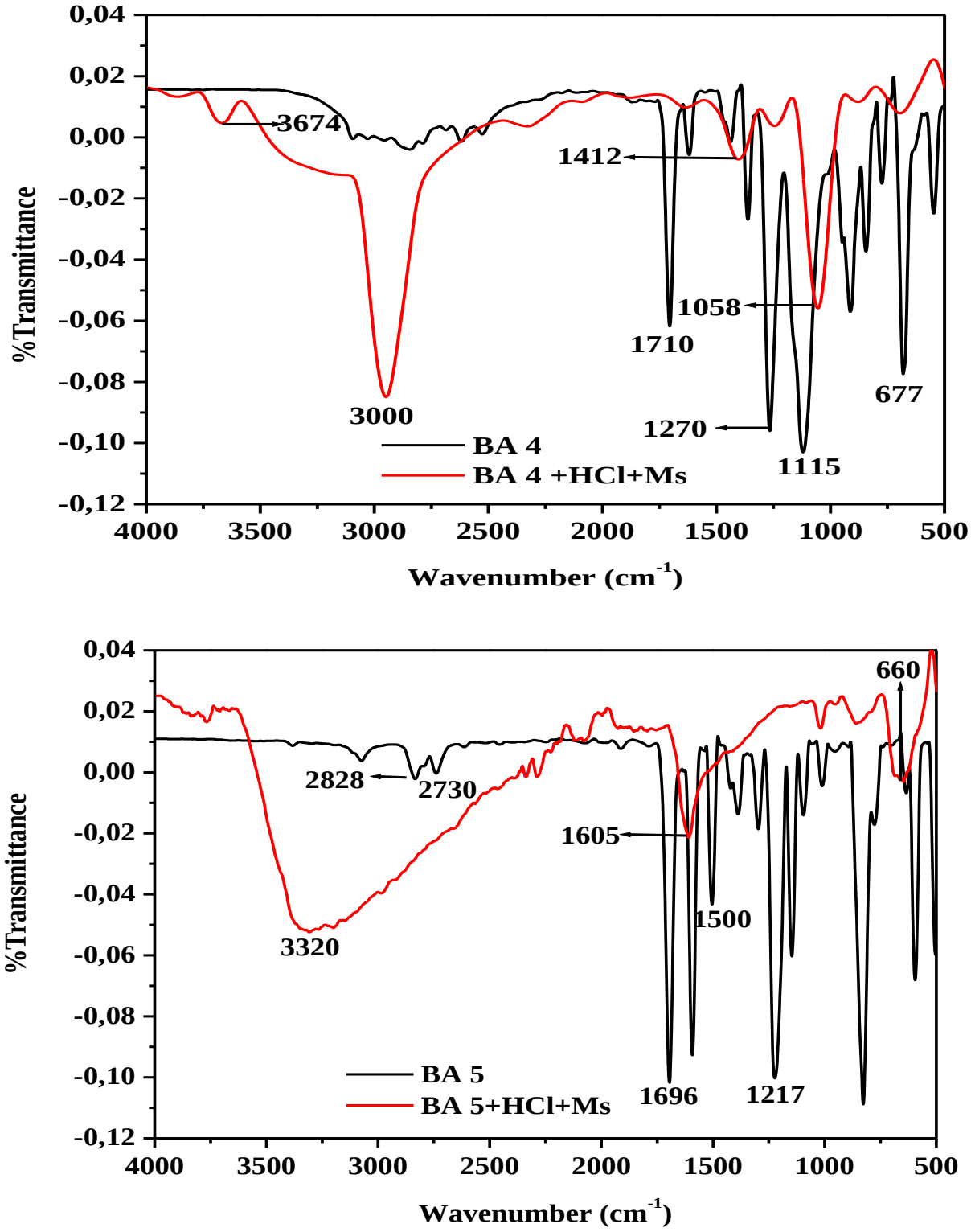

Figure 4.8 FTIR spectra of the pure inhibitor molecules, and the adsorbed film formed on the mild steel surface after 7 days of exposure to the inhibitor-acid solution.

4.4.2. Ultraviolet-visible (UV-Vis) Spectroscopy

The UV-Vis absorbance spectroscopy technique measures the property of the compounds to absorb certain wavelengths of the UV-Vis spectrum and examine the complexation of iron in the acid medium with the inhibitive molecules. The UV-Vis absorption spectra of pure benzaldehyde and benzaldehyde derivatives with mild steel at an optimum concentration of inhibitor (500 ppm) after seven days' immersion of mild steel specimen is shown in Figure 4.9. Benzaldehyde derivatives exhibit absorption peaks between 200 nm and 300 nm, which can be attributed to $n \rightarrow \pi^*$ transitions [114]. For the mild steel, HCl and inhibitors solutions, the observed shift in the position and absorbance of the absorption maximum, indicates the interaction between the inhibitors and the iron in the solution. The spectrum of BA 1 after immersion of mild steel shows a red shift, with the sharp peak initially observed at 300 nm now appearing at 295 nm. The spectrum of BA 2 showed apparent blue-shift after mild steel immersion, as the broad peak that initially centred at 320 nm now appears at 300 nm and showed significance decrease in absorbance. For BA 3, before the immersion of mild steel only one peak is appearing at around 288 nm but after immersion of mild steel two absorption peaks are appearing at 288 nm and 390 nm. A change was observed for BA 4, initially a sharp peak was observed around 280 nm, after the mild steel was immersed, the peak appeared at 315 nm, shifting to the red region. The results of these experiments offer robust evidence for the formation of a complex between Fe^{2+} ions and the inhibitors in 1 M HCl solution [115]. The UV-Vis spectroscopic analysis confirms the formation of a protective layer of metal-inhibitor complex on the metal surface, indicating the creation of a barrier that prevents corrosion.

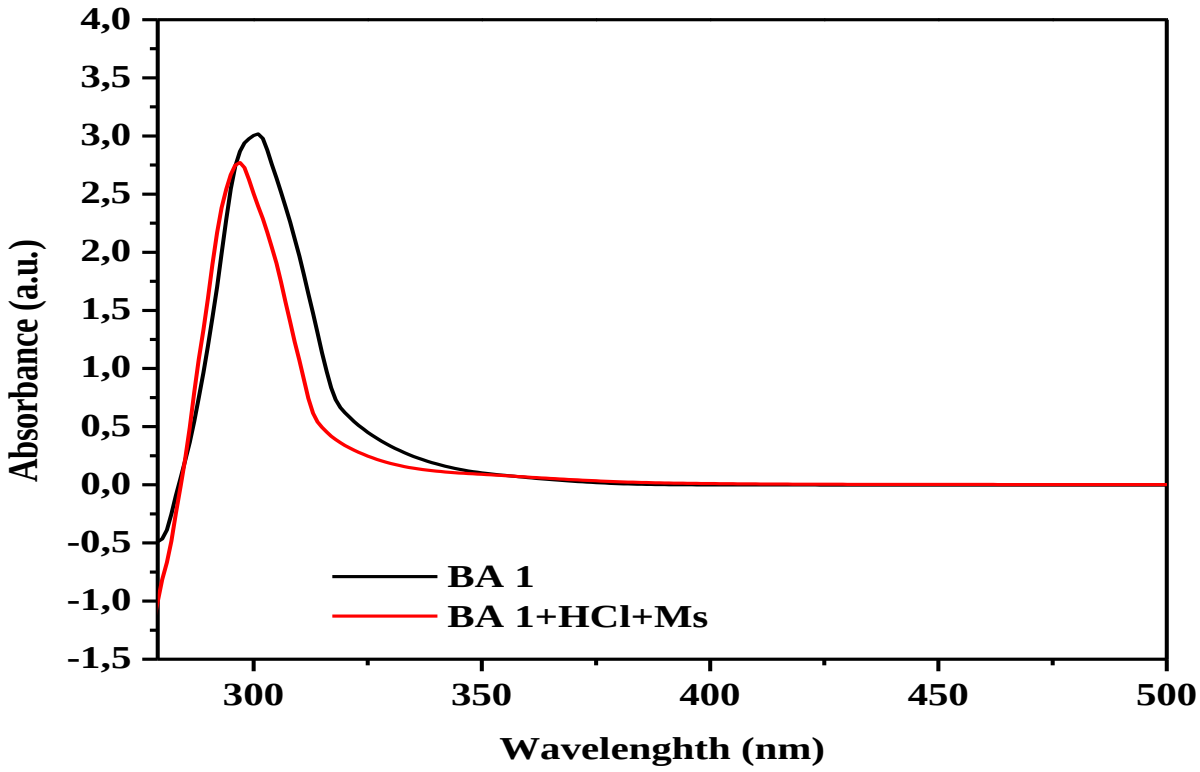
4,0
3,5
3,0
2,5
2,0
1,5
1,0
0,5
0,0
-0,5
-1,0
-1,5
Absorbance (a.u.)
300
350
400
450
500
Wavelenghth (nm)
BA 1
BA 1+HCl+Ms

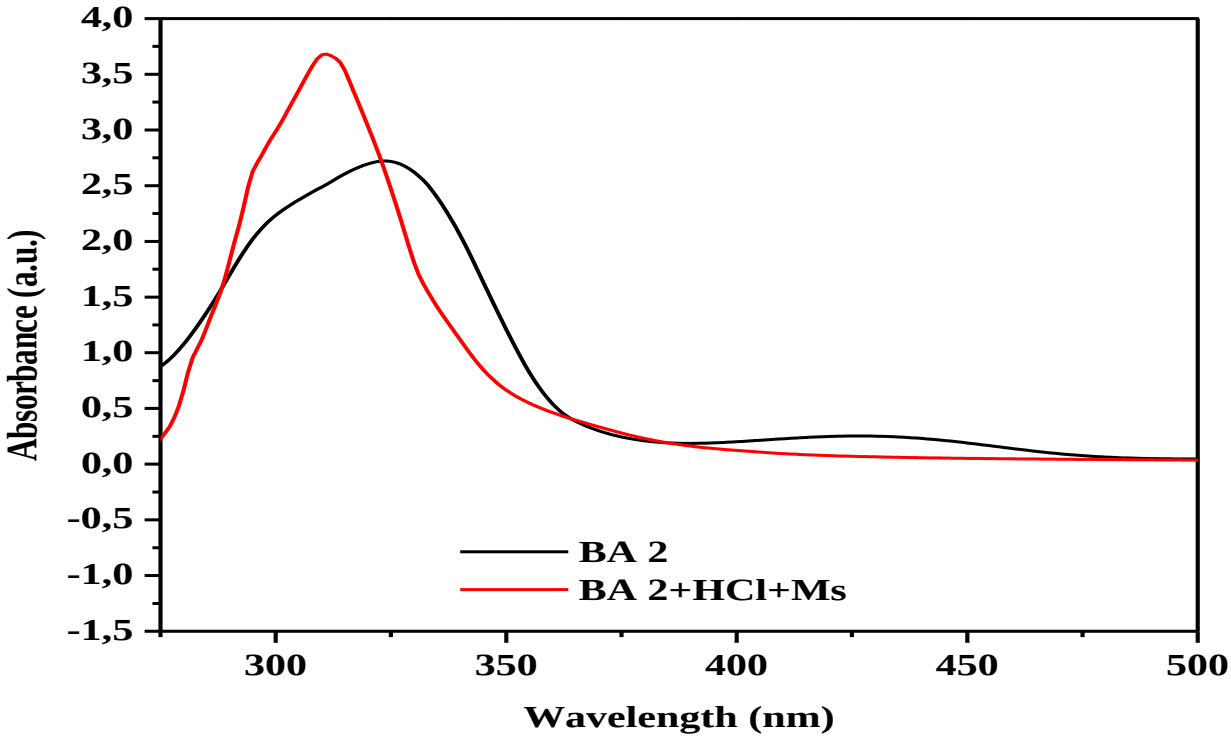
4,0
3,5
3,0
2,5
2,0
1,5
1,0
0,5
0,0
-0,5
-1,0
-1,5
Absorbance (a.u.)
300
350
400
450
500
Wavelength (nm)
BA 2
BA 2+HCl+Ms

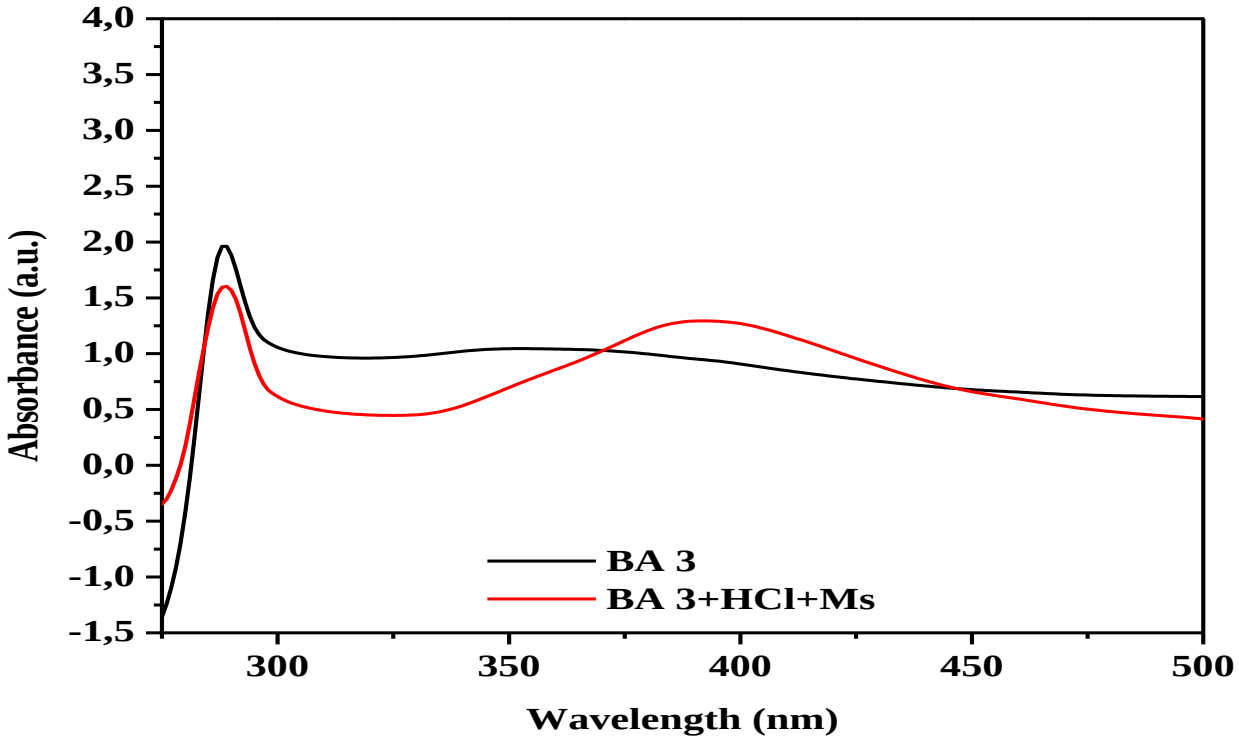
4,0
3,5
3,0
2,5
2,0
1,5
1,0
0,5
0,0
-0,5
-1,0
-1,5
Absorbance (a.u.)
300
350
400
450
500
Wavelength (nm)
BA 3
BA 3+HCl+Ms

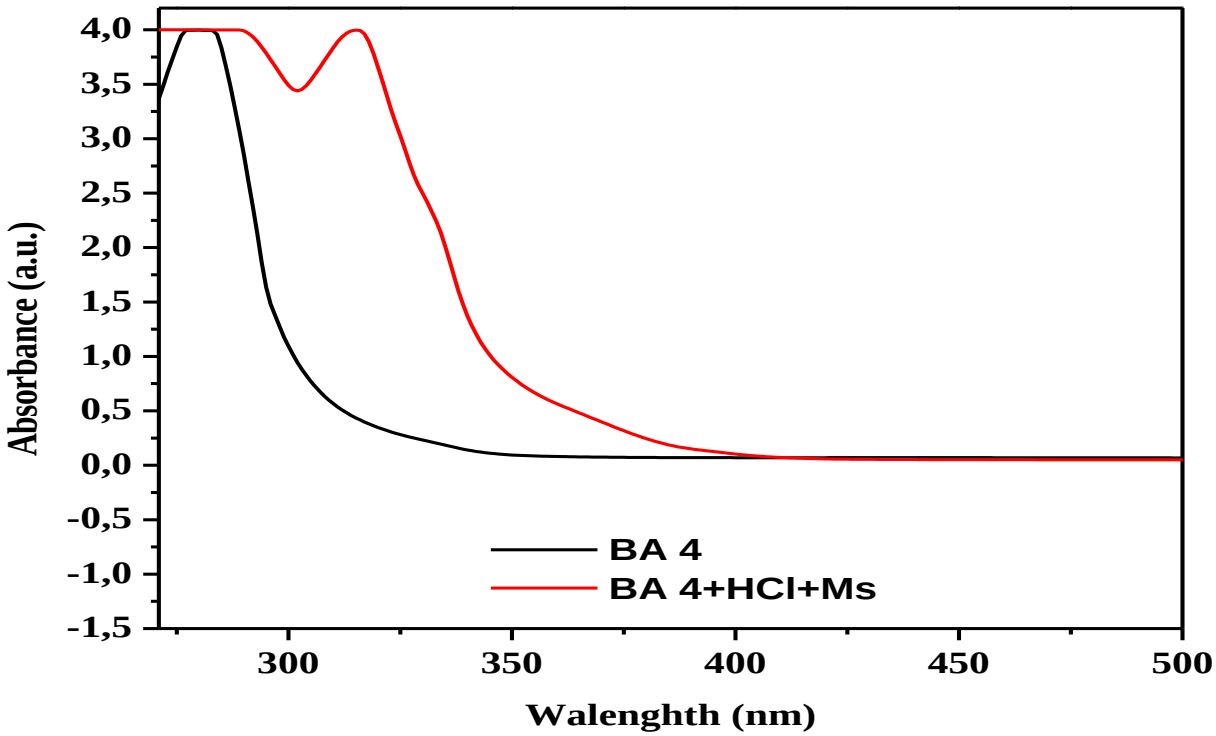
4,0
3,5
3,0
2,5
2,0
1,5
1,0
0,5
0,0
-0,5
-1,0
-1,5
Absorbance (a.u.)
300
350
400
450
500
Walenghth (nm)
BA 4
BA 4+HCl+Ms

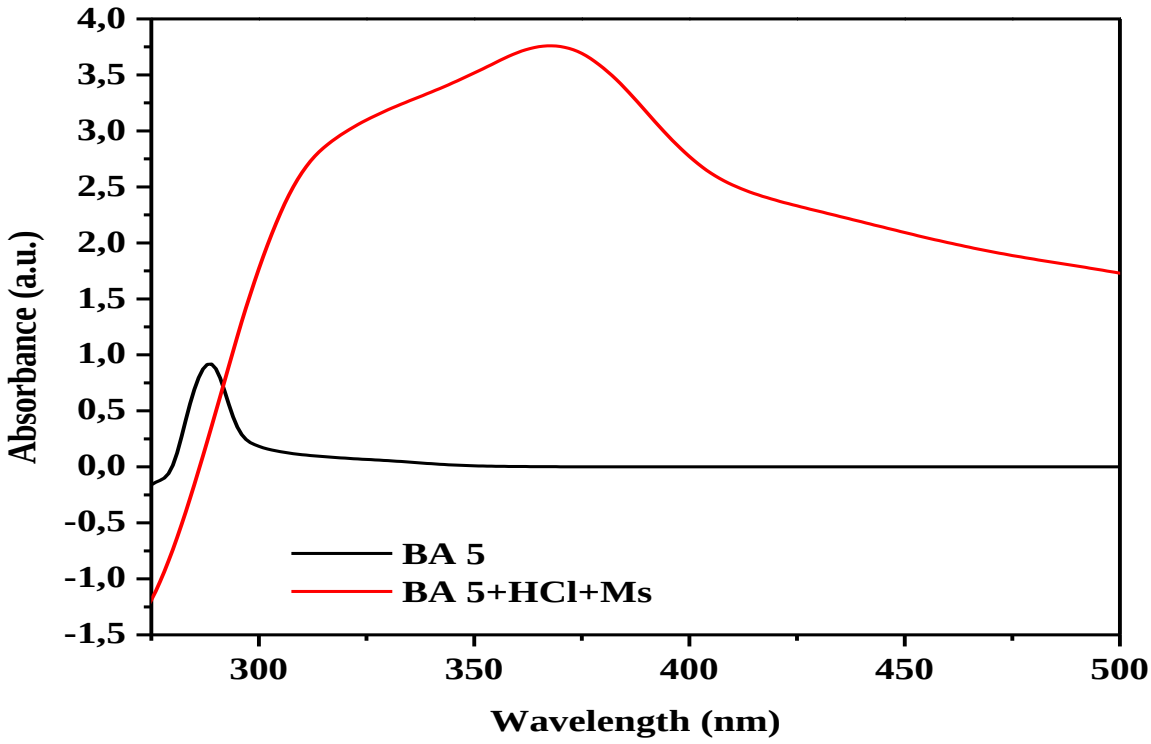

Figure 4.9 UV-Vis spectra of benzaldehyde derivative inhibitors in acidic solutions before and after exposure to mild steel.

CHAPTER 5 – CONCLUSIONS AND RECOMMENDATIONS

5.1 Conclusion

This research investigated the corrosion inhibition properties and adsorption behaviour of five benzaldehyde derivatives on mild steel in 1 M HCl solution. A comprehensive approach was employed, combining electrochemical techniques, spectroscopic methods, and quantum chemical methods to evaluate the inhibitors' performance. The study's findings and conclusions are presented below.

5.1.1Tafel analysis

All five benzaldehyde derivatives demonstrated excellent inhibition performance for mild steel in 1 M HCl, with the highest concentration 500 ppm, and the inhibition efficiency ranking of the five benzaldehyde inhibitors is as follows:

BA2 > BA1 > BA3 > BA4 > BA5.

All these inhibitors interact with the metal surface through both cathodic and anodic sites, classifying them as mixed-type inhibitors. However, it is worth noting that in some cases, the cathodic site may be more dominant, while in others, the anodic site may be more prevalent, indicating a varying degree of interaction between the inhibitors and the metal surface.

5.1.2 Electrochemical impedance spectroscopy (EIS)

The five benzaldehyde derivatives exhibited excellent performance in protecting mild steel against corrosion in 1 M HCl, with a maximum concentration of 500 ppm. Their inhibition efficiency order is as follows.

BA2 > BA1 > BA3 > BA4 > BA5.

The results of the Tafel and EIS analyses exhibited a remarkable correlation, indicating that all the benzaldehydes' derivatives demonstrated substantial solution resistance and displayed exceptional corrosion protection capabilities for mild steel. The consistent trend across both analyses reaffirms the outstanding performance of the inhibitors in mitigating corrosion. Additionally, the findings suggest that these inhibitors have great potential for practical applications in corrosion protection.

5.1.3 Adsorption isotherms

The benzaldehyde inhibitors exhibited excellent conformity to the Langmuir adsorption isotherm, with R^2 values approaching unity, indicating a strong fit. Additionally, the high K_{ads} values observed for all benzaldehyde inhibitors suggest robust interactions between the inhibitors and the mild steel surface. Furthermore, the ΔG_{ads} values, ranging from -20 to -40 kJ/mol, indicate that the inhibitors interact with the metal surface through physisorption, a strong and stable adsorption mechanism, which confirms the effectiveness of these inhibitors in protecting the metal surface from corrosion.

5.1.4 Spectroscopic Studies

Both FTIR and UV-Vis spectroscopy for all the studied benzaldehyde inhibitors demonstrated the inhibitors' interaction with the mild steel surface, indicating the potential creation of an inhibitor/mild steel complex formation.

5.1.5 Computational study

The HOMO and LUMO analysis of the benzaldehyde corrosion inhibitors revealed that the benzaldehyde ring exhibits both electron-donating and electron-accepting capabilities. The presence of pi-electrons from the double bonds in these heterocyclic compounds, along with the partially filled orbitals of the N-atoms, enables these inhibitors to engage in both electron donation

and acceptance. Moreover, the quantum chemical calculations reveal that the studied inhibitors possess the essential electronic and structural properties required to interact strongly with the metal surface, underscoring their promising potential as effective corrosion inhibitors.

5.2 Future recommendations

Benzaldehydes are generally considered non-toxic and environmentally friendly, making them an attractive alternative to traditional corrosion inhibitors, and they can be readily prepared through a straightforward synthesis process using easily accessible starting materials, making them cost-effective. Therefore, it is highly recommended for industries struggling with corrosion issues to consider implementing benzaldehyde inhibitors as a solution. By doing so, they can effectively reduce corrosion-related problems, extend the lifespan of their equipment, and improve overall operational efficiency and safety.

Researchers investigating the adsorption behaviour of organic molecules for corrosion protection are advised to:

a. Focus on environmentally friendly and non-toxic inhibitors to ensure sustainable applications.

b. Utilise established electrochemical techniques, such as Tafel and EIS, to assess corrosion inhibition performance.

c. Support experimental findings with advanced characterization tools, including:

- AFM for surface analysis and adsorption studies
- XPS for surface chemical composition analysis
- SEM for morphology

d. Complement experimental results with computational studies, including:

- Quantum mechanical calculations for molecular modelling and reactivity predictions
- Molecular dynamics simulations for adsorption and diffusion studies.

By adhering to these guidelines, scientists can significantly enhance our knowledge of corrosion prevention and organic molecule adsorption, paving the way for the creation of innovative, eco-friendly, and sustainable solutions that effectively address corrosion challenges.

REFERENCES

1. Moloto, B.P., Experimental quantum chemical, Monte Carlo simulations and QSAR studies of some hydantoin derivatives as corrosion inhibitors for mild steel in 0.5 M HCI solution. 2017, North-West University (South Africa).
2. François, R., Khan I. and Dang V.H., Impact of corrosion on mechanical properties of steel embedded in 27-year-old corroded reinforced concrete beams. Materials and structures, 2013. 46: p. 899-910.
3. Yunovich, M. and Thompson , N.G., Corrosion of highway bridges: Economic impact and control methodologies. Concrete International, 2003. 25(1): p. 52-57.
4. Bahadori, A., Corrosion and materials selection: a guide for the chemical and petroleum industries. 2014: John Wiley & Sons.
5. Popova, A., E. Sokolova, S. Raicheva and Christov M.J.C.s., AC and DC study of the temperature effect on mild steel corrosion in acid media in the presence of benzimidazole derivatives. 2003. 45(1): p. 33-58.
6. Tshikhudo, F., Investigation of substituted thiazolidinediones as corrosion inhibitors on different metals in acidic media. 2021.
7. Akiyama, M., Frangopol, D.M.and Ishibashi, H., Toward life-cycle reliability-, risk-and resilience-based design and assessment of bridges and bridge networks under independent and interacting hazards: emphasis on earthquake, tsunami and corrosion. Structure and Infrastructure Engineering, 2020. 16(1): p. 26-50.
8. Spitz, K. and Trudinger J., Converting Minerals to Metals: From Ore to Finished Product, in Mining and the Environment. 2019, CRC Press. p. 195-224.

9. Ebenso, E. and Oguzie, E, Corrosion inhibition of mild steel in acidic media by some organic dyes. Materials Letters, 2005. 59(17): p. 2163-2165.
10. Sharma, C.P., Engineering materials: properties and applications of metals and alloys. 2003: PHI Learning Pvt. Ltd.
11. Motsilanyane, A.R., Corrosion inhibition potential of imidazolium and pyrollidinium based ionic liquids on mild steel surfaces in acidic medium. 2017, North-West University (South Africa).
12. Murulana, L.C., Singh, A.K., Shukla, S.K., Kabanda, M.M. and Ebenso, E.E., Experimental and quantum chemical studies of some bis (trifluoromethyl-sulfonyl) imide imidazolium-based ionic liquids as corrosion inhibitors for mild steel in hydrochloric acid solution. Industrial & Engineering Chemistry Research, 2012. 51(40): p. 13282-13299.
13. Chandran, D.,. Ng, H.K, Lau, H.L.N., Gan, S and Choo, Y.M., Investigation of the effects of palm biodiesel dissolved oxygen and conductivity on metal corrosion and elastomer degradation under novel immersion method. Applied Thermal Engineering, 2016. 104: p. 294-308.
14. Ahmad, Z., Principles of corrosion engineering and corrosion control. 2006: Elsevier.
15. Dillon, C., Forms of Corrosion Recognition and Prevention: NACE handbook 1. Corros. Underst. Basics,(81), 1982: p. 99-143.
16. Pedeferri, P. and Pedeferri, P., Uniform Corrosion in Acidic and Aerated Solutions. Corrosion Science and Engineering, 2018: p. 145-167.
17. Zhang, X., Galvanic corrosion. Uhlig's Corrosion Handbook, 2011. 51: p. 123.
18. Jafarzadeh, S., Chen, Z and Bobaru, F., Computational modeling of pitting corrosion. Corrosion reviews, 2019. 37(5): p. 419-439.

19. Kim, Y.-J., Bahn, C.B., Baek, S.H., Choi, W. and Song, G.D., Crevice chemistry and corrosion in high temperature water: A review. Nuclear Engineering and Technology, 2024.

20. Larrosa, N., Akid, R. and Ainsworth, R., Corrosion-fatigue: a review of damage tolerance models. International Materials Reviews, 2018. 63(5): p. 283-308.

21. Khalifeh, A., Stress corrosion cracking damages, in Failure analysis. 2019, IntechOpen.

22. Phull, B., Evaluating intergranular corrosion. 2003.

23. Kalenda, P. and Petrášek, M., Study of the resistances of organic coatings to filiform corrosion. in Macromolecular Symposia. 2002. Wiley Online Library.

24. Singh, A.K., Singh, A.K. and D'Silva, Microbially induced corrosion and its mitigation. 2020: Springer.

25. Wright, K., An investigation of fretting corrosion. Proceedings of the Institution of Mechanical Engineers, 1953. 167(1b): p. 556-574.

26. Tozar, A. and Karahan, I., Structural and corrosion protection properties of electrochemically deposited nano-sized Zn–Ni alloy coatings. Applied Surface Science, 2014. 318: p. 15-23.

27. Fernandes, M., Latanision, R. and Searson, P., Morphological aspects of anodic dissolution. Physical Review B, 1993. 47(18): p. 11749.

28. Noor, E.A. and Al-Moubaraki, A.H., Corrosion behavior of mild steel in hydrochloric acid solutions. International Journal of Electrochemical Science, 2008. 3(7): p. 806-818.

29. Esfandiari, K., Banihashemi, M. and Soleimani, P., Influence of impressed current cathodic protection systems on chemical characteristics of underground water. Water Environment Research, 2020. 92(12): p. 2105-2111.

30. Skoog, D.A., Holler, F.J. and Crouch, S.R., Textbook" Principles of Instrumental Analysis". 2019: Cengage Learning; 6 edition.

31. Kemell, M., Ritala, M. and Leskelä, M., Thin film deposition methods for CuInSe 2 solar cells. Critical Reviews in Solid State and Materials Sciences, 2005. 30(1): p. 1-31.

32. Mashuga, M.E., Adsorption, thermodynamic and quantum chemical studies of some ionic liquids as corrosion inhibitors for mild steel in HCl. 2014, North-West University.

33. Zhang, X., Jiang Z.H., Yao, Z.P., Song Y. and Wu Z.D., Effects of scan rate on the potentiodynamic polarization curve obtained to determine the Tafel slopes and corrosion current density. Corrosion science, 2009. 51(3): p. 581-587.

34. Anaee, R.A.M. and Abdulmajeed, M.H., Tribocorrosion. Advances in Tribology, 2016.

35. Choi, H. and W. Kim., The improvement of corrosion resistance of AZ91 magnesium alloy through development of dense and tight network structure of Al-rich α phase by addition of a trace amount of Ti. Journal of Alloys and Compounds, 2017. 696: p. 736-745.

36. Peng, H., Zhang L., Soeller C. and Travas-Sejdic J., Conducting polymers for electrochemical DNA sensing. Biomaterials, 2009. 30(11): p. 2132-2148.

37. Aparicio, M. and Mosa J., Electrochemical characterization of sol–gel coatings for corrosion protection of metal substrates. Journal of Sol-Gel Science and Technology, 2018. 88: p. 77-89.

38. Cano, E., Lafuente, D. and Bastidas, D.M., Use of EIS for the evaluation of the protective properties of coatings for metallic cultural heritage: a review. Journal of Solid State Electrochemistry, 2010. 14: p. 381-391.

39. Gonzalez-Garcia, Garcia, Y., S. and Mol J., Electrochemical techniques for the study of self healing coatings. Active Protective Coatings: New-Generation Coatings for Metals, 2016: p. 203-240.

40. Feliu Jr, S., Electrochemical impedance spectroscopy for the measurement of the corrosion rate of magnesium alloys: Brief review and challenges. Metals, 2020. 10(6): p. 775.

41. Walczak, M., F. Pineda, A.G. Fernandez, C. Mata, T. and Escobar, R.A., Materials corrosion for thermal energy storage systems in concentrated solar power plants. Renewable and Sustainable Energy Reviews, 2018. 86: p. 22-44.

42. Durán, A., Y. Castro, A. Campo., C . and Damborenea, J.d., Sol-gel protective coatings for metals. 2005.

43. Kirkland, N., Birbilis, N. and Staiger, M., Assessing the corrosion of biodegradable magnesium implants: A critical review of current methodologies and their limitations. Acta biomaterialia, 2012. 8(3): p. 925-936.

44. Cesiulis, H., Tsyntsaru, N., Ramanavicius, A. and Ragoisha, G., The study of thin films by electrochemical impedance spectroscopy. Nanostructures and thin films for multifunctional applications: technology, properties and devices, 2016: p. 3-42.

45. Orazem, M.E. and Tribollet, B., Electrochemical impedance spectroscopy. New Jersey, 2008. 1: p. 383-389.

46. Amirudin, A. and Thieny, D., Application of electrochemical impedance spectroscopy to study the degradation of polymer-coated metals. Progress in organic coatings, 1995. 26(1): p. 1-28.

47. Choi, W., Shin, H.-C., Kim, J.M., Choi, J.-Y. and Yoon, W.-S., Modeling and applications of electrochemical impedance spectroscopy (EIS) for lithium-ion batteries. Journal of Electrochemical Science and Technology, 2020. 11(1): p. 1-13.

48. Macdonald, D.D., Reflections on the history of electrochemical impedance spectroscopy. Electrochimica Acta, 2006. 51(8-9): p. 1376-1388.

49. Frolick, M.N. and Robichaux, B.P., EIS information requirements determination: Using a group support system to enhance the strategic business objectives method. Decision Support Systems, 1995. 14(2): p. 157-170.

50. Mansfeld, F., Shih, H., Greene, H. and Tsai, C., Analysis of EIS data for common corrosion processes, in Electrochemical impedance: analysis and interpretation. 1993, ASTM International.

51. Kraka, E. and Cremer D., Computer design of anticancer drugs. A new enediyne warhead. Journal of the American Chemical Society, 2000. 122(34): p. 8245-8264.

52. Adamo, C. and Barone, V., A TDDFT study of the electronic spectrum of s-tetrazine in the gas-phase and in aqueous solution. Chemical Physics Letters, 2000. 330(1-2): p. 152-160.

53. Parac, M. and Grimme, S., All calculations were done by GAUSSIAN 03 W software. J. Phys. Chem. A, 2003. 106: p. 6844-6850.

54. Becke, A.D., A new mixing of Hartree–Fock and local density-functional theories. The Journal of chemical physics, 1993. 98(2): p. 1372-1377.

55. Lee, C., Yang, W. and Parr, R.G., Development of the Colle-Salvetti correlation-energy formula into a functional of the electron density. Physical review B, 1988. 37(2): p. 785.

56. Parr, R.G., Gadre S.R. and Bartolotti, L.J., Local density functional theory of atoms and molecules. Proceedings of the National Academy of Sciences, 1979. 76(6): p. 2522-2526.

57. Parr, R.G. and Pearson, R.G., Absolute hardness: companion parameter to absolute electronegativity. Journal of the American chemical society, 1983. 105(26): p. 7512-7516.

58. Lesar, A. and Milošev, I., Density functional study of the corrosion inhibition properties of 1, 2, 4-triazole and its amino derivatives. Chemical physics letters, 2009. 483(4-6): p. 198-203.

59. Masoud, M., M. Awad, Shaker M.A. and El-Tahawy, M., The role of structural chemistry in the inhibitive performance of some aminopyrimidines on the corrosion of steel. Corrosion Science, 2010. 52(7): p. 2387-2396.

60. Legut, D., Kądzielawa, A.P., Pánek, P., K. Marková, P. Váňová,. Konečná, K. and Langová, Š., Inhibition of steel corrosion with imidazolium-based compounds–Experimental and theoretical study. Corrosion Science, 2021. 191: p. 109716.

61. Wei, H., B. Heidarshenas, L. Zhou, G. Hussain, Q. Li and Ostrikov, K.K., Green inhibitors for steel corrosion in acidic environment: state of art. Materials Today Sustainability, 2020. 10: p. 100044.

62. Brycki, B.E., Kowalczyk, I.H., Szulc, A., Kaczerewska O. and Pakiet, M., Organic corrosion inhibitors. Corrosion inhibitors, principles and recent applications, 2018. 3: p. 33.

63. Goyal, M., Kumar, S., Bahadur, I., Verma C. and Ebenso, E.E., Organic corrosion inhibitors for industrial cleaning of ferrous and non-ferrous metals in acidic solutions: A review. Journal of Molecular Liquids, 2018. 256: p. 565-573.

64. Odewole, O.A., Ibeji, C.U., Oluwasola, H.O., Oyeneyin, O.E., Akpomie, K.G., Ugwu, C.M., Ugwu, C.G. and Bakare, T.E., Synthesis and anti-corrosive potential of Schiff bases

derived 4-nitrocinnamaldehyde for mild steel in HCl medium: Experimental and DFT studies. Journal of Molecular Structure, 2021. 1223: p. 129214.

65. Saha, S.K., Dutta A., Ghosh, P., Sukul, D. and Banerjee, P., Adsorption and corrosion inhibition effect of Schiff base molecules on the mild steel surface in 1 M HCl medium: a combined experimental and theoretical approach. Physical Chemistry Chemical Physics, 2015. 17(8): p. 5679-5690.

66. Pritzl, M.D., Tabatabai, H. and Ghorbanpoor, A., Laboratory evaluation of select methods of corrosion prevention in reinforced concrete bridges. International Journal of Concrete Structures and Materials, 2014. 8(3): p. 201-212.

67. Negm, N., Ghuiba, F. and Tawfik, S., Novel isoxazolium cationic Schiff base compounds as corrosion inhibitors for carbon steel in hydrochloric acid. Corrosion Science, 2011. 53(11): p. 3566-3575.

68. Touir, R., Dkhireche, N., Touhami, M.E., Sfaira, M., Senhaji, O., Robin, J., Boutevin B. and Cherkaoui, M., Study of phosphonate addition and hydrodynamic conditions on ordinary steel corrosion inhibition in simulated cooling water. Materials Chemistry and Physics, 2010. 122(1): p. 1-9.

69. Hassani, A. and Kamali, M.R., Optimization of acid injection rate in high rate acidizing to enhance the production rate: an experimental study in Abteymour oil field, Iran. Journal of Petroleum Science and Engineering, 2017. 156: p. 553-562.

70. Chen, H., Ji, H., Zhou, X. and Wang, L., Green synthesis of natural benzaldehyde from cinnamon oil catalyzed by hydroxypropyl-β-cyclodextrin. Tetrahedron, 2010. 66(52): p. 9888-9893.

71. Sarma, B.B., Efremenko I. and Neumann, R., Oxygenation of methylarenes to benzaldehyde derivatives by a polyoxometalate mediated electron transfer–oxygen transfer reaction in aqueous sulfuric acid. Journal of the American Chemical Society, 2015. 137(18): p. 5916-5922.

72. Kosmider, L., A. Sobczak, A. Prokopowicz, J. Kurek, M. Zaciera, J. Knysak, D. Smith and Goniewicz, M.L., Cherry-flavoured electronic cigarettes expose users to the inhalation irritant, benzaldehyde. Thorax, 2016. 71(4): p. 376-377.

73. Singh, D.K., S. Kumar, G. Udayabhanu and R.P. John, 4 (N, N-dimethylamino) benzaldehyde nicotinic hydrazone as corrosion inhibitor for mild steel in 1 M HCl solution: An experimental and theoretical study. Journal of molecular liquids, 2016. 216: p. 738-746.

74. Zhang, H. and Chen, Y., Experimental and theoretical studies of benzaldehyde thiosemicarbazone derivatives as corrosion inhibitors for mild steel in acid media. Journal of Molecular Structure, 2019. 1177: p. 90-100.

75. Arrousse, N., Salim, R., Houari, G.A., Hajjaji, F.E., Zarrouk, A., Rais, Z., Taleb, M., Chauhan D.S., Experimental and theoretical insights on the adsorption and inhibition mechanism of (2E)-2-(acetylamino)-3-(4-nitrophenyl) prop-2-enoic acid and 4-nitrobenzaldehyde on mild steel corrosion. Journal of Chemical Sciences, 2020. 132: p. 1-10.

76. Erdoğan, Ş., Safi, Z.S., Kaya, S., Işın, D.Ö., Guo, L. and Kaya, C., A computational study on corrosion inhibition performances of novel quinoline derivatives against the corrosion of iron. Journal of Molecular Structure, 2017. 1134: p. 751-761.

77. Ebenso, E.E., Kaband,a M.M., Murulana, L.C., Singh, A.K. and Shukla, S.K., Electrochemical and quantum chemical investigation of some azine and thiazine dyes as potential corrosion inhibitors for mild steel in hydrochloric acid solution. Industrial & engineering chemistry research, 2012. 51(39): p. 12940-12958.

78. Lowmunkhong, P., Ungthararak, D.and Sutthivaiyakit, P., Tryptamine as a corrosion inhibitor of mild steel in hydrochloric acid solution. Corrosion Science, 2010. 52(1): p. 30-36.

79. Döner, A., Solmaz, R., Özcan, M.and Kardaş, G., Experimental and theoretical studies of thiazoles as corrosion inhibitors for mild steel in sulphuric acid solution. Corrosion Science, 2011. 53(9): p. 2902-2913.

80. Oguzie, E., Li, Y.and Wang, F., Effect of surface nanocrystallization on corrosion and corrosion inhibition of low carbon steel: Synergistic effect of methionine and iodide ion. Electrochimica Acta, 2007. 52(24): p. 6988-6996.

81. Lahmady, S., Anor, O., Forsal, I., Hanine, H.and Benbouya, K., Electrochemical Examination of an Eco-friendly Corrosion Inhibitor. Analytical and Bioanalytical Electrochemistry, 2022. 14(3): p. 303-318.

82. Shylesha, B., Venkatesha, T. and Praveen, B., Corrosion inhibition studies of mild steel by new inhibitor in different corrosive medium. Research Journal of Chemical Sciences ISSN, 2011. 2231: p. 606X.

83. Verma, C., Olasunkanmi, L., Ebenso, E.E. and Quraishi, M., Substituents effect on corrosion inhibition performance of organic compounds in aggressive ionic solutions: a review. Journal of Molecular Liquids, 2018. 251: p. 100-118.

84. McCafferty, E., Introduction to corrosion science. 2010: Springer Science & Business Media.

85. Martinez, S. and Metikoš-Huković, M., A nonlinear kinetic model introduced for the corrosion inhibitive properties of some organic inhibitors. Journal of Applied Electrochemistry, 2003. 33: p. 1137-1142.

86. Bentiss, F., Lagrenee, M., Traisnel, M. and Hornez, J., The corrosion inhibition of mild steel in acidic media by a new triazole derivative. Corrosion science, 1999. 41(4): p. 789-803.

87. Leth-Olsen, H., CO2 Corrosion of Steel in Formate Brines for Well Applications. in NACE CORROSION. 2004. NACE.

88. Zarrouk, A., Hammouti, B., Zarrok, H., Al-Deyab, S.and Warad, I., Thermodynamic study of metal corrosion and inhibitor adsorption processes in copper/N-1-naphthylethylenediamine dihydrochloride monomethanolate/nitric acid system: part 2. Research on Chemical Intermediates, 2012. 38(7): p. 1655-1668.

89. Singh, A.K. and Quraishi, M., Adsorption properties and inhibition of mild steel corrosion in hydrochloric acid solution by ceftobiprole. Journal of Applied Electrochemistry, 2011. 41: p. 7-18.

90. Mashuga, M.E., Olasunkanmi, L.O. and Ebenso, E.E., Experimental and theoretical investigation of the inhibitory effect of new pyridazine derivatives for the corrosion of mild steel in 1 M HCl. Journal of Molecular Structure, 2017. 1136: p. 127-139.

91. Chopra, D. and Row, T.N.G., Role of organic fluorine in crystal engineering. CrystEngComm, 2011. 13(7): p. 2175-2186.

92. Ramachandran, A., Anitha, P., Gnanavel, S.and Angaiah, S., Development of 1-phenyl-3-(4-(pyridin-4-ylmethyl) phenyl) urea derivatives as robust corrosion inhibitors for mild steel in 1 M HCl environment: Insight from, molecular, experimental, and microscopic-scale modelling approaches. Journal of Environmental Chemical Engineering, 2024. 12(1): p. 111648.

93. Yadav, D.K., Maiti, B. and Quraishi, M., Electrochemical and quantum chemical studies of 3, 4-dihydropyrimidin-2 (1H)-ones as corrosion inhibitors for mild steel in hydrochloric acid solution. Corrosion Science, 2010. 52(11): p. 3586-3598.

94. Iroha, N.B. and Maduelosi, N.J., Corrosion inhibitive action and adsorption behaviour of justicia secunda leaves extract as an eco-friendly inhibitor for aluminium in acidic media. Biointerface Res. Appl. Chem, 2021. 11: p. 13019-13030.

95. Mashuga, M.E., Olasunkanmi, L.O., Lgaz, H., Sherif, E.-S.M. and Ebenso, E.E., Aminomethylpyridazine isomers as corrosion inhibitors for mild steel in 1 M HCl: Electrochemical, DFT and Monte Carlo simulation studies. Journal of Molecular Liquids, 2021. 344: p. 117882.

96. Zulkifli, F., Yusof, M.S.M., Isa, M., Yabuki, A. and Nik, W.W., Henna leaves extract as a corrosion inhibitor in acrylic resin coating. Progress in Organic Coatings, 2017. 105: p. 310-319.

97. Zarrouk, A., Hammouti, B., Al-Deyab, S., Salghi, R., Zarrok H., Jama, C. and Bentiss, F., Corrosion inhibition performance of 3, 5-diamino-1, 2, 4-triazole for protection of copper in nitric acid solution. International Journal of Electrochemical Science, 2012. 7(7): p. 5997-6011.

98. Ituen, E., Akaranta O. and James, A., Evaluation of performance of corrosion inhibitors using adsorption isotherm models: an overview. Chem. Sci. Int. J, 2017. 18(1): p. 1-34.

99. Vaszilcsin, C.G., Putz , M.V., A. Kellenberger and M.L. Dan, On the evaluation of metal-corrosion inhibitor interactions by adsorption isotherms. Journal of Molecular Structure, 2023. 1286: p. 135643.

100. Saha, P. and Chowdhury, S., Insight into adsorption thermodynamics. Thermodynamics, 2011. 16: p. 349-364.

101. Harvey, Walsh, T., F. and Nahlé, A., A review of inhibitors for the corrosion of transition metals in aqueous acids. Journal of Molecular Liquids, 2018. 266: p. 160-175.

102. Eddy, N.O. and Ebenso, E.E., Quantum chemical studies on the inhibition potentials of some penicillin compounds for the corrosion of mild steel in 0.1 M HCl. Journal of molecular modeling, 2010. 16: p. 1291-1306.

103. Hepworth, J.D., Waring, D.R. and Waring, M.J., Aromatic chemistry. Vol. 13. 2002: Royal Society of Chemistry.

104. Jezuita, A., Ejsmont, K. and Szatylowicz, H., Substituent effects of nitro group in cyclic compounds. Structural Chemistry, 2021. 32(1): p. 179-203.

105. Lebrini, M., Lagrenée, M., Traisnel, M., Gengembre, L., Vezin, H. and Bentiss, F., Enhanced corrosion resistance of mild steel in normal sulfuric acid medium by 2, 5-bis (n-thienyl)-1, 3, 4-thiadiazoles: electrochemical, X-ray photoelectron spectroscopy and theoretical studies. Applied Surface Science, 2007. 253(23): p. 9267-9276.

106. Murulana, L.C., Kabanda, M.M. and Ebenso, E.E., Experimental and theoretical studies on the corrosion inhibition of mild steel by some sulphonamides in aqueous HCl. RSC advances, 2015. 5(36): p. 28743-28761.

107. Ebenso, E.E., Arslan, T., Kandemirlı, F., Love ,I., Öğretır, C.l., Saracoğlu, M. and Umoren, S.A., Theoretical studies of some sulphonamides as corrosion inhibitors for mild steel in acidic medium. International Journal of Quantum Chemistry, 2010. 110(14): p. 2614-2636.

108. de Oliveira, L.F., Edwards, H.G., Velozo, E.S. and Nesbitt, M., Vibrational spectroscopic study of brazilin and brazilein, the main constituents of brazilwood from Brazil. Vibrational Spectroscopy, 2002. 28(2): p. 243-249.

109. James, C., Ra,j A.A., Reghunathan, R., Jayakumar, V. and Joe, I.H., Structural conformation and vibrational spectroscopic studies of 2, 6-bis (p-N, N-dimethyl benzylidene) cyclohexanone using density functional theory. Journal of Raman Spectroscopy: An International Journal for Original Work in all Aspects of Raman Spectroscopy, Including Higher Order Processes, and also Brillouin and Rayleigh Scattering, 2006. 37(12): p. 1381-1392.

110. Bernstein, M.P., Sandford, S.A. and Allamandola, L.J., The infrared spectra of nitriles and related compounds frozen in Ar and H2O. The Astrophysical Journal, 1997. 476(2): p. 932.

111. Kang, I.P.S., Spectral Studies of Compounds Containing the Carboxylate Ion, Nitro and Related Groupings. 1970: The Australian National University (Australia).

112. Badger, R.M. and Bauer, S.H., Spectroscopic studies of the hydrogen bond I. A photometric investigation of the association equilibrium in the vapor of acetic acid. The Journal of Chemical Physics, 1937. 5(8): p. 605-608.

113. Olasunkanmi, L.O., Kabanda, M.M. and Ebenso, E.E., Quinoxaline derivatives as corrosion inhibitors for mild steel in hydrochloric acid medium: Electrochemical and quantum chemical studies. Physica E: Low-dimensional Systems and Nanostructures, 2016. 76: p. 109-126.

114. Minami, K., Ohashi, T., Suzuki, M., Aizawa, T., Adschiri, T. and Arai, K., Estimation of local density augmentation and hydrogen bonding between pyridazine and water under sub-and supercritical conditions using UV-vis spectroscopy. Analytical sciences, 2006. 22(11): p. 1417-1423.

115. Rbaa, M., F. Benhiba, I. Obot, H. Oudda, I. Warad, B. Lakhrissi and Zarrouk, A., Two new 8-hydroxyquinoline derivatives as an efficient corrosion inhibitors for mild steel in hydrochloric acid: synthesis, electrochemical, surface morphological, UV–visible and theoretical studies. Journal of Molecular Liquids, 2019. 276: p. 120-133.

APPENDIX: FORMULAE USED

1. Potentiodynamic polarization ihibition efficiency:

$$E_{PDP}\% = \frac{i^{o}corr - i^{i}corr}{i^{o}corr}$$

2. Electrochemical impedance spectroscopy inhibition efficiency:

$$E_{EIS}\% = \left(1 - \frac{R^{o}ct}{R_{ct}}\right) x\ 100$$

3. The energy gap:

$$\Delta E = E_{LUMO} - E_{HOMO}$$

4. Dipole moment

$$\mu = Q \times r$$

5. Global chemical hardness

$$\sigma = \frac{1}{\eta} \cong -2/(E_{HOMO} - E_{LUMO})$$

6. Electronegativity

$$X \cong -(\frac{1}{2})(E_{HOMO} + E_{LUMO})$$

7. Current response, constant phase element (CPE):

$Z_{CPE} = Y_0^{-1}(i\omega)^{-n}$

8. Double layer resistance (Cdl):

C_{dI}= $(Y_0 R_{ct}^{1-n})^{1/n}$

9. Surface coverage (with thermodynamic parameters):

$\theta = \frac{K_{ads}C_{inh}}{1+K_{ads}C_{inh}}$

10. Surface coverage (with thermodynamic parameters) rearranged:

$\frac{C}{\theta} = C + \frac{1}{K_{ads}}$

11. Gibb's free energy of adsorption

$\Delta G^{O}{}_{ads}$= - RT In (55.5K_{ads})